Inaugural dissertation

for

obtaining the doctoral degree

of the

Combined Faculty of Mathematics, Engineering and Natural Sciences

of the

Ruprecht - Karls - University

Heidelberg

Presented by

M. Sc. Niklas Peters

born in: Nettetal, Germany

Oral examination: 03.12.2024

Regulation of the ubiquitin ligase Ubr1 during protein quality control

Referees: Prof. Dr. Matthias Mayer
Prof. Dr. Sebastian Schuck

I. Summary

Cells control the degradation of aberrant or damaged proteins through ubiquitin ligases. When yeast faces protein folding imbalance, the disordered protein Roq1 binds the ubiquitin ligase Ubr1 as a substrate mimic that profoundly changes Ubr1 activity and substrate specificity from N-degron substrates to misfolded proteins. How Roq1 reprograms Ubr1 is not known on a mechanistic level.

In my PhD thesis I biochemically dissected the underlying principles how Roq1 controls Ubr1 using a defined *in vitro* system. I could demonstrate that Roq1 governs the ubiquitination of Ubr1 substrates through two cooperating motifs. The Roq1 N-terminus controls N-degron substrate ubiquitination. The Roq1 hydrophobic motif enhances the ubiquitination of endogenous Ubr1 substrates with internal degrons and of misfolded proteins. The N-terminus and hydrophobic motif allow Roq1 to bind Ubr1 heterobivalently to generate avidity for efficient Ubr1 reprograming. Furthermore, I could show that amino acid residues C-terminal of the hydrophobic motif are dispensable for Roq1 function. How does Roq1 regulate Ubr1? Instead of promoting ubiquitin-conjugating enzyme or substrate recruitment, Roq1 enhances the ubiquitin transfer by increasing the efficiency of ubiquitin chain initiation. To understand how Roq1 manipulates Ubr1 on a structural level I determined the cryogenic electron microscopy structure of a Roq1-Ubr1 complex with an overall resolution of 6.3 Ångström, which awaits further optimization.

Overall, I unraveled in my PhD thesis how the small, disordered protein Roq1 comprehensively regulates the complex ubiquitin ligase Ubr1. Given the essential role of ubiquitin ligases in diseases, the Roq1 bipartite mode of action could therefore inspire the design of new therapeutic modulators for other ubiquitin ligases.

II. Zusammenfassung

Zellen kontrollieren den Abbau von überflüssigen oder beschädigten Proteinen mithilfe von Ubiquitin-Protein-Ligasen. Wenn fehlgefaltete Proteine in der Hefezelle akkumulieren, entsteht eine zelluläre Stressreaktion. Während dieser bindet das kleine, intrinsisch ungeordnete Protein Roq1 als Pseudosubstrat die Ubiquitin-Protein-Ligase Ubr1 und steuert so nachhaltig deren Aktivität und Substratspezifität. Anstelle von N-Degron-Substraten erkennt Ubr1 nun hauptsächlich fehlgefaltete Proteine und baut diese ab. Wie Roq1 auf mechanistischer Ebene Ubr1 umprogrammiert, ist nicht bekannt.

In meiner Doktorarbeit habe ich die grundlegenden Prinzipien der Ubr1-Regulation durch Roq1 in einem definierten *in vitro* System biochemisch untersucht. Ich konnte zeigen, dass Roq1 die Ubiquitinierung von Ubr1-Substraten über zwei miteinander agierende Motive steuert. Mittels N-Terminus kontrolliert Roq1 die Ubiquitinierung von N-Degron-Substraten. Über ein hydrophobes Element verbessert Roq1 die Ubiquitinierung von fehlgefalteten Proteinen und endogenen Ubr1 Substraten mit internen Abbausequenzen. Der N-Terminus und das hydrophobe Motiv befähigen Roq1 über einen heterobivalenten Mechanismus Ubr1 zu binden, der die benötigte Avidität für eine effiziente Umprogrammierung von Ubr1 bereitstellt. Darüber hinaus konnte ich zeigen, dass Aminosäuren C-Terminal des hydrophoben Motivs nicht für die Funktion von Roq1 benötigt werden. Wie reguliert Roq1 Ubr1? Anstatt die Affinität zwischen des Ubiquitin-konjugierenden Enzyms oder Substrates und Ubr1 zu erhöhen, steigert Roq1 die Ubiquitinierungseffizienz über eine Beschleunigung der initialen Ubiquitinkettenbildung. Um zu verstehen, wie Roq1 auf Strukturebene Ubr1 beeinflusst, habe ich mittels Kryoelektronenmikroskopie die Struktur eines Roq1-Ubr1 Komplexes gelöst bei einer globalen Auflösung von 6,3 Ångström, welche weiter optimiert werden wird.

Zusammengefasst konnte ich in meiner Doktorarbeit zeigen, wie das kleine, intrinsisch ungeordnete Protein Roq1 nachhaltig die komplexe Ubiquitin-Protein-Ligase Ubr1 modulieren kann. Unter dem Gesichtspunkt, dass Ubiquitin-Protein-Ligasen Schlüsselrollen bei diversen Krankheiten einnehmen, könnten die hier gewonnen Erkenntnisse als Inspiration dienen für die Entwicklung therapeutischer Regulatoren anderer Ubiquitin-Protein-Ligasen.

Table of contents

III. Contributions by co-workers

A significant portion of the data was recently published as a preprint article (Peters *et al*, 2024). This includes figures 2B, 4, 5B+C, 6, 7A+D, 9A-C, 10, 11B, D, E, 14, 15B+C. Cartoons in figures 1, 10A and 20 and the AlphaFold structure predicition of Roq1 in figure 9A were adapted from Peters *et al*., 2024 by me. Sibylle Kanngießer and Sebastian Schuck contributed to the conceptualization and data acquisition. All experiments were conceptualized and performed by me, unless otherwise stated here, in the text and figure legends.

Pho8*, unfolded luciferase and Cup9 ubiquitination assays in figures 3, 5A and 15D were conceptualized and first performed by Sibylle Kanngießer and reproduced by me. The depicted experiments in these figures were carried out by me.

Photo-crosslinking experiments in figure 10B, re-purification of Ulp1, Ubr1 and Rad6 and ubiquitination assay implementation were done collaboratively with Sibylle Kanngießer.

Cryo electron microscopy data acquisition and processing for figures 17B-G were done by Dirk Flemming and Jan Rheinberger. Graphical representation of the dataset was performed by me.

The Roq1-Ubr1 AlphaFold predictions in figures 18B-E were run by Bram Vermeulen and analyzed collaboratively by Bram Vermeulen, Stefan Pfeffer, Sibylle Kanngießer and me.

The Roq1 disorder predictions and homology alignments in figures 9B+C, respectively, were conceptualized and initially visualized by Sebastian Schuck, but re-run and re-plotted by me.

Co-immunoprecipitations, biolayer interferometry experiments, flow cytometry assays and the purification and characterization of Roq1 mutants were conceptualized and performed by Sibylle Kanngießer.

The yeast genetic screen that led to the identification of the Roq1 hydrophobic motif (Fig. 9D) was initially carried out by Oliver Pajonk and finalized by Sibylle Kanngießer.

The generation of the pCA528-His_6-SUMO-Roq1 (22-60)-HA and pCA528-His_6-SUMO-Roq1 (22-104)-HA plasmids, the purification of Roq1 (22-104)-HA and initial testing of Roq1 (22-104)-HA activity in yeast reporter assays were carried out by Rafael Salazar Claros.

Jörg Malsam provided technical assistance and reagent support for the photo-crosslinking experiments in figure 10B.
The Rad6 and N-degron substrate purification protocols were from Chi-Ting Ho.
Purification of ubiquitin was done collaboratively with Gerry Meese (Melchior lab) using a protocol from Jörg Schweiggert.

IV. List of Abbreviations

Ala	Alanine
APF-1	ATP-dependent proteolysis factor 1
Arg	Arginine
APS	Ammonium persulfate
ATP	Adenosine triphosphate
ATPase	Adenosine triphosphatase
dNTP	Deoxynucleotide triphosphate
Bpa	p-Benzyol-L-phenylalanine
BSA	Bovine serum albumin
CHAPS	3-(Dimethyl[3-(3α,7α,12α-trihydroxy-5β-cholan-24-amido) propyl]azaniumyl) propane-1-sulfonate
CRBN	Cereblon
CRL	Cullin-RING ligase
Cryo-EM	Cryo-electron microscopy
DTT	Dithiothreitol
DUB	Deubiquitinating enzyme
E1	Ubiquitin-activating enzyme 1
E2	Ubiquitin-conjugating enzyme 2
E3	Ubiquitin ligase
E. coli	Escherichia coli
EDTA	Ethylenediaminetetraacetic acid
EM	Electron microscopy
ER	Endoplasmic reticulum
ERAD	ER-associated degradation
GID	Glucose-induced degradation-deficient
GST	Glutathione S-transferase
HECT	Homologous to the E6-AP Carboxyl Terminus
HEPES	2-[4-(2-Hydroxyethyl)piperazin-1-yl]ethane-1-sulfonic acid
IAP	Inhibitor of apoptosis
IMAC	Immobilized metal affinity chromatography
IPOD	Insoluble protein deposit
IPTG	Isopropyl β-D-1-thiogalactopyranoside
JUNQ	Juxtanuclear quality control compartment
LB	Lysogeny broth
Leu	Leucine
LUBAC	Linear ubiquitin chain assembly complex
Luciferase^{N}	Native Firefly Luciferase
Luciferase^{U}	Unfolded Firefly Luciferase
MBP	Maltose binding protein
NEB	New England Biolabs
NEF	Nucleotide Exchange Factor
NP-40	Nonidet P-40 (NP-40)

OD	Optical density
PAGE	Polyacrylamide gel electrophoresis
PBS	Phosphate-buffered saline
PCR	Polymerase chain reaction
PDB	Protein Data Bank
PEG	Polyethylene glycol
PMSF	Phenylmethylsulfonyl fluoride
PROTAC	Proteolysis targeting chimera
PQC	Protein quality control
PTM	Post-translational modification
RBR	RING-Between-RING
RING	Really interesting new gene
S. cerevisiae	Saccharomyces cerevisiae
SCD	Synthetic complete dextrose
SDS	Sodium dodecyl sulfate
SEC	Size exclusion chromatography
SHRED	Stress-induced homeostatically regulated protein degradation
SLiM	Short linear motif
TBS	Tris-buffered saline
TBST	TBS/Tween
UBD	Ubiquitin binding domain
UBIP	Ubiquitous immunopoietic polypeptide
UBLM	Ubiquitin binding loop motif
UPS	Ubiquitin proteasome system
VHL	Von Hippel-Lindau
YNB	Yeast nitrogen base
YPD	Yeast extract peptone dextrose
YT	Yeast extract tryptone

V. List of Figures

VI. List of Tables

1. Introduction

The ancient Egyptians created a code to document their secular legacy, express ideas and to communicate: the hieroglyphs. Comprising sequences of single symbols, they convert sophisticated and perhaps pivotal messages, which remain enigmatic unless the recipient knows how to decode them.

Cells employ similar methods to instruct proteins what they need to do. Damaged or aberrant proteins, for instance, are marked with ubiquitin molecules for their degradation. Ubiquitin is part of a cellular mechanism reminiscent of hieroglyphs: the ubiquitin code (Figure 1) (Komander & Rape, 2012).

Writers of the ubiquitin code include ubiquitin-activating enzymes (E1), ubiquitin-conjugating enzymes (E2) and ubiquitin ligases (E3). Cooperatively, they attach though a multistep cascade one or more ubiquitin molecules to dedicated substrates, which sequentially builds sophisticated ubiquitin chains of different topologies (see Figure 1 legend for details). Erasers of the ubiquitin code, deubiquitinating enzymes (DUBs), can trim the ubiquitin chains to add further layers of complexity. Ubiquitin signals translate into intricate messages, which are deciphered by ubiquitin binding proteins, the decoders. A comprehensive translation of the ubiquitin code is essential for a cell to control the fate of a substrate, which covers nonproteolytic and proteolytic roles.

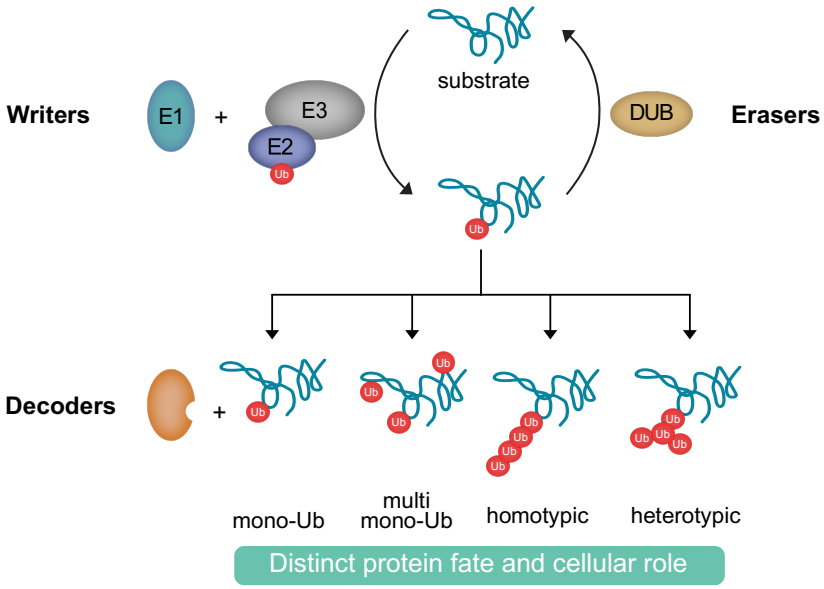

Figure 1. Components of the ubiquitin code. Writers of the ubiquitin code include ubiquitin-activating enzymes (E1), ubiquitin-conjugating enzymes (E2) and ubiquitin ligases (E3s). In cooperation with their E1 and E2 enzymes, ubiquitin ligases conjugate ubiquitin through an enzymatic cascade to one or more residues of a distinct substrate they bind. Ubiquitination can also be deleted by deubiquitinating enzymes (DUBs), which serve as erasers of the ubiquitin code. The single ubiquitin conjugation to a substrate leads to its monoubiquitination (mono-Ub), whereas numerous single ubiquitin binding events to different substrate residues cause multi-monoubiquitination (multi-mono-Ub). The repetitive attachment of ubiquitin molecules to acceptor ubiquitins guides the formation of a distinct chain. Based on the E2/E3 pair that drives the chain elongation, different ubiquitin lysines or even the N-terminus of ubiquitin can be employed to form ubiquitin chains with various chain topologies. Depending on whether they share the same or a different acceptor side within ubiquitin, they form homotypic or heterotypic ubiquitin chains, respectively. Discrete ubiquitin signals (be it mono- or polyubiquitination) are deciphered by distinct decoders with ubiquitin binding domains (UBDs) that determine the protein fate and cellular roles, ranging from nonproteolytic to proteolytic functions. The cartoon was conceptualized by (Dikic & Schulman, 2022), created and further modified by me with permission from Springer Nature.

Here, I will first introduce the biochemical and cellular aspects of the ubiquitin code that are needed to ubiquitinate substrates (section 1.1). Next, I will describe how the writers of the ubiquitin code, ubiquitin ligases, can be biochemically finetuned and manipulated to more efficiently ubiquitinate their substrates (section 1.2). Given the significance of ubiquitinated substrates for cellular functions, I will subsequently unravel the roles of E3s in various nonproteolytic and proteolytic pathways (section 1.3). For a more thorough dissection, I will then focus on biochemical and cellular aspects of two distinct proteolytic pathways that share the same ubiquitin ligase in different cellular contexts (sections 1.4 and 1.5).

1.1 Writing, erasing and deciphering the ubiquitin code

1.1.1 Writers

Writing the ubiquitin code requires sequential action of three enzymes: a ubiquitin-activating enzyme (E1), a ubiquitin-conjugating enzyme (E2) and a ubiquitin ligase (E3) that, together with ubiquitin, initiate the synthesis of a ubiquitin chain covalently linked to target proteins (Deshaies & Joazeiro, 2009). The enzymatic cascade that drives ubiquitin chain synthesis is conserved among eukaryotes (Hershko & Ciechanover, 1998), but a mechanistically similar pathway involving E1-E2 and ubiquitin-like proteins has only recently been identified in bacteria (Chambers *et al*, 2024).

Ubiquitin, the hieroglyphic symbol so to say of the ubiquitin code, consists of 76 amino acids, is conserved and was first isolated in 1975 by Gideon Goldstein, who attempted to purify thymopoietin, and termed it as ubiquitous immunopoietic polypeptide (UBIP) (Goldstein *et al*, 1975). In 1978, Hershko and Ciechanover discovered that proteins undergo adenosine triphosphate (ATP)-dependent proteolysis once they conjugate the ATP-dependent proteolysis factor 1 (APF-1) (Ciehanover *et al*, 1978). Two years later, Wilkinson identified APF-1 as UBIP and, considering its ubiquitous role in life, gave the protein its final name, ubiquitin (Wilkinson *et al*, 1980).

Since the first isolation of UPS components and the identification of a sequential E1-E2-E3 ubiquitin transfer in 1983, the number of identified proteins significantly increased (Hershko *et al*, 1983). Today, there are two E1s, 50 E2s and more than 600 E3s known in humans (George *et al*, 2018). Yeast, in contrast, only possess one E1, 11 E2s and roughly 100 E3s (Fang *et al*, 2023).

The enzymatic E1-E2-E3 ubiquitin transfer cascade starts with a ubiquitin-charging step of the ubiquitin-activating enzyme (Cappadocia & Lima, 2018; Streich & Lima, 2014). First, the E1 binds ATP, magnesium, and ubiquitin to adenylate the C-terminal glycine of bound ubiquitin. Next, the E1 catalytic cysteine binds the Ub~adenylate ("~" denotes a thioester bond) to form a E1~Ub, which causes the release of AMP. Subsequently, the E1~Ub adenylates a second ubiquitin, thus forging a ternary ubiquitin-E1~ubiquitin complex. The ternary complex then transfers ubiquitin to the E2 via transthioesterification to form E2~Ub (Cappadocia & Lima, 2018).

Despite their diversity, E2s share common features: They possess a catalytic α/β fold UBC domain that comprises an active site cysteine, a backside that allows binding of a second ubiquitin or different proteins for regulation (see also section 1.2.1) and overlapping E1/E3 binding sites (Stewart *et al*, 2016). The overlap prevents simultaneous E1/E3 binding and accounts for the sequential binding order in the ubiquitination cascade. E2~Ub, which is a high-energy complex, exhibits intrinsic activity towards small nucleophiles such as free lysines, resulting in spontaneous aminolysis independently of an E3 (Bracher *et al*, 2011; Pickart & Rose, 1985). Accounting for this is the C-terminus of ubiquitin, which is very dynamic and shows a high degree of freedom in an open state (Buetow & Huang, 2016).

E2~Ubs have an increased reactivity in presence of ubiquitin ligases. Depending on the type, they transfer ubiquitin indirectly via two-step thioesterification and

aminolysis reactions (Homologous to the E6-AP Carboxyl Terminus (HECT) and RING-Between-RING (RBR) E3s) or directly via a single aminolysis step (Really Interesting New Gene (RING) E3s) to bound substrates (Deshaies & Joazeiro, 2009). RING ubiquitin ligases possess a RING domain comprising histidine and cysteine residues that bind two zinc ions. RING E3s that lack zinc ions but act similarly are U box proteins. Both RING E3s and U box proteins directly transfer ubiquitin from the E2 to a bound substrate (Buetow & Huang, 2016). Remarkably, ubiquitin transfer is universal for all RING E3s and requires a so called closed E2~Ub-E3 conformation (Branigan *et al*, 2020). The RING domain binds E2~Ub and restricts the flexibility of the C-terminus of ubiquitin, folds it back to I44 of ubiquitin and positions E2~Ub ideally for a substrate nucleophilic attack on E2~Ub. During the nucleophilic attack, a substrate ubiquitin acceptor, canonically a lysine via its ε-amino group, binds the carboxyl group of the C-terminal glycine of ubiquitin. Typically, this involves a RING linchpin residue, in most cases an arginine, that assists in further positioning of the glycine. The ternary E2~Ub-RING-substrate complex allows ubiquitin discharge from the E2 and efficient ubiquitin transfer to the bound substrate (Cappadocia & Lima, 2018; Dou *et al*, 2012b; Plechanovova *et al*, 2012; Pruneda *et al*, 2012; Stewart *et al.*, 2016).

The transfer of multiple ubiquitin molecules to a substrate generates a polymeric, elongated ubiquitin chain, whose assembly underlies two different mechanisms: en bloc or sequential chain formation (Deshaies & Joazeiro, 2009). En bloc formation describes the simultaneous transfer of multiple ubiquitin molecules to a substrate and was first described for HECT ubiquitin ligases, but later also for some E2/RING E3 pairs (Li *et al*, 2007; Masuda *et al*, 2012). In contrast, sequential chain formation conveys that the most distal substrate ubiquitin serves as an acceptor for the next donor molecule, thus representing single encounter reactions (Pierce *et al*, 2009). Priming a substrate with the first ubiquitin occurs in most cases with less sequence specificity, whereas ubiquitin chain elongation appears to be more precise due to the monoubiquitin orientation (Fischer *et al*, 2011; Nakasone *et al*, 2022; Petroski & Deshaies, 2003; Tang *et al*, 2007). Thus, the priming rate represents the limiting step during ubiquitin chain assembly (Williamson *et al*, 2011).

To compensate for different spatio-temporal parameters during ubiquitin chain initiation and elongation, several strategies exist: Some E3s, such as the anaphase promoting complex APC/C, have distinct E2s for chain initiation and elongation

(Brown *et al*, 2016). Since an increasing chain length demands more conformational space, some E3s such as the N-degron ubiquitin ligase Ubr1 restrict the degree of freedom through a non-RING motif that binds the elongating ubiquitin chain and thereby favors a nucleophilic attack of the distal ubiquitin acceptor (Deol *et al*, 2019; Pan *et al*, 2021).

While the RING domain mediates the substrate ubiquitin accessibility to the E2~Ub, it is the E2 that dictates the chain topology (Buetow & Huang, 2016). Ubiquitin chains form either homotypic or heterotypic chain linkages, depending on whether they share the same or a different acceptor site within ubiquitin, respectively (see section 1.3). Heterotypic chains can be generated by a single E3 that shows no linkage specificity, such as the HECT E3 ligase WWP1. Alternatively, either two E3 ligases can act cooperatively on one substrate by sharing ubiquitin binding domains (UBDs) or different E2s mediate ubiquitin chain initiation and elongation (French *et al*, 2017; Koegl *et al*, 1999; Meyer & Rape, 2014). The total ubiquitin chain length and overall chain building kinetics are affected by the ratio of ubiquitin association and substrate dissociations rates. In combination with the chain linkage topology, they determine the cellular fate of a substrate (see below).

Altogether, writers of the ubiquitin code include E1, E2 and E3 enzymes, which orchestrate, through a catalytic cascade, the transfer of ubiquitin molecules to dedicated substrates.

1.1.2 Erasers

To prevent permanent ubiquitination of a substrate, ubiquitin chains must be trimmed or erased by dedicated proteases, the deubiquitinating enzymes (DUBs). Roughly 100 DUBs exist in humans and 22 DUBs in yeast (Suresh *et al*, 2020). One major task of DUBs is to maintain a free pool of ubiquitin. Ubiquitinated substrates that are marked for destruction are sent to the proteasome, where they are degraded. To prevent degradation of ubiquitin, proteasome-bound DUBs such as Ubp6 in yeast (USP14 in humans) hydrolyze ubiquitin chains from substrates, thus keeping a pool of free ubiquitin (Finley, 2009).

In concert with E3s, DUBs edit the chain topology of a ubiquitinated substrate for additional linkage specificity to exert distinct cellular functions, including protein

degradation, cell morphology and signaling or quality control of ER-targeted proteins (Suresh *et al.*, 2020). The yeast DUB Ubp1, for instance, opposes the ER-bound E3 ligase Doa10 and serves as molecular timer that determines the protein fate (Ast *et al*, 2014).

1.1.3 Decoders

Once a ubiquitin chain is built, the ubiquitin code needs to be deciphered to fulfill its physiological function. Ubiquitin decoders contain dedicated domains or motifs through which they bind ubiquitin. Once bound, they determine the cellular fate of the ubiquitinated substrate, including enzymatic activation, post-translational modification (PTM), or protein degradation (Komander & Rape, 2012). Depending on the substrate, protein degradation involves the AAA adenosine triphosphatase (ATPase) CDC48, which exhibits unfoldase activity and extracts ubiquitinated proteins from the ER membrane in a conveyor belt-like mechanism (Twomey *et al*, 2019). Remarkably, threading of the substrate through CDC48 also leads to the unfolding of proximal ubiquitins, which would need to refold after the substrate emerges from CDC48. The extracted and unfolded but still ubiquitinated substrate is recognized by the 19S proteasomal subunit receptors Rpn10, Rpn1 and Rpn13, which bind the L8-I44-H68-V70 patch of ubiquitin (Bard *et al*, 2018; Dikic *et al*, 2009; Finley *et al*, 2012; Randles & Walters, 2012). Once bound, the substrate engages with the proteasome by inserting its unfolded tail. Rpn11, as part of the 19S proteasomal cap, deubiquitinates the substrate to admit threading into the 20S proteasomal core for its final destruction (Bard *et al.*, 2018).

In contrast to the proteasome and CDC48, many other ubiquitin decoders either further post-translationally modify ubiquitinated substrates or require them for their activity. For instance, the ubiquitin-like protein Nedd8 allosterically stimulates Cullin RING ubiquitin ligase (CRL) activity to promote ubiquitin chain formation (Baek *et al*, 2020). Moreover, Vps27 of the ESCRT-0 complex contains a ubiquitin-interacting motif for the recruitment of downstream ESCRT components that are needed for endosomal trafficking and cargo sorting (Bilodeau *et al*, 2002). The monoubiquitin attached to histone2B has a distinct orientation that dictates where downstream methylation by MLL methyltransferases takes place (Xue *et al*, 2019).

Together, ubiquitin decoders are crucial components of the ubiquitin code, which enable a cell to decipher the physiological function of ubiquitinated substrates.

1.2 Regulation and manipulation of ubiquitin ligases

1.2.1 Regulation of ubiquitin ligases

As illustrated above, achieving a closed conformation of a E2~Ub/E3 pair is crucial for efficient ubiquitin transfer. Controlling the involved machinery allows the precise finetuning according to cellular demands, where control over ubiquitin ligase activity and substrate specificity is pivotal.

Due to its essential role in controlling the ubiquitin transfer, E2s represent the ideal target to regulate ubiquitin chain building activity. Non-covalent attachment of a second ubiquitin molecule to their backside, as it has been reported for Rad6, facilitates the closed conformation, and thus stimulates ubiquitin transfer (Brzovic *et al*, 2006; Buetow *et al*, 2015; Kumar *et al*, 2015). Besides ubiquitin, non-RING elements in E3 ligases can also stimulate ubiquitin ligase activity, which involves the interaction of alpha-helical segments with the E2 backside (Stewart *et al.*, 2016). Examples include the UB2R domain of the E3 Ubr1, which stabilizes Rad6 (Pan *et al.*, 2021), the U7BR domain of Cue1 that cooperates with Ubc7 (Metzger *et al*, 2013), and G2BR of Gp78 that binds Ube2g2 (Das *et al*, 2009). Paradoxically, non-RING element binding of the ubiquitin ligase Bre1 to Rad6 impairs polyubiquitination. Instead, it promotes monoubiquitination by fixating Rad6 in a rigid conformation that sterically allows only the conjugation of a single ubiquitin to its substrate, the histone H2B (Deng *et al*, 2023; Gallego *et al*, 2016; Shi *et al*, 2023; Turco *et al*, 2015). There are also a few reports showing that fixing of the E2~Ub conformation can be achieved independently of the E2 backside, as recently demonstrated for UbcH5b, whose activity is governed by the E3 RNF125 through a zinc finger motif that does not overlap with the ubiquitin backside binding side (Middleton *et al*, 2023).

Beyond the importance of ubiquitin-conjugating enzymes, proteins or ligands that directly bind ubiquitin ligases control ubiquitin transfer efficiency as well. For instance, poly(ADP-ribosyl)ation of the RNF146 ubiquitin ligase promotes ubiquitination by activating an allosteric switch that favors the E2~Ub closed conformation (DaRosa *et al*, 2015). Moreover, binding of the ubiquitin-like protein Nedd8 to CRLs promotes

chain initiation (Baek *et al.*, 2020; Saha & Deshaies, 2008) and, as recently demonstrated, chain elongation (Liwocha *et al*, 2024). To achieve this, Nedd8 binds to a Cullin lysine residue, which causes the release of the RING domain from Cullin to interact with UBE2R2 and an acceptor ubiquitin. Protein phosphorylation, the most common type of PTM (Ubersax & Ferrell, 2007), plays substantial roles in regulating ubiquitin ligases. For instance, the RING E3 ubiquitin ligase Cbl binds its cognate E2 far away from the substrate in its unphosphorylated state. Phosphorylation of residue Y371 allosterically activates Cbl by flipping the E2 and RING domain to favor substrate interaction (Dou *et al*, 2012a).

Another mechanism to regulate RING ubiquitin ligase activity is dimerization. In their autoinhibited state, the E3s BIRC7 and RNF4 are monomers, but dimerize through their RING tails to become active (Dou *et al.*, 2012b; Plechanovova *et al.*, 2012). How protein oligomerization stirs ligase activity has also recently been demonstrated by structural investigations of the HECT ubiquitin ligase Ubr5 (Wang *et al*, 2023). Ubr5 exists both as a homodimer and cage-like tetrameric structure in solution. While dimerization occurs via helical scaffolds, tetramer formation requires the interplay between two SBB2-SBB2 regions of two Ubr5 dimers. How oligomerization affects Ubr5 activity is not entirely clear, but first evidence suggests that oligomerization is a prerequisite for effective substrate recruitment (Hodakova *et al*, 2023; Tsai *et al*, 2023).

Taken together, cells have established powerful strategies to manipulate ubiquitin ligase activity and substrate specificity to meet their changing demands. This includes but is not limited to exploiting E2 binding, PTMs or ubiquitin ligase oligomerization.

1.2.3 Manipulation of ubiquitin ligases

Ubiquitin ligases are associated with numerous diseases (Cruz Walma *et al*, 2022; George *et al.*, 2018). With a deeper understanding of their structure-function relationship, their perception underwent a rapid transformation from disease-causing proteins to promising candidates for targeted protein degradation (Konstantinidou & Arkin, 2024; Tsai *et al*, 2024). To induce the degradation of target substrate proteins the UPS needs to be manipulated in such way that it recruits a target protein to an E3

enzyme. This is achieved by molecules that are called degraders. They can be classified into molecular glue degraders and proteolysis targeting chimeras (PROTACs) (Tsai *et al.*, 2024).

PROTACs consist of two binding sites, which are also called warheads. While one binds to the target protein, the other warhead, which is connected through a short linker, binds the respective ubiquitin ligase (Tsai *et al.*, 2024). So far, mainly CRLs with Cereblon (CRBN) or von Hippel-Lindau (VHL) receptor subunits haven been intensively studied, but recent developments also considered other RING domain-containing E3s such as Ubr1 (Jevtic *et al*, 2021). Being the major ubiquitin ligase of the N-degron pathway (see section 1.4), Ubr1 was recently hijacked to degrade the oncogenic kinase BCR-ABL in a xenograft mouse model by a PROTAC ligand that binds Ubr1 by mimicking its natural N-degron pathway substrates (see sections 1.4.1 and 1.4.3) (Zhang *et al*, 2023). Moreover, a Ubr1 *in silico* peptidometrics screen recently identified N-degron recruiters for a rational PROTAC design (Maria-Solano *et al*, 2024). However, modulators of Ubr1 and ubiquitin ligases in general need to be carefully evaluated in every case, as they are drawn away from their natural substrates, which could promote developmental and neurodegenerative disorders (Demir *et al*, 2022; Sukalo *et al*, 2014; Zenker *et al*, 2005).

In contrast to PROTACs, molecular glue degraders consist of monovalent small molecules that interact either with the target protein or ubiquitin ligase, thus promoting a ternary E3-glue-substrate neo-interface (Tsai *et al.*, 2024). Most molecular glue degraders were discovered either retrospectively and/or by serendipity, such as thalidomide and its derivatives, which are now being used as therapeutics in clinic (Mullard, 2021).

Despite their use in clinical applications, there are also a handful of endogenous molecular glue degraders that target neo-substrates for degradation in nature. Among them are viral peptides, which hijack host ubiquitin ligases for targeted degradation of host proteins. A prominent example is the human immunodeficiency virus protein Vif, which binds CRL5 to degrade A3 proteins that would otherwise repress viral invasion. It was only recently shown that the molecular glue that creates the Vif-A3 neo interface is RNA (Ito *et al*, 2023; Li *et al*, 2023). Apart from viruses, plants have also evolved natural molecular glue degraders to cope with fluctuating conditions. One example is the auxin phytohormone class that controls gene expression and plant development (Teale *et al*, 2006). Auxins such as indole-3-acetic

acid bind to the F-box containing E3 ligase SCF^{TIR1} (with TIR1 being the substrate receptor) to create a neo-complex that allows binding of auxin response proteins for their degradation (Tan *et al*, 2007).

Together, understanding the complex interplay between ubiquitin ligases and their substrates together with serendipitous discoveries in the past now enable the synthesis of rational molecular glue degraders and PROTACs for clinical applications. As such, some degraders, including those against androgen receptors to treat breast cancer, have already entered phase III in clinical trials (Tsai *et al.*, 2024).

1.3 The cellular role of the ubiquitin code

The interplay of writing, erasing, and deciphering the ubiquitin code determines the cellular fate of a substrate, which can be either non-proteolytic (section 1.3.1) or proteolytic (1.3.3).

1.3.1 Nonproteolytic functions

Substrate ubiquitination does not necessarily lead to degradation. Ubiquitin, the "hieroglyph" of the ubiquitin code, possesses seven lysine residues (K6, K11, K27, K29, K33, K48, K63) and an N-terminal methionine, which can function as anchoring points to build a ubiquitin chain (Haakonsen & Rape, 2019). Depending on the topology of such a ubiquitin chain, many ubiquitination events do not lead to proteasomal degradation but are crucial PTMs that control diverse cellular functions, including protein trafficking, DNA damage response or signaling events (Liao *et al*, 2022).

The linear ubiquitin chain assembly complex (LUBAC), for instance, regulates necroptosis through synthetizing linear M1-linked ubiquitin chains (Weinelt *et al*, 2024). Other chain linkages, such as via K27 or K63, are important for cell cycle progression (Shearer *et al*, 2022) or endocytic trafficking and DNA damage response, respectively (Erpapazoglou *et al*, 2014; Uckelmann & Sixma, 2017).

Substrate monoubiquitination is equally important to control cellular processes such as trafficking, transcriptional regulation, viral budding, endocytosis, or DNA repair mechanisms (Chen *et al*, 2022; Hicke & Dunn, 2003). For example, the Rad6/Rad18 E2/E3 pair monoubiquitinates the proliferating cell nuclear antigen to initiate DNA repair mechanisms (Hoege *et al*, 2002; Kannouche *et al*, 2004). Moreover, the oncoprotein Mdm2 multi-monoubiquitinates the transcription factor p53, when expressed at low levels, for nuclear export (Li *et al*, 2003). The DUB USP10 trims p53 ubiquitination and allows its re-import into the nucleus (Yuan *et al*, 2010).
In sum, the diverse spectrum of ubiquitin chain topologies enables a cell to respond to changing demands beyond the proteolytic destruction of proteins.

1.3.2 Emerging roles of a non-canonical ubiquitin code

A first crack in the ubiquitin code came from E3 LUBAC, which ubiquitinates its substrates via M1-linked linear ubiquitin chains (Kirisako *et al*, 2006). Until then, the central proposition was that only lysine residues were targets for ubiquitination. Recent expansion of ubiquitin chain linkage types showed that also serine or threonine residues can get ubiquitinated, as demonstrated for the neuron-associated ubiquitin ligase MYCBP2 (Pao *et al*, 2018). Apart from the ubiquitination of proteins, recent evidence suggests that ubiquitin ligases also ubiquitinate biomolecules such as bacterial lipopolysaccharides, saccharides, and ADP-Ribose (Kelsall *et al*, 2022; Otten *et al*, 2021; Zhu *et al*, 2022). Moreover, the yeast E3 Tul1, together with its cognate E2s Ubc4 and Ubc5, ubiquitinates phosphatidylethanolamine in endosomal and vacuolar membranes, which implies contributions to membrane dynamics and ESCRT recruitment (Sakamaki *et al*, 2022). Concomitant with the identification of new ubiquitination targets, ubiquitin itself can also be post-translationally modified. For instance, acetylation of ubiquitin lysine residues inhibits ubiquitin chain formation (Ohtake *et al*, 2015).
The recent findings of non-canonical substrate ubiquitination still await further dissection to identify their cellular roles, but they have already now considerably challenged the hypothesis of a canonical ubiquitin code.

1.3.3 Functions in protein quality control

Cells survive fluctuating environmental conditions by a diverse array of protein quality control (PQC) mechanisms. Members of the PQC machinery sense damaged proteins and degrade them, if refolding fails (Labbadia & Morimoto, 2015).

Chaperones are essential PQC components whose major task is to fold nascent peptide chains *de novo* or refold damaged proteins. This way they shield exposed hydrophobic amino acids from aqueous surroundings (Arhar *et al*, 2021). Major eukaryotic chaperones are the ATPases Hsp70 and Hsp90, the co-chaperone Hsp40 and nucleotide exchange factors (NEFs). The same chaperone complex that refolds damaged proteins can also initiate their degradation. The triage decision whether such proteins are refolded, degraded or sequestered is mainly driven by co-chaperones (Arhar *et al.*, 2021; Kim *et al*, 2013).

If refolding fails, irreversibly damaged proteins can be sequestered into subcellular deposits, which avoids an accumulation of toxic proteins inside the cell (Kaganovich *et al*, 2008). Aggregated, insoluble proteins are stored in insoluble protein deposits (IPODs), which reside close to the yeast vacuole. Large protein aggregates that accumulate during starvation are cleared through autophagic processes, which involves ubiquitin-like proteins such as Atg12 and Atg8 (Mizushima, 2024). Soluble but misfolded cytosolic proteins, on the other hand, are transported to Q-bodies for further degradation via the UPS or to an intranuclear quality control compartment (INQ) for temporary storage (Miller *et al*, 2015). The spatial sequestration of damaged proteins also depends on chaperones and on co-chaperones, which drive the overall selectivity (Sontag *et al*, 2017).

Many ubiquitin ligases do not bind misfolded proteins on their own but interact with chaperones to exploit their capability to recognize them. The recognition of misfolded proteins through chaperones might therefore shift E3 activity towards protein degradation, particularly during acute stress conditions. During activated cellular stress response pathways, including the unfolded protein response and heat shock response, more heat shock proteins are synthesized (Higuchi-Sanabria *et al*, 2018). This means that more E3s are likely to bind chaperones, such as the human E3 ligase CHIP which binds Hsp70 and Hsp90 (Balaji *et al*, 2022).

What does it take for a protein to be degraded by the proteasome? Essential for proteasomal degradation is the equipment of a substrate with at least four ubiquitin molecules that form a chain (Thrower *et al*, 2000). Despite having eight ubiquitin

acceptor sites (seven lysines and M1), K48-linked ubiquitin chains show the highest preference among homotypic chains for proteasomal recognition. As illustrated above, the 19S proteasomal subunit receptors Rpn10, Rpn1 and Rpn13 can all bind ubiquitin. However, degradation of homotypic K48-linked chains mainly depends on Rpn10, whereas Rpn1 and Rpn13 recognize multiple short chains (Martinez-Fonts *et al*, 2020). In contrast to homotypic chains, branched ubiquitin chains in particular give priority signals for proteasomal degradation due to a better signal amplification and efficient recognition by Rpn10, leading to faster degradation (Haakonsen & Rape, 2019; Meyer & Rape, 2014). The generation of mixed chains can involve multiple E3s, which coordinate the installment of distinct ubiquitin chains. For instance, the E3 Ufd4 first ubiquitinates its substrates via K29-linked chains, before the ubiquitin ligase Ufd2 elongates them in an “E4-like” manner via K48, which leads to proteasomal degradation (Liu *et al*, 2017).

Each cellular compartment has its own PQC machinery consisting of chaperones and ubiquitin ligases, which may have overlapping substrates depending on their localization in a cell. The main PQC pathway for damaged ER proteins is the ER-associated degradation (ERAD) pathway (Christianson & Carvalho, 2022). Key E3 ligases involved in this pathway are Doa10 and Hrd1, both of which are conserved from yeast to humans (Ruggiano *et al*, 2014). While Hrd1 mainly ubiquitinates ER luminal and membrane proteins, Doa10 preferentially targets cytosolic and ER membrane proteins with cytosolic domains, apart from the Rtn1-Pho8*-GFP model reporter substrate (see section 1.5) (Bays *et al*, 2001; Huyer *et al*, 2004; Ruggiano *et al.*, 2014; Szoradi *et al*, 2018). Doa10 recognizes substrates that are rich in hydrophobic stretches (Geffen *et al*, 2016; Wu *et al*, 2024) and ubiquitinates them with two different E2s via K11/K48 linkages for proteasomal degradation (Samant *et al*, 2018; Yau *et al*, 2017).

In the nucleus, where most proteasomes are located, the major ubiquitin ligase is San1 (Breckel & Hochstrasser, 2021; Wojcik & DeMartino, 2003). Despite possessing a well-folded RING domain, the protein is mainly intrinsically disordered (Rosenbaum *et al*, 2011). This accounts for its versatility in recognizing many misfolded proteins with local hydrophobic patches of five or more amino acids (Fredrickson *et al*, 2011; Ibarra *et al*, 2021). Interestingly, some nuclear ubiquitin ligases also ubiquitinate cytosolic proteins (Prasad *et al*, 2010). The degradation of cytosolic proteins in the nucleus requires the nucleocytoplasmic shuttling of

substrates, which is mediated by the Ssa1/2-Sis1-Sse1-Ydj1 chaperone system in yeast (Prasad *et al*, 2018). Such a chaperone-dependent substrate shuttling has been described for the ubiquitin ligase Ubr1, which localizes primarily to the nucleus, but possesses also a small cytosolic pool (Eisele & Wolf, 2008; Heck *et al*, 2010; Prasad *et al.*, 2018).

In the cytosol, substrate degradation is mainly orchestrated by five ubiquitin ligases. One such candidate, Rsp5, eliminates misfolded proteins during heat stress (Fang *et al*, 2014). Hul5, which shares a partial substrate overlap with Rsp5, ubiquitinates heat-damaged misfolded proteins but also stalled polypeptides at the ribosome (Fang *et al*, 2011; Sitron & Brandman, 2019). To ensure the rapid elimination of unwanted proteins and compensate for defects in any of the E3s, the E3s Doa10, Ubr1 and Ubr2 share an overlapping substrate spectrum by ubiquitinating misfolded proteins (Muller & Hoppe, 2024). In contrast to Ubr2, which exclusively eliminates misfolded proteins, Ubr1 also recognizes native proteins and those with exposed N-termini via the so-called N-degron pathway (see section 1.4) (Hochstrasser, 1996; Nillegoda *et al*, 2010; Varshavsky, 2019a).

1.4 The N-degron pathway

The term “degron” describes a degradation determinant in a protein that consists of the minimal sequence that is required to catalyze its degradation via the UPS (Varshavsky, 1991). Key features of PQC degrons may include exposed hydrophobicity upon protein damage, amino acid additions after translation errors, N-terminal modifications, or exposed destabilizing N- or C-termini after protease cleavage (Kampmeyer *et al*, 2022; Mashahreh *et al*, 2022; Muller & Hoppe, 2024). N- or C-terminal amino acids that are recognized as degrons via specialized cellular recognition pathways are called N- and C-degrons, respectively (Varshavsky, 2019b). All amino acids can serve as degradation determinants, depending on the cellular context and degradation pathway.

1.4.1 Arg/N-degron pathway

The conserved Arg/N-degron pathway degrades proteins with non-acetylated N-terminal residues that are exposed upon endoproteolytic cleavage or removal of the N-terminal methionine. The main ubiquitin Ligase of the N-degron pathway is Ubr1. It recognizes distinct classes of proteins with N-terminal degrons, which are called N-degron substrates (Varshavsky, 2019a). Those with a basic polar or bulky hydrophobic amino acid such as R/K/H/MΦ/W/L/F/Y/I (where MΦ represents a methionine followed by a bulky residue) are substrates with primary N-degrons. Those with D/E or N/Q N-termini possess secondary and tertiary N-degrons, respectively (Bachmair *et al*, 1986; Varshavsky, 2019b). While substrates with primary N-degrons bind Ubr1 directly via dedicated substrate binding sites (see section 1.4.3), those possessing secondary or tertiary N-degrons need to be further post-translationally modified (Figure 2). First, the N-terminal amidase Nta1 removes the amide group from tertiary N/Q N-degron substrates, yielding secondary N-degron substrates with D/E termini (Baker & Varshavsky, 1995). The R-transferase Ate1 further arginylates them, yielding primary N-degron substrates with an N-terminal arginine that Ubr1 recognizes (Balzi *et al*, 1990).

To efficiently ubiquitinate its substrates, Ubr1 forms a stable complex with the Ubc4/Ufd4 E2/E3 pair. While they do not show any inherent activity in the N-degron pathway on their own, they help Ubr1 to elongate ubiquitin chains on N-degron substrates, thus promoting proteasomal degradation (Hwang *et al*, 2010a). Apart from binding Ubc4/Ufd4, Ubr1 also interacts with Ate1 and the proteasome (Oh *et al*, 2020; Xie & Varshavsky, 2000). Thus, Ubr1 forms an enzymatic hub with Rad6, Ubc4, Ufd4 and Ate1. According to one hypothesis, this spatial orchestration of binding and substrate processing events may account for a proteasomal degradation of N-degrons without the need of a substrate to dissociate from the complex (Oh *et al.*, 2020).

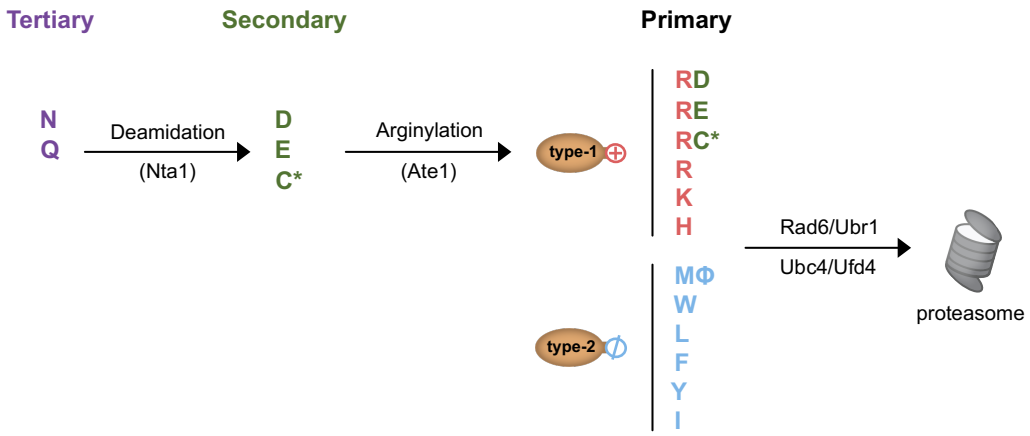

Figure 2. The eukaryotic Arg/N-degron pathway. "Tertiary", "secondary" and "primary" denote different classes of substrates with exposed N-terminal amino acid residues that are eliminated via the Arg/N-degron pathway (Varshavsky, 2019a). Tertiary N-degron substrates with N-terminal asparagine (N) or glutamine (Q) are deamidated by the N-terminal deamidase Nta1, yielding secondary N-degron substrates with N-terminal aspartate (D) or glutamate (E), respectively (Bachmair *et al.*, 1986; Baker & Varshavsky, 1995). The R-transferase Ate1 arginylates the secondary N-degron substrates, which results in primary N-degron substrates with an N-terminal arginine (R) (Balzi *et al.*, 1990). In mammals, Ate1 also arginylates oxidized cysteine (C*) (Hu *et al*, 2005). Primary N-degron substrates can be categorized into type-1 and type-2 N-degron substrates, depending on the properties of their N-terminal amino acid. Type-1 N-degron substrates possess a basic polar N-terminus such as an arginine (R), lysine (K) or histidine (H), whereas type-2 N-degron substrates have a bulky hydrophobic N-terminal residues such as a methionine followed by a bulky residue (MΦ), tryptophane (W), leucine (L), phenylalanine (F), tyrosine (Y) or isoleucine (I) (Varshavsky, 2019a). Primary N-degron substrates are recognized by the Rad6/Ubr1-Ubc4/Ufd4 E2/E3 pairs for proteasomal degradation (Hwang *et al.*, 2010a). The cartoon was conceptualized by (Hwang *et al.*, 2010a), created and further modified by me with permission from Springer Nature.

The Arg/N-degron pathway fulfills several physiological roles. For instance, it controls the degradation of cohesin, which is needed for proper chromosome segregation (Rao *et al*, 2001). Moreover, it also mediates the peptide uptake by regulating the transcriptional repressor Cup9 (Turner *et al*, 2000) (see section 1.4.3) and senses heme levels through Ate1, which is inhibited by hemin (Hu *et al*, 2008). In mammals, the Arg/N-degron pathway also acts as a detector of oxygen through the NO/O_2-dependent oxidation of N-terminal cysteine to cysteine-sulfonate, which gets arginylated by Ate1 (Hu *et al.*, 2005). Furthermore, it regulates apoptotic processes by eliminating C-terminal proapoptotic fragments that contain N-terminal degrons (Piatkov *et al*, 2012).

1.4.2 Other N- and C-degron pathways

Apart from the Arg/N-degron pathway, many other degradation pathways exist that exploit either N- or C-terminal degrons for recognition. Some of the pathways are briefly discussed below.

Roughly 60-80% of the yeast and mammalian proteins are N-terminally acetylated to increase protein longevity and complex stability by protecting them from degradation (Aksnes *et al*, 2016; Scott *et al*, 2011; Varland *et al*, 2023). Paradoxically, the Ac/N-degron pathway specifically degrades acetylated proteins (Hwang *et al*, 2010b). To achieve this, methionine aminopeptidases remove the initial methionine before N-terminal acetylates modify the exposed A/S/T/V/C N-degrons. The final degradation of acetylated proteins is mediated by Doa10 (Hwang *et al.*, 2010b).

In the Pro/N-degron pathway, proteins with a proline at position 1, 2 or 3 are degraded (Chen *et al*, 2017b; Shimshon *et al*, 2024). The major ubiquitin ligase in this pathway is the glucose-induced degradation-deficient (GID) complex, which eliminates enzymes that are involved gluconeogenesis such as the fructose-1,6-bisphosphatase (Chen *et al.*, 2017b). The GID complex forms a supramolecular assembly with substrate subunit receptors, which are exchanged depending on the substrate and cellular condition. For instance, the Gid4 receptor recognizes substrates involved in glucose recovery, whereas Gid10 binds substrates particularly during heat and osmotic stress and Gid11 in presence of other stressors (Chen *et al.*, 2017b; Chrustowicz *et al*, 2022; Sherpa *et al*, 2021).

In the Gly/N-degron pathway, the Cullin-RING ligase Cul2 ubiquitinates substrates bearing N-terminal glycines through its CRL receptors ZYG11B and ZER1 (Timms *et al*, 2019). Upon cleavage of the initiator methionine and exposure of an N-terminal glycine, the protein gets *N*-myristoylated for stabilization and to ensure a correct cellular location (Wright *et al*, 2010). Failure of *N*-myristoylation and the Gly/N-degron pathway to eliminate substrates can have deleterious effects on the innate immune response (Wang *et al*, 2021).

C-degron pathways exploit the distinct nature of an exposed C-terminal carboxy group after proteolytic cleavage to degrade a substrate. This is mainly but not exclusively mediated via CRLs such as Cul2, Cul4 or Cul5 with different receptor domains (Timms & Koren, 2020). Depending on the substrate receptor, the C-degron pathway degrades proteins bearing a C-terminal arginine or glycine. Interestingly,

ubiquitin and Nedd8 with their C-terminal Gly-Gly motif do not bind to CRL substrate receptors due to their low binding affinity (Lin *et al*, 2018; Scott *et al*, 2023).
Together, depending on the cellular condition and presence of substrates bearing N- or C-terminal degrons, various pathways exist to eliminate them via specialized ubiquitin ligases such as CRLs or Ubr1.

1.4.3 Mechanism and regulation of the N-degron ubiquitin ligase Ubr1

Ubr1 is the key ubiquitin ligase of the Arg/N-degron pathway and was the first E3 to be cloned using molecular biology techniques. Deletion of Ubr1 and its cognate E3 Ubr2 in mice is lethal at early embryonic stage and mutations in human Ubr1 are associated with severe developmental disorders (Demir *et al.*, 2022; Tasaki *et al*, 2005; Zenker *et al.*, 2005). This underlines why Ubr1 is both from a medicinal, historical and biochemical perspective an interesting candidate E3 to study (Bartel *et al*, 1990).
Despite being a RING E3 ubiquitin ligase of roughly 200 kDa, Ubr1 consists of only a single subunit that possesses a sailboat-shaped structure (Pan *et al.*, 2021). With its helical UB2R domain it binds the backside of its cognate E2 Rad6 to facilitate the closed conformation. The RING domain located in the head region interacts with Rad6 and ubiquitin to promote efficient ubiquitin transfer. In comparison with other ubiquitin ligases, the ubiquitin chain priming of Ubr1 is slightly faster than its chain building activity (Pan *et al.*, 2021).
In terms of conservation, yeast Ubr1 has both sequential and functional homologs with mammalian Ubr1 and Ubr2, which together regulate the mammalian Arg/N-degron pathway, including sensing heme and oxygen, controlling chromosome signaling and mediating apoptosis (Varshavsky, 2019b). To recognize N-degron substrates, yeast Ubr1 possesses two dedicated binding sites, the UBR-Boxes. Depending on the N-terminal degron, the UBR-Boxes allow a differentiation between basic polar and bulky hydrophobic destabilizing N-termini. Via the UBR-Box-1, Ubr1 recognizes basic polar N-termini such as R/K/H, which are called type-1 N-degron substrates. Via the UBR-Box-2, Ubr1 binds bulky hydrophobic N-termini such as W/L/F/Y/I, the so-called type-2 N-degron substrates (Sherpa *et al*, 2022; Varshavsky, 1996). The UBR-Boxes do not act individually but are intertwined. For instance,

occupancy of the UBR-Box-1 promotes the recognition and degradation of type-2 N-degron substrates via the UBR-Box-2 (Baker & Varshavsky, 1991). In contrast, the UBR-Box-2 does not affect type-1 N-degron substrate degradation (Szoradi *et al.*, 2018; Xia *et al*, 2008b).

Apart from N-degron substrates, Ubr1 also binds native proteins with internal degrons. Among such is the transcriptional repressor Cup9, which represses the synthesis of the peptide transporter Ptr2 and thus limits the cellular uptake of peptides (Turner *et al.*, 2000). Ubr1 only marginally ubiquitinates Cup9 under endogenous conditions. However, in presence of short peptides, Ubr1 ubiquitinates Cup9, lowers its cellular levels and promotes this way through stabilizing Ptr2 the uptake of more peptides. The effect of short peptides on Ubr1 activity towards Cup9 stems from allosteric effects. Short peptides with destabilizing N-termini can mimic N-degron substrates and bind to the UBR-Boxes. Instead of being ubiquitinated, they allosterically activate Ubr1 to promote Cup9 degradation. This is achieved through the release of the autoinhibitory UBLC domain of Ubr1, which prevents Cup9 binding under basal conditions (Du *et al*, 2002; Turner *et al.*, 2000). A similar mechanism has recently been described in hepatocyte-like cells for the regulation of Plin2 ubiquitination, which determines lipid droplet stability and is thus relevant for nonalcoholic fatty liver disease (Zhang *et al*, 2022). Concomitant to its role in regulating lipid droplet stability, recent findings underpin Ubr1's role in mediating fatty acid synthesis by targeting the fatty acid synthetase Fas2 for degradation in yeast (Jang *et al*, 2024).

Apart from Cup9, Ubr1 also recognizes the mitotic checkpoint kinase Chk1 and the alkyltransferase Mgt1 through internal degrons (Hwang *et al.*, 2010a; Hwang *et al*, 2009; Oh *et al*, 2017).

As a third substrate class, Ubr1 binds and ubiquitinates, supposedly through a distinct fourth binding site, damaged outer mitochondrial membrane proteins or misfolded cytosolic substrates (Eisele & Wolf, 2008; Heck *et al.*, 2010; Metzger *et al*, 2020).

1.5 The SHRED pathway

Ubr1 degrades misfolded cytosolic proteins preferentially via the UPS-dependent stress-induced homeostatically regulated protein degradation (SHRED) pathway (Figure 3; Szoradi *et al.*, 2018).

The uprise of misfolded proteins induces the expression of the intrinsically disordered protein Roq1 that comprises 104 amino acid residues. To become functionally active, the nuclear endopeptidase Ynm3 removes the first 21 amino acids, generating Roq1 (22-104). With its positively charged N-terminal arginine Roq1 (22-104) mimics a type-1 N-degron substrate and binds as such to the UBR-Box-1. Roq1 binding thoroughly alters Ubr1 activity and its preference for certain substrate classes: It impairs the elimination of type-1 N-degron substrates, stimulates the removal of type-2 N-degron substrates and favors the degradation of misfolded proteins.

Despite the complexity how Roq1 reprograms Ubr1, surprisingly little is known about the mechanism: How does Roq1 regulate Ubr1 on a biochemical and structural level? Which are the functionally relevant features of Roq1, and how is Roq1 degraded as soon as protein folding stress ceases?

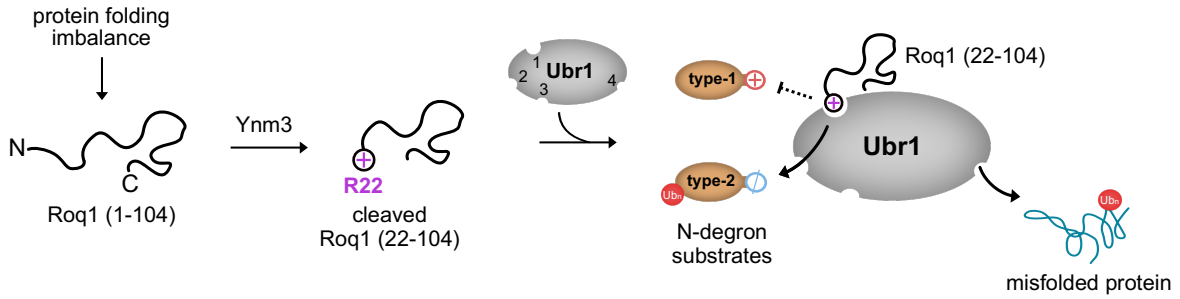

Figure 3. Schematic illustrating the stress-induced homeostatically regulated protein degradation (SHRED) pathway.
When yeast is exposed to protein folding imbalance, it induces the expression of the 104 amino acids-containing and intrinsically disordered protein Roq1. The nuclear endopeptidase Ynm3 removes the N-terminal 21 amino acid residues of Roq1, which results in a cleaved variant, Roq1 (22-104). It harbors a positively charged arginine (R22) as new N-terminus that binds to the UBR-Box-1 of the N-degron ubiquitin ligase Ubr1. Through binding Ubr1, Roq1 promotes the degradation of misfolded proteins, stabilizes type-1 N-degron substrates and enhances the degradation of type-2 N-degron substrates. Ubr1 has four sites for substrate binding: (1) type-1 N-degron substrates, (2) type-2 N-degron substrates, (3) substrates with internal degrons and (4) misfolded proteins. $(Ub)_n$ denotes a polyubiquitin chain for proteasomal degradation. Conceptualized by Sibylle Kanngießer, Sebastian Schuck and me. Adapted by me from (Peters *et al.*, 2024).

2. Aims of this thesis

Ubiquitin ligases maintain cellular homeostasis by promoting protein ubiquitination and degradation. Protein folding imbalance in yeast triggers the expression of the disordered protein Roq1, which binds the ubiquitin ligase Ubr1 as a substrate mimic. Roq1 binding regulates the elimination of N-degron substrates and enhances the degradation misfolded proteins, thus reprograming Ubr1. How Roq1 achieves Ubr1 reprograming on a mechanistic level is unknown. The goal of my PhD thesis was to unravel how Roq1 regulates Ubr1 activity and achieves substrate-specificity by *in vitro* reconstitution experiments. My specific aims were:

1. Dissect how Roq1 regulates Ubr1 via *in vitro* reconstitution experiments
2. Define the essential molecular features of Roq1 that are required to modulate Ubr1
3. Characterize the Roq1-Ubr1 complex and determine its structure

3. Results

3.1 *In vitro* reconstitution of SHRED

3.1.1 *Ubr1 ubiquitinates Roq1 in vitro*

To mechanistically investigate the SHRED machinery, I investigated how Roq1 regulates Ubr1 utilizing a defined *in vitro* system. Full length Roq1 undergoes Ynm3 cleavage *in vivo*, yielding SHRED-active Roq1 (22-104) (Szoradi *et al.*, 2018). To probe for Roq1 effects on Ubr1 activity, I purified Roq1 (22-104), the ubiquitin ligase Ubr1, ubiquitin, the ubiquitin-conjugating enzyme Rad6 (Figure S1) and mixed them with ATP and the ubiquitin-activating enzyme Ube1. Surprisingly, Ubr1 ubiquitinated Roq1 (22-104) in absence of any substrates (Figure 4, Pan *et al*, 2021), which is an undesired side reaction that interferes with my assay readout. Roq1 does not possess any lysine residues so that ubiquitination likely happens on serine, threonine or cysteine residues (Kelsall, 2022). Ubiquitinated Roq1 was resistant to dithiothreitol in sample buffer but sensitive to alkaline hydrolysis in my assays, indicating the formation of oxyester rather than thioester or amide bonds (Figure 4). To eliminate the unwanted Roq1 ubiquitination and solely concentrate on Ubr1 activity towards authentic substrates, Rafael Salazar designed, and I purified a C-terminally truncated Roq1 variant, Roq1 (22-60). Roq1 (22-60) is SHRED-active *in vivo* (shown by Rafael Salazar) and Ubr1 barely ubiquitinates it in my experiments (Figure 4). Hence, I utilized Roq1 (22-60) for *in vitro* ubiquitination assays and Roq1 (22-104) for binding experiments, unless stated otherwise.

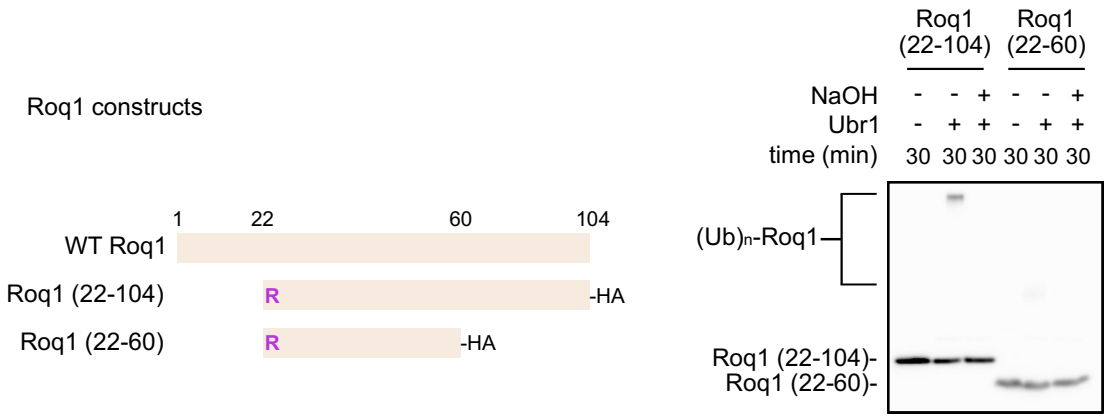

Figure 4. Ubr1 ubiquitinates Roq1 (22-104) *in vitro*.
Left: Cartoon overview of Roq1 constructs used for the *in vitro* reconstitution of SHRED. Roq1 (22-104) mimics the proteolytically cleaved and SHRED-active Roq1 variant with an N-terminal arginine (highlighted in purple) but possesses an additional C-terminal, lysine-free HA tag for visualization of ubiquitination via immunoblotting. The Roq1 (22-60) variant was designed in a similar manner as Roq1 (22-104) with N-terminal R22 and a C-terminal HA tag but lacks amino acid residues 61-104. Wild type (WT) Roq1 is shown for better visualization.
Right: HA tag immunoblot from ubiquitination assays with Roq1 (22-104)-HA or Roq1 (22-60)-HA without Ubr1 substrates. To monitor Roq1 ubiquitination, the Roq1 variants were mixed with the ubiquitin-activating enzyme Ube1, the ubiquitin-conjugating enzyme Rad6, the ubiquitin ligase Ubr1, ubiquitin and ATP. Ubiquitination reactions were performed at 30°C for 30 minutes before termination with dithiothreitol-containing sample buffer. NaOH was added to break oxyester bonds formed between ubiquitin and Roq1. Ubr1 builds NaOH-sensitive ubiquitin chains on Roq1 (22-104) but only marginally ubiquitinates Roq1 (22-60). The experiment was designed and performed by me and the right figure was adapted from (Peters *et al.*, 2024).

3.1.2 *Roq1 promotes the ubiquitination of folding-deficient Ubr1 substrates*

Utilizing the established ubiquitination assay and Roq1 (22-60), I tested Ubr1 activity and the effect of Roq1 on the ubiquitination of various Ubr1 substrates. As a first substrate class, I focused on misfolded proteins. Ubr1 binds and ubiquitinates misfolded proteins with cytosolic domains (Eisele & Wolf, 2008; Heck *et al.*, 2010; Szoradi *et al.*, 2018). A model substrate to study protein misfolding is Pho8*, a derivative of yeast alkaline phosphatase carrying mutations that make it prone for misfolding (Szoradi *et al.*, 2018). Pho8* gets eliminated by Ubr1 *in vivo* and Roq1 accelerates the degradation (Szoradi *et al*, 2018). To study Pho8* ubiquitination and effects of Roq1 *in vitro*, I purified misfolded Pho8* and folded Pho8 (Figure S2) and tested their capability for getting ubiquitinated. Ubr1 ubiquitinates Pho8* on its own,

and Roq1 further promotes the ubiquitination. In contrast, Ubr1 barely ubiquitinates native Pho8 in absence or presence of Roq1 (Figures 5A+B). Next, I employed Firefly Luciferase as a model substrate, of which an unstable variant gets degraded via SHRED in yeast (Szoradi *et al*, 2018). Ubr1 efficiently ubiquitinated unfolded Firefly Luciferase, Luciferase^{U}, in my experiments. Addition of Roq1 further enhanced the ubiquitination. Native Firefly Luciferase, Luciferase^{N}, barely showed ubiquitination in absence or presence of Roq1 (Figures 5C+D). Taken together, Roq1 promotes through Ubr1 the ubiquitination of misfolded proteins but not their native counterparts.

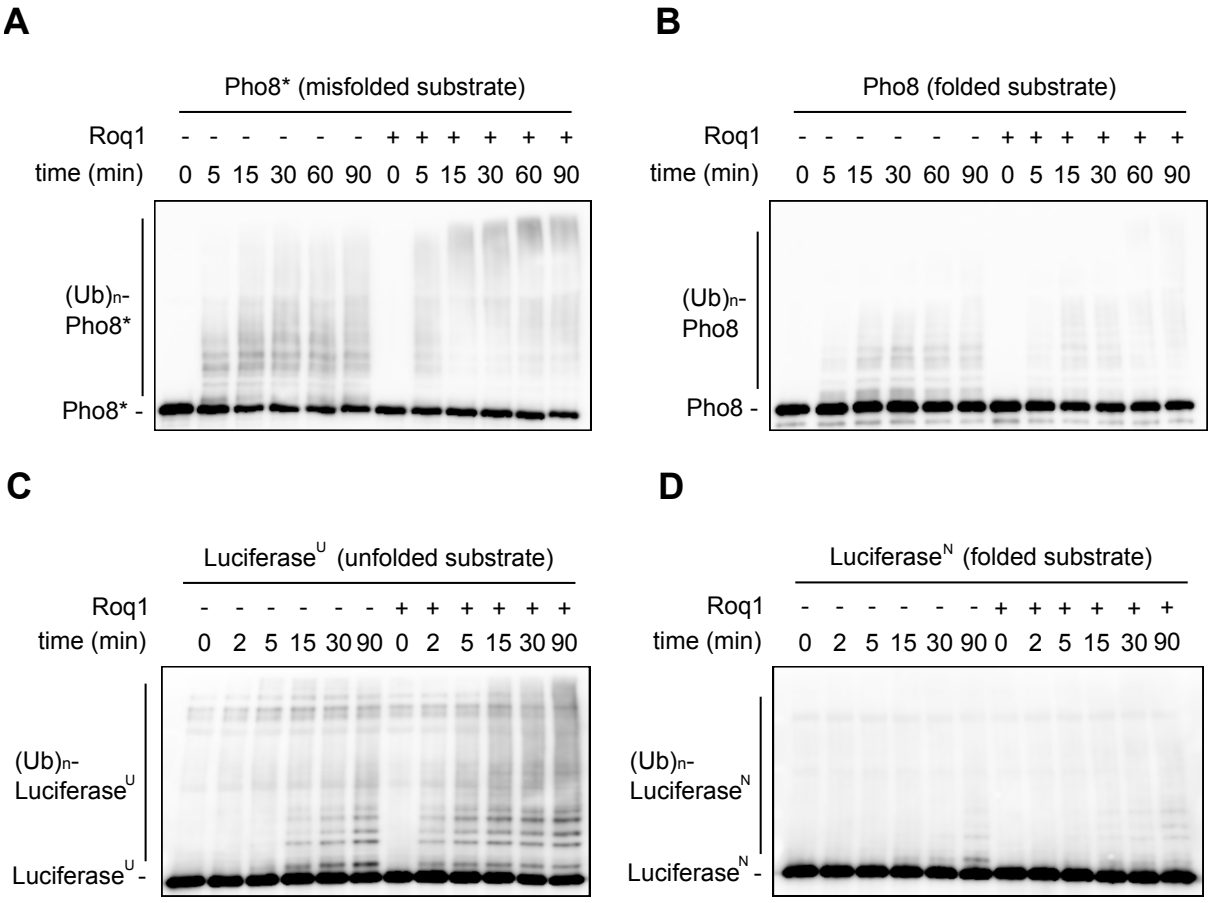

Figure 5. Roq1 promotes the ubiquitination of misfolded and unfolded substrates.
(A), (B) Pho8 immunoblot from Pho8* or Pho8 ubiquitination assays in presence or absence of Roq1 (22-60)-HA. Ubiquitination of misfolded Pho8* or folded Pho8 was monitored at 30°C over 0, 5, 15, 30, 60 or 90 minutes. Roq1 (22-60)-HA was added at 10-fold molar excess over Ubr1 where indicated. Experiments were initially performed by Sibylle Kanngießer, published in (Peters *et al.*, 2024) and replicated by me. The replicated experiments are depicted here.
(C), (D) Luciferase immunoblot from luciferase ubiquitination assays. Ubiquitination of unfolded (Luciferase^{U}) or folded luciferase (Luciferase^{N}) was monitored at 30°C over 0, 2, 5, 15, 30 or 90 minutes. Note that, instead of Roq1 (22-60)-HA, Roq1 (22-104) was added at 10-fold molar excess

over Ubr1 where indicated. This experiment was designed and performed by me. An experiment with Roq1 (22-60)-HA showed similar effects but was designed and performed by Sibylle Kanngießer.

3.1.3 Reconstituting Ubr1 regulation by Roq1 *in vitro*

To test the robustness of the ubiquitination assay, I performed various control experiments using Pho8* or Luciferase^{U} as model substrates. First, I compared Roq1 (22-104) and Roq1 (22-60) for their efficiency in promoting Pho8* ubiquitination. While Roq1 (22-60) strongly promoted Pho8* ubiquitination, Roq1 (22-104) was less efficient (Figure 6A). This can be attributed to Roq1 (22-104) being ubiquitinated by Ubr1, which drives Ubr1 molecules away from Pho8*. Since Ubr1 ubiquitinates lysine-free Roq1 (22-104) via serine or threonine residues, I tested whether Ubr1 creates amide or oxyester linkages between ubiquitin and Pho8*. Ubiquitinated Pho8* was resistant to alkaline hydrolysis and dithiothreitol, suggesting the formation of amide bonds between substrate lysine residues and ubiquitin (Figure 6B). To evaluate the efficiency of Roq1 (22-60) in promoting Pho8* ubiquitination, I titrated Roq1 (22-60) into ubiquitination reactions. Roq1 (22-60) promoted Pho8* ubiquitination already at equimolar Ubr1 concentrations, suggesting a tight interaction with Ubr1 (Figure 6C). Increasing the concentration resulted in further decrease of nonubiquitinated Pho8*. I therefore employed a 10-fold molar excess of Roq1 (22-60) in all ubiquitination assays unless stated otherwise. Roq1 alone was not sufficient to promote Pho8* ubiquitination in absence of Ubr1, as shown by Sibylle Kanngießer. The ubiquitination reactions do not go to full completion, with nonubiquitinated Pho8* or Luciferase^{U} remaining. A potential explanation could be their aggregation over the course of the assay. To test this hypothesis, I performed fractionation experiments with Pho8* or Luciferase^{U} before and after ubiquitination assays and separated soluble from insoluble proteins (Figures 6D+E). Both Pho8* and Luciferase^{U} remained soluble during the assay, indicating that either another factor becomes limiting in my experiments or that protein aggregates remain soluble but inaccessible to Ubr1.

Taken together, the control experiments identified the minimal requirements needed to robustly assay Roq1 efficacy in promoting Ubr1 model substrate ubiquitination.

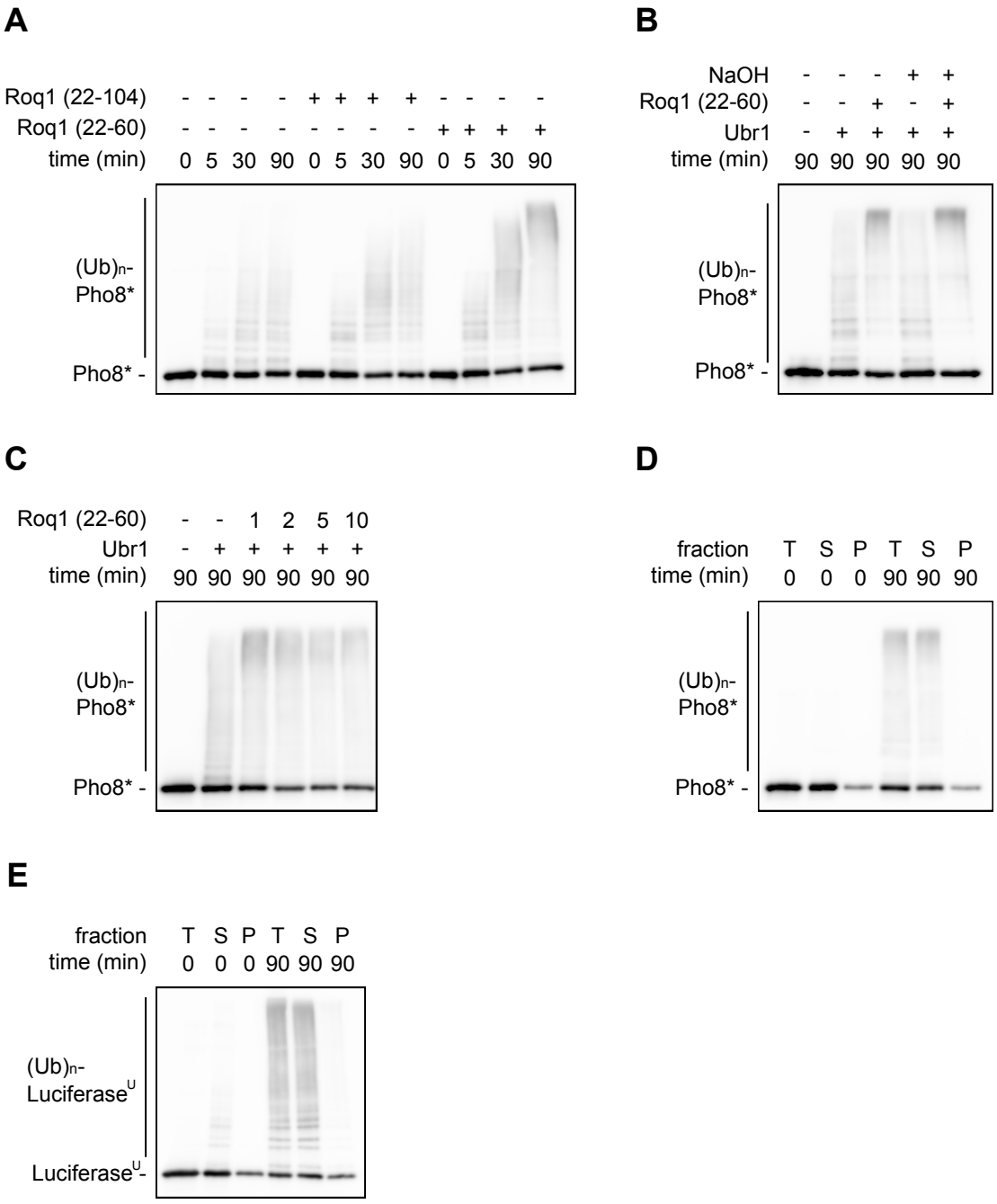

Figure 6. *In vitro* reconstitution of SHRED.
(A) Pho8 immunoblot from Pho8* ubiquitination assay in presence or absence of Roq1 (22-104)-HA or Roq1 (22-60)-HA. Pho8* ubiquitination was monitored at 30°C over 0, 5, 30 or 90 minutes. Roq1 (22-104)-HA or Roq1 (22-60)-HA were added at 10-fold excess over Ubr1 where indicated. The experiment was designed and performed by me. The figure is adapted from (Peters *et al.*, 2024).
(B) Pho8 immunoblot from Pho8* ubiquitination assays in presence or absence of Roq1 (22-60)-HA. The ubiquitination reactions were performed at 30°C for 90 minutes prior termination with dithiothreitol-containing sample buffer. NaOH was added to hydrolyze any oxyester bonds formed between ubiquitin and Pho8*. The Pho8* ubiquitination products were NaOH resistant, confirming they consist of amide rather than oxyester bonds between Pho8* lysines and ubiquitin. Addition of Roq1 (22-60)-HA had no further effect on NaOH resistance. The experiment was designed and performed by me. The figure is adapted from (Peters *et al.*, 2024).

(C) Pho8 immunoblot from Pho8* ubiquitination assays with increasing amounts of Roq1 (22-60)-HA. Pho8* ubiquitination reactions were performed at 30°C for 90 minutes in presence or absence of 1, 2, 5 or 10-fold molar excess of Roq1 over Ubr1. Note that with increasing Roq1 concentration the amount of non-ubiquitinated Pho8* becomes less, indicating efficient Pho8* ubiquitination at higher concentrations of Roq1. Thus, I used as default assay conditions a 10-fold molar excess of Roq1 over Ubr1 unless stated otherwise. The experiment was designed and performed by me. The figure is adapted from (Peters *et al.*, 2024).
(D) Pho8 immunoblot from Pho8* fractionation assays. Pho8* ubiquitination reactions were set up with Roq1 (22-60)-HA and incubated at 30°C for 0 or 90 minutes. Soluble Pho8* was separated from insoluble Pho8* via a high-speed centrifugation step. T = total, S = soluble, P = pellet. The experiment was designed and performed by me. The figure is adapted from (Peters *et al.*, 2024).
(E) As in panel (D), but with unfolded Luciferase (Luciferase^{U}).

3.1.4 *Roq1 enhances the ubiquitination of substrates with internal degrons*

As a second class of substrates, I analyzed together with Sibylle Kanngießer native Ubr1 substrates containing internal degrons. Among those were the transcriptional repressor Cup9 (Du *et al.*, 2002; Turner *et al.*, 2000), the O^6-alkylguanine-DNA alkyltransferase Mgt1 (Hwang *et al.*, 2009) and the mitotic checkpoint kinase Chk1 (Oh *et al.*, 2017). First, I purified them (Figure S. 3) and tested subsequently with Sibylle Kanngießer the effect of Roq1 on their Ubr1-mediated ubiquitination. Roq1 (22-60) accelerated and enhanced the ubiquitination of all three substrates (Figure 7).

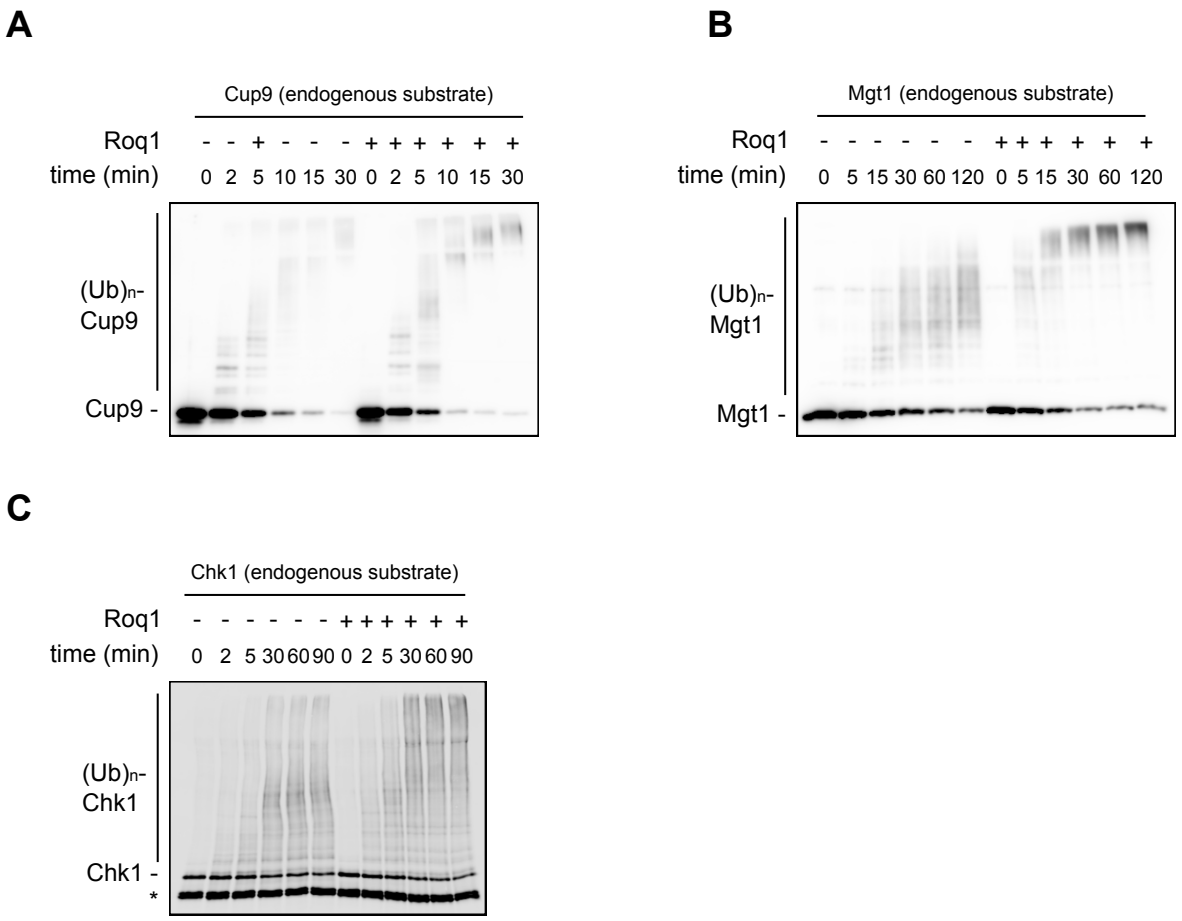

Figure 7. Roq1 promotes the ubiquitination of endogenous Ubr1 substrates with internal degrons.
(A) Strep tag immunoblot from Cup9-Strep ubiquitination assays. Ubiquitination of Cup9 was monitored at 30°C over 0, 2, 5, 10, 15 or 30 minutes in absence or presence of Roq1 (22-60)-HA. The experiment was initially designed and conducted by Sibylle Kanngießer. The replicate shown in this figure was performed by me.
(B) Maltose-binding protein (MBP) tag immunoblot from Mgt1-MBP ubiquitination assays. Ubiquitination of Mgt1 was monitored at 30°C over 0, 5, 15, 30, 60 or 120 minutes in absence or presence of Roq1 (22-60)-HA. The experiment was designed and performed by me. The figure is adapted from (Peters *et al.*, 2024).
(C) ALFA tag immunoblot from Chk1-ALFA-FLAG ubiquitination assays. Ubiquitination of Chk1 was monitored at 30°C over 0, 2, 5, 30, 60 or 90 minutes in absence or presence of Roq1 (22-60)-HA. The asterisk indicates an inactive N-terminal cleavage product of Chk1 that appeared during protein expression or purification. The experiment was designed and performed by me. The figure is adapted from (Peters *et al.*, 2024).

3.1.5 *Roq1 governs the ubiquitination of N-degron substrates*

As a third substrate category, I tested the impact of Roq1 on Ubr1 substrates possessing N-terminal degrons. Ubr1 mediates as the major ubiquitin ligase the

turnover of type-1 and type-2 N-degron substrates in the N-degron pathway (Varshavsky, 2019a). Cleaved Roq1 binds to the UBR-Box-1, thereby inhibiting the degradation of type-1 N-degron substrates with basic polar N-termini (Szoradi *et al*, 2018). I purified R-GFP (Figure S4A), a model type-1 N-degron substrate, and tested the effect of Roq1 on its Ubr1-mediated ubiquitination. Roq1 (22-60) inhibited R-GFP ubiquitination, as expected (Figure 8A).

Binding of type-1 N-degron substrates encourages the degradation of type-2 N-degron substrates (Baker & Varshavsky, 1991). Ynm3-cleaved Roq1, through binding to the UBR-Box-1, stimulates type-2 N-degron substrate elimination in yeast (Szoradi *et al*, 2018). To test this *in vitro*, I purified F-GFP as model type-2 N-degron substrate (Figure S4B). Accordingly, Roq1 (22-60) promoted through Ubr1 the ubiquitination of F-GFP (Figure 8B). Simultaneous addition of two substrates such as Pho8* and F-GFP had no further effect on their individual ubiquitination (data not shown).

Taken together, Roq1 enhances the ubiquitination of misfolded or unfolded substrates, improves the ubiquitination efficiency of substrates containing internal degrons, encourages the ubiquitination of type-2 N-degron substrates and inhibits type-1 N-degron substate ubiquitination. Thus, Roq1 comprehensively reprograms Ubr1.

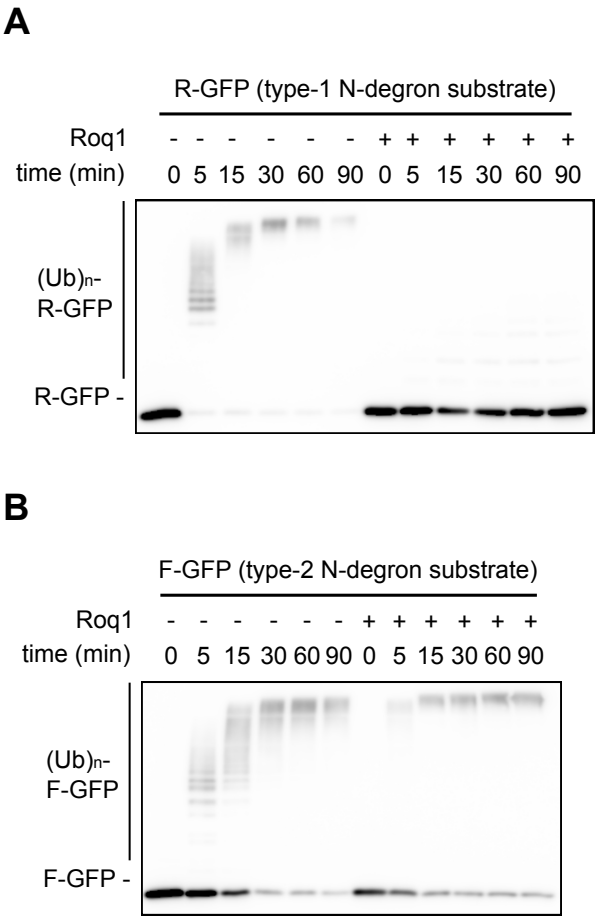

Figure 8. Roq1 governs the ubiquitination of Ubr1 N-degron substrates.
(A) GFP immunoblot from R-GFP ubiquitination assays. Ubiquitination of the model type-1 N-degron substrate R-GFP was monitored at 30°C over 0, 5, 15, 30, 60 or 90 minutes in absence or presence of Roq1 (22-60)-HA. The experiment was designed and performed by me. The figure is adapted from (Peters *et al.*, 2024).
(B) As in panel (A), but with F-GFP as model type-2 N-degron substrate.

3.2 Roq1 harbors a functionally important hydrophobic motif

3.2.1 *Ubr1 regulation by Roq1 requires R22 and an additional feature*

What is the functionally relevant architecture of Roq1 to reprogram Ubr1? Binding of cleaved Roq1 to the UBR-Box-1 requires R22 *in vivo* (Szoradi *et al*, 2018). Consistently, a binding-deficient Roq1 variant, Roq1 (22-60) (R22A), did not enhance Pho8* ubiquitination in my *in vitro* assays (Figure 9A). Since occupancy of the UBR-Box-1 by Roq1 or any other type-1 N-degron substrate allosterically facilitates the

degradation of type-2 N-degron substrates *in vivo* (Baker & Varshavsky, 1991), one explanation could be that occupancy of the UBR-Box-1 also regulates the recognition of misfolded proteins. To test this hypothesis, I made use of synthesized Arg-Ala (RA) and Leu-Ala (LA) dipeptides mimicking type-1 and type-2 N-degron substrates, respectively (Baker & Varshavsky, 1991). As expected, while the LA dipeptide abolished F-GFP ubiquitination, the RA dipeptide stimulated it (Figure 9B). Next, I tested the effect of the RA dipeptide on Pho8* ubiquitination. While Roq1 enhanced Pho8* ubiquitination as expected, the RA dipeptide had no effect (Figure 9C). Of note, simultaneous addition of the RA dipeptide and Roq1 (22-60) (R22A), as shown by Sibylle Kanngießer, did not stimulate Pho8* ubiquitination. Thus, occupancy of the UBR-Box-1 does not drive Ubr1 activity towards misfolded proteins but might be a pre-requisite, assuming there is at least one other element in Roq1 that is essential to reprogram Ubr1. This hypothesis is further supported by biolayer interferometry (BLI) experiments Sibylle Kanngießer performed between Ubr1 and immobilized Roq1 (22-104) (R22A). While showing no activity *in vivo* or *in vitro*, Roq1 (22-104) (R22A) still bound Ubr1 to some extent *in vitro*. Concomitantly, further increasing the concentration of Roq1 (22-60) (R22A) in my Pho8* ubiquitination assays resulted in partial regain of Ubr1 activity (Figure 9D, compare lanes with 10-fold and 40-fold molar excess of Roq1 (22-60) (R22A)). Thus, Roq1 harbors beyond R22 at least one other functional element that is required to accelerate the ubiquitination of misfolded substrates through Ubr1.

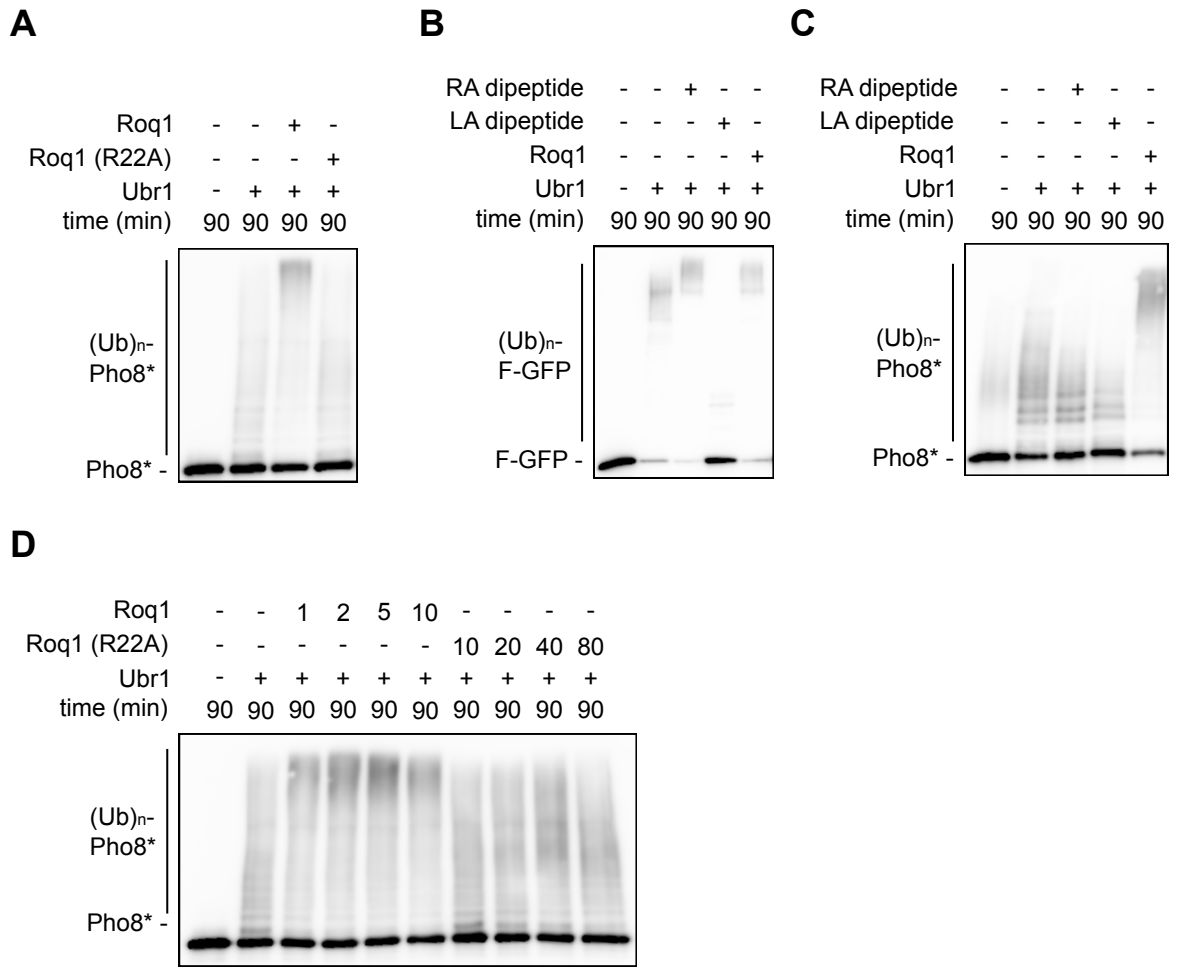

Figure 9. Ubr1 regulation by Roq1 requires R22 and an additional feature.
(A) Pho8 immunoblot from Pho8* ubiquitination assays in presence of Roq1 (22-60)-HA or Roq1 (22-60) (R22A)-HA. Roq1 variants were added at 10-fold molar excess over Ubr1. Ubiquitination reactions were incubated at 30°C for 90 minutes. The experiment was designed and performed by me. The figure is adapted from (Peters *et al.*, 2024).
(B) GFP immunoblot from F-GFP ubiquitination assays in presence of Roq1 (22-60)-HA, Arg-Ala (RA) or Leu-Ala (LA) dipeptides. The RA and LA dipeptides mimic type-1 and 2 N-degron substrates, respectively. Dipeptides were added at 4000-fold excess over Ubr1. Molar Roq1 (22-60)-HA: Ubr1 ratio was 10:1. Ubiquitination reactions were performed at 30°C for 90 minutes. Conceptualization and performance of the experiment was done by me.
(C) As in panel (B), but with Pho8* as Ubr1 substrate.
(D) Pho8 immunoblot from Pho8* ubiquitination assays using Roq1 (22-60)-HA or Roq1 (22-60) (R22A)-HA. Roq1 (22-60)-HA was added at 1, 2, 5 or 10-fold molar excess over Ubr1 where indicated. Roq1 (22-60) (R22A)-HA : Ubr1 ratio was 10, 20, 40 or 80:1. Ubiquitination reactions were incubated at 30°C for 90 minutes. Note that at a 40-fold excess Roq1 (22-60) (R22A)-HA stimulates Pho8* ubiquitination. The experiment was designed and performed by me. The figure is adapted from (Peters *et al.*, 2024).

Ubr1 also recognizes substrates with internal degrons. Whether the effect of Roq1 on enhanced Cup9, Mgt1 and Chk1 ubiquitination (Figure 7) is exclusively mediated

through R22 binding to the UBR-Box-1 of Ubr1 is not clear. To test this hypothesis, I performed Cup9, Mgt1 and Chk1 ubiquitination assays with Roq1, RA or LA dipeptides (Figure 10). While Roq1 enhanced the ubiquitination of all three substrates, the RA and LA dipeptides stimulated only Cup9 ubiquitination (Figure 10A). Concomitantly, dipeptide addition has been previously shown to regulate Cup9 ubiquitination through allosteric mechanisms (Du *et al.*, 2002; Hwang *et al.*, 2010a). Roq1 promotes Cup9 ubiquitination through its N-terminal R22 that binds to the UBR-box-1. In contrast, Roq1 regulates Mgt1 and Chk1 ubiquitination through at least one other determinant.

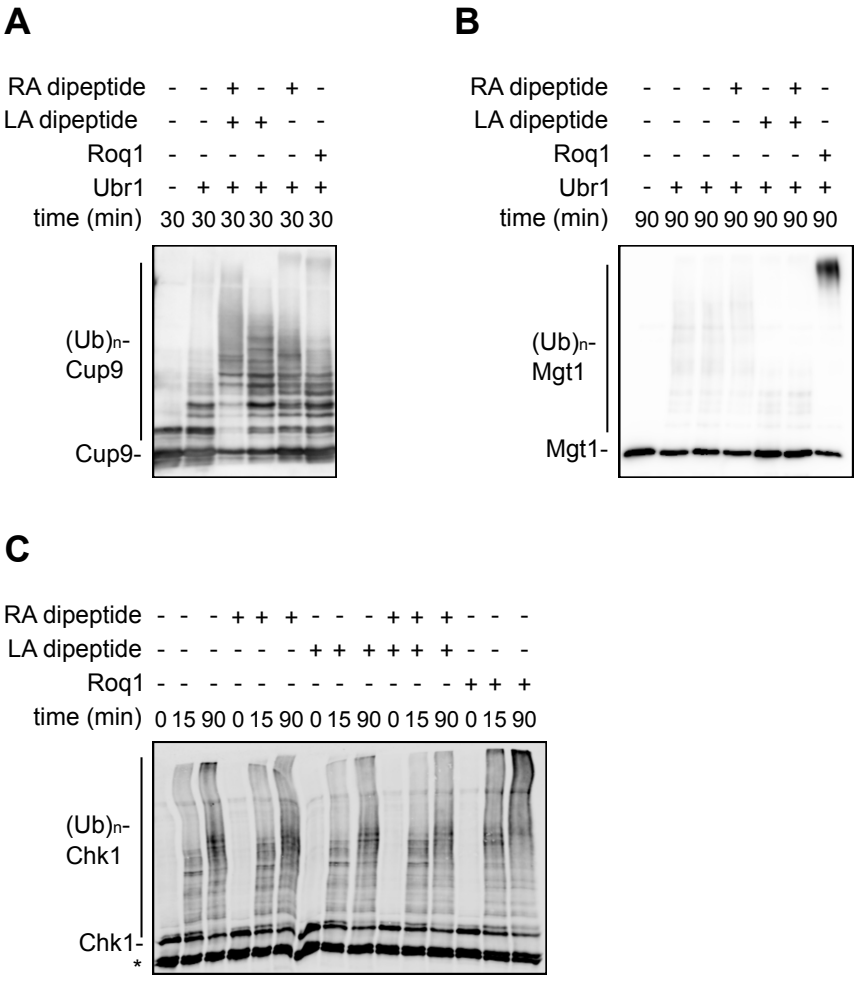

Figure 10. Roq1 stimulates the ubiquitination of some but not all Ubr1 substrates with internal degrons through R22.

(A) Strep tag immunoblot from Cup9-Strep ubiquitination assays. The following assay parameters were adjusted for better visualization of dipeptide and Roq1-dependent effects on Cup9 ubiquitination: RA or LA dipeptide:Ubr1 molar ratio was 400:1, Roq1 (22-104):Ubr1 ratio was 40:1 and Cup9-Strep concentration was 5 μM. Ubiquitination reactions were incubated at 30°C for 30 minutes. The experiment was conceptualized and performed by me.

(B) MBP tag immunoblot from Mgt1-MBP ubiquitination assays. RA and LA dipeptides were added at 4000-fold molar excess over Roq1. The Roq1 (22-60)-HA:Ubr1 molar ratio was 10:1. Ubiquitination reactions were incubated at 30°C for 90 minutes. Note that the LA dipeptide marginally inhibited Mgt1 ubiquitination while the RA dipeptide had no effect. This experiment was conceptualized and performed by me.
(C) ALFA tag immunoblot from Chk1-ALFA-FLAG ubiquitination assays. RA/LA:Ubr1 molar ratio was 4000:1 and Roq1 (22-60)-HA:Ubr1 molar ratio was 10:1. Ubiquitination reactions were incubated at 30°C for 0, 15 or 90 minutes. The asterisk (*) denotes a degradation product from protein expression or purification. This experiment was conceptualized and performed by me.

3.2.2 *Roq1 encompasses a hydrophobic motif that associates with Ubr1*

Which other Roq1 determinant beyond R22 is required for Ubr1 reprograming? Roq1 is predicted to be almost completely disordered, with having no defined tertiary structure elements (Figure 11A). Yet, residues 53-60 show less disorder tendency in predictions initially run by Sebastian Schuck and re-run by me (Figure 11B). Multiple sequence alignments initially run by Sebastian Schuck and subsequently replicated by me using Roq1 and closely related fungi species reveal two conserved regions within Roq1: The Ynm3 proteolytic cleavage site (residues 20-25) and a hydrophobic stretch in the center covering residues 53-60 (Figure 11C). To identify in an unbiased manner whether Roq1 harbors functionally relevant elements beyond R22, Sebastian Schuck, Oliver Pajonk and Sibylle Kanngießer conceptualized and performed a genetic screen. In brief, they generated error-prone Roq1 (22-104) PCR products, incorporated them into a yeast strain that lacks Roq1 but harbors a reporter substrate, and monitored SHRED activity. Strikingly, SHRED-inactive Roq1 variants harbored polar mutations within a hydrophobic region of Roq1 spanning residues 55-58. Further hit validation by Oliver Pajonk and Sibylle Kanngießer defined the Y55-Y56-F57-V58 region as crucial for Roq1 activity *in vivo* (Figure 11D). Thus, we refer to the Roq1 YYFV sequence as the hydrophobic motif (Peters *et al.*, 2024). Altogether, the hydrophobic motif of Roq1 defines a second determinant that is required for regulating Ubr1 activity *in vivo*.

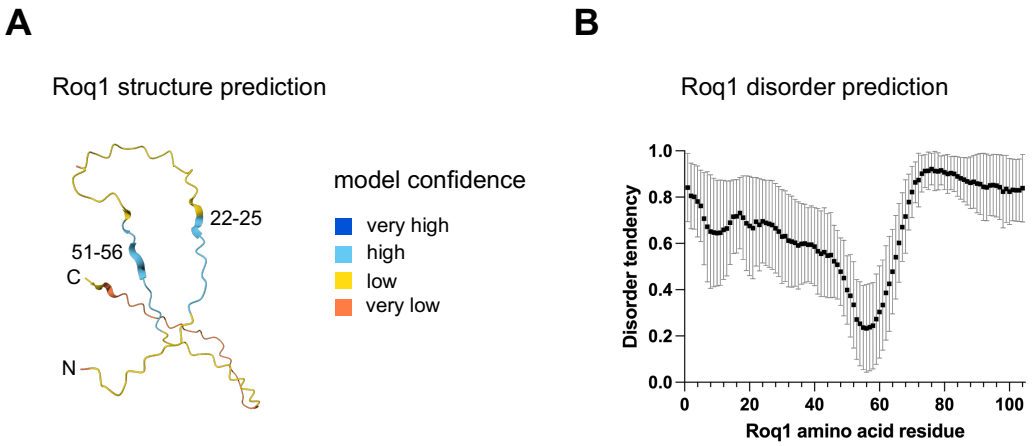

C

Multiple sequence alignment of Roq1 homologs from different yeast species

```
                    1                   22
S. cerevisiae       MLRRETSTIYRTHKK----SNSSILRSQRDQTRVDSLVE--------------ESPMGDFGINNQPTQ
S. eubayanus        MLRKSTSTIYTTHKK----SNSSILRSRKDQTKVDPLVE--------------EYPMGEFGTTNQPAQ
S. uvarum           MLRKSTSTIYTAHKK----SNCSILRSRKEQTKVDSLVE--------------EYPMGDFGTHNQLVQ
S. boulardii        MLRRETSTIYRTHKK----SNSSILRSQRDQTRVDSLVE--------------ESPMGDFGINNQPTQ
S. paradoxus        MLRKGTSTIYRTHKK----TNSSILRSQRDQTKVDSLVE--------------ESPMGDFGIHNQPTQ
S. mikatae          MLRKGTSTIYTAHKK----SNSSILRSQRDQTKVESLVE--------------ESPIGDFGIHNQPTQ
S. kudriavzevii     MLRKGTSTIYKTHKK----SNSSILRSQRDQTRMDSLVE--------------ESPMGDFGVHNQPTQ
S. arboricola       MLRKGTSTIYTAHKK----SNGSILRSQRDQSKADLLVE--------------ESPMGDFGVSDQPPQ
K. barnettii        MLRRDTANIHNNHTR----TKHTILRSKRVIPQYSDTLC-EESPDAQ------EYRFGDFSVLNHRNH
K. saulgeensis      MLRRDTASIHNNHTR----TKHTIFRSKRVIPQYSDTLCGDVAPDAQ------EYRFGDFSVLNHTNH
K. bulderi          MLRRDTATIRNNHAR----TKHSIFRSKRVIPQYNETICDGGLQDTE------EQRFGDFSVLNHNNH
K. naganishii       MLRRNTTHIFNNSKR----VPHRVLRSRKSVPQYSDSINLGLGNEYQQE----EARFGNFSVLNENTH
K. unispora         MLRTSTSSILQSRKNNRNHTNHTILRSRRNIPQYQDTLINEVN---NMNGYTEENRYGDFNVLNESNH
K. heterogenica     MLRTTTSQAYQKRK-----TNQTILRSRRKIPQYSDTLNNSLYGYTDDNNNNSNNRYGNFNVLNETNH
                    *** *:               ::**::  .: .  :             :   *:*.  :.  :

                      53     60
S. cerevisiae       PGVIYYFVELTNLGIQENTSSNNNNNNN----------HGDDENGSRYGHGSSLGGDVHSRRCS--
S. eubayanus        PSVIYYFVELTNAGIQENTSSNNNNNNNNNNN------HDGGESGARYGHGSSLGGNVHLRRYS--
S. uvarum           PSVIYYFVELTNAGIQENTSSNNNNNNNNNN--------RNGGDGGTRYGHGDSLSGNVHSHRYS--
S. boulardii        PGVIYYFVELTNLGIQENTSSNNNNNNN----------HGDDENGSRYGHGSSLGGDVHSRRCS--
S. paradoxus        PGVIYYFVELTNLGIQENTSSNNNNNNN----------HSDDENGGRYGHGSSLGGDVHSHRCSST
S. mikatae          PGVIYYFVELTNLGIHDNTSSNNNNNNNN----------HSDDENGSRYGQGSSLGRNVHSRRYS--
S. kudriavzevii     PGVIYYFVELTNLGIQENSSSNNNNNNNNNNNNNGENSNNENDENGTRYGHGSSSGGNVHSRRYS--
S. arboricola       PGVIYYFVELNNLGIQENTSSNNNNNNNNDN--------HNDNENGTRYGHGDSLGGSVHSHRYS--
K. barnettii        PGVVYYFIELTDPNGNPISGRSGNNTSNNNNS-------INNSSNTHRI----------------
K. saulgeensis      PGVVYYFIELTDPNGNPISSRSGNNNNDNNN-------------NTHRI----------------
K. bulderi          PGVVYYFIELTDPNGNPISSRGGLNNNNDNN---------HDHHDTHRT----------------
K. naganishii       PGVVYYFIELRNSGDDSSTPGRGNNNNNNNNE--------GDRSRGSDAHI--------------
K. unispora         PGVVYYFVEVANPEVTTSSSSSGVGGVGNNGS--------QNGNVNGSI----------------
K. heterogenica     PGIVYYFIEIRNSAVNNNRNDHERN-NGNNNN--------NNGNSSGSNSLYT-----------
                    *.::***:*: :           .  .   .: .  :      .
```

D

Roq1 mutagenesis screen hits

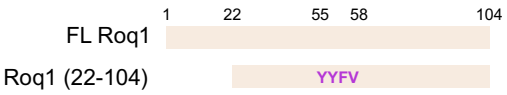

Figure 11. Roq1 harbors a distinct hydrophobic motif.
(A) Roq1 AlphaFold structure prediction. The structure is accessible with Uniprot number P47009 via the AlphaFold Protein Structure Database. N- and C-terminus, as well as regions with high confidence prediction (22-25, 51-56) are highlighted in the figure. Region 22-25 is part of the Ynm3 cleavage site.

Residues 51-56 are in the center of Roq1 and predicted to form together with residues 22-25 alpha-helical elements with high model confidence. The per-residue model confidence score (pLDDT) indicates the likelihood of correct structure prediction. Values range from 0 to 100, with 100 being the highest possible confidence score. Models with a very high confidence have a pLDDT of > 90 (dark blue) and those with high confidence range between 90 > pLDDT > 70 (mint blue). Low confidence structures range between 70 > pLDDT > 50 (yellow), and those with a very low a model confidence have a pLDDT < 50. Regions below 50 pLDDT may represent unstructured regions. Note that the majority of the Roq1 structure prediction has a low or very low confidence score, confirming its unstructured character. The figure is adapted from (Peters *et al.*, 2024).
(B) Roq1 sequence disorder prediction. The disorder tendency for each amino acid residue of Roq1 (1-104) was calculated by 11 different algorithms (Table 16 in *Materials and Methods*). Individual scores were averaged and plotted with standard deviations against the respective amino acid residue number. Note that amino acid residues 54-60 are predicted to be less disordered. Disorder predictions were initially run by Sebastian Schuck and replicated by me. The figure is adapted from (Peters *et al.*, 2024).
(C) Multiple sequence alignment of Roq1 homologs from different yeast species. The *S. cerevisiae* Roq1 amino acid sequence was aligned with homologs from 13 different yeast species, as indicated. *S. = saccharomyces; K. = Kazachstania*. Amino acid residue numbers are denoted. Conserved motifs among the analyzed species span residues 1-3, 20-25 and 53-60. The latter two motifs are highlighted in beige pink. R22, which becomes exposed upon proteolytic cleavage, is highlighted in purple. "*" = fully conserved; ":" = strongly conserved; "." = weakly conserved. The initial multiple sequence alignment was performed by Sebastian Schuck and is displayed in (Peters *et al.*, 2024). The sequence alignment depicted here was performed by me and modified for better visualization.
(D) Functionally relevant Roq1 residues identified by a mutagenesis screen. Cartoons of the full-length (FL) Roq1 (1-104) and Roq1 (22-104) with highlighted screen hits in pink. The mutagenesis screen aimed to identify Roq1 amino acid residues that are important for SHRED function. It was conceptualized by Sebastian Schuck, Oliver Pajonk and Sibylle Kanngießer and performed by Oliver Pajonk and Sibylle Kanngießer. In brief, Roq1 (22-104) was taken as DNA template for error-prone PCR. The PCR product was used to transform a *roq1*Δ yeast strain carrying the previously described Rtn1-Pho8*GFP (RPG) reporter (Szoradi *et al,* 2018). Reporter degradation efficiency was monitored and SHRED-deficient Roq1 variants were subsequently sequenced. The depicted cartoon was designed and produced by me.

3.2.3 *The hydrophobic motif directly associates with Ubr1*

To evaluate if the hydrophobic motif was relevant for the Roq1-Ubr1 association, Sibylle Kanngießer performed biolayer interferometry experiments using purified Ubr1 as analyte in solution and Roq1 variants that were immobilized on the sensor. While Roq1 variants with individual R22A or hydrophobic motif mutations bound Ubr1 to some extent, mutating both R22 and the hydrophobic motif completely disrupted Ubr1 interaction in her experiments. To further ask if the hydrophobic motif was not only needed to mediate the Roq1-Ubr1 communication but directly bound Ubr1, Sibylle Kanngießer and I collaboratively designed and performed photo-crosslinking experiments (Figure 12A). We designed Roq1 variants harboring amber stop codons

at position Y55 or Y56 inside the hydrophobic motif to incorporate the photo-reactive unnatural amino acid p-benzoyl-L-phenylalanine (Bpa; (Chin *et al*, 2002)). Using an *E. coli* strain that carries the corresponding suppressor tRNA/tRNA synthetase pair allowed us to express and purify Roq1 (22-104) (Y55Bpa)-ALFA and Roq1 (22-104) (Y56Bpa)-ALFA. Purified variants and wild type Roq1 (22-104)-ALFA were used in anti-ALFA pulldowns to isolate the Roq1-Ubr1 complex. Reconstituted complexes were subsequently illuminated with UV light to generate photo-crosslinked products. Roq1 (Y55Bpa) and Roq1 (Y56Bpa) formed crosslinks with Ubr1, as judged by the shift in their apparent molecular weight from 15 kDa to 250 kDa (Figure 12B). As expected, wild type Roq1 (22-104)-ALFA formed no crosslinks with Ubr1. Thus, the Roq1 hydrophobic motif directly binds Ubr1.

Altogether, Roq1 binds Ubr1 via a heterobivalent binding mechanism: Cleaved Roq1 binds with its N-terminal R22 to the UBR-Box-1 through a first binding site. The hydrophobic motif establishes a second binding interface with an unknown binding site in Ubr1.

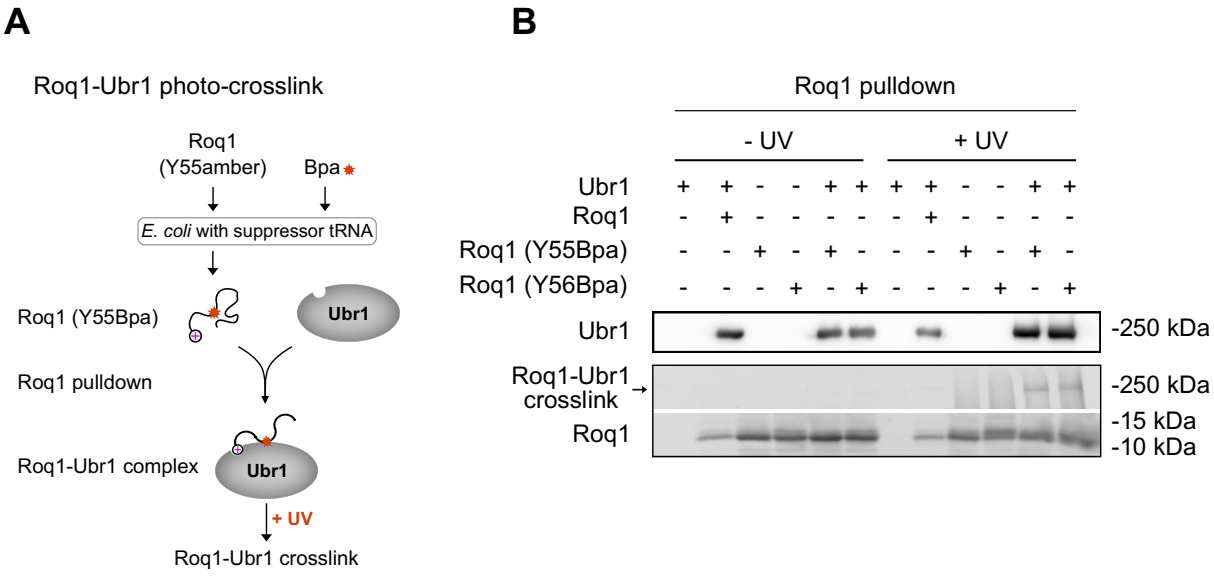

Figure 12. The hydrophobic motif of Roq1 directly binds Ubr1.
(A) Cartoon of Roq1-Ubr1 photo-crosslinking workflow. The workflow is shown with Roq1 (Y55amber) as an example but was also conducted using Roq1 (Y56amber). Roq1 (Y55amber or Y56amber)-ALFA harbors an amber stop codon at position Y55 or Y56 for the insertion of the photoreactive unnatural amino acid *p*-benzoyl-L-phenylalanine (Bpa). Roq1 (Y55Bpa or Y56Bpa)-ALFA was expressed in *E. coli* containing the appropriate tRNA synthetase/tRNA pair and Bpa. Roq1 (Y55Bpa)-ALFA or Roq1 (Y56Bpa)-ALFA was immobilized after expression and mixed with Ubr1 to allow

complex formation. Bound Roq1-Ubr1 was eluted with ALFA peptide, and the complex was left untreated or treated with UV light to obtain photo-crosslinks. The cartoon was adapted from (Peters *et al.*, 2024).
(B) FLAG tag and ALFA tag immunoblots from FLAG-Ubr1 and Roq1-ALFA crosslinking experiments, respectively. Bpa was incorporated into Roq1 instead of Y55 or Y56, yielding Roq1 (Y55Bpa)-ALFA or Roq1 (Y56Bpa)-ALFA. Wild-type Roq1 (22-104)-ALFA was used as control. Note that an arrow marks Roq1-Ubr1 crosslinks. Upon crosslinking with Ubr1, the apparent molecular weight of Roq1 shifts from roughly 15 kDa to 250 kDa, thereby co-migrating with Ubr1. The conceptualization of the photo-crosslinking experiment was done by Sebastian Schuck, Sibylle Kanngießer and me. Sibylle Kanngießer and I collaboratively performed the experiment.

3.3 The hydrophobic motif enhances misfolded substrate ubiquitination

3.3.1 *The hydrophobic motif promotes misfolded protein ubiquitination*

Next, I asked whether the Roq1 hydrophobic motif not only binds Ubr1 but also acts as a functional element like R22 to regulate its activity. Roq1 (V58E), a hydrophobic motif variant Sibylle Kanngießer identified from the mutagenesis screen, harbors a polar mutation that made it SHRED-inactive *in vivo* (shown by Sibylle Kanngießer). However, *in vitro* pulldowns performed by me and biolayer interferometry experiments done by Sibylle Kanngießer showed that Roq1 (V58E) bound Ubr1, but less strongly than wild type Roq1. (Figure 13A). This suggests that Roq1-Ubr1 binding might involve V58 but does not strictly depend on it. Moreover, it also indicates that the hydrophobic motif could regulate Ubr1 activity through V58. To test this, Sebastian Schuck, Sibylle Kanngießer and I conceptualized *in vitro* ubiquitination assays with Roq1 (V58E), and I subsequently tested the effect on ubiquitination efficiency for different Ubr1 substrate classes. As a first substrate class, I tested the impact of Roq1 (V58E) on misfolded Pho8* or unfolded Luciferase^{U} ubiquitination. Roq1 (V58E) did not, in contrast to wild type Roq1, stimulate their ubiquitination, even when used at higher concentrations (Figures 13B+C). Next, I tested their effect on the N-degron substrate ubiquitination. Both Roq1 (V58E) and wild type Roq1 inhibited R-GFP ubiquitination (Figure 13D) but promoted F-GFP ubiquitination (Figure 13E) to the same extent.

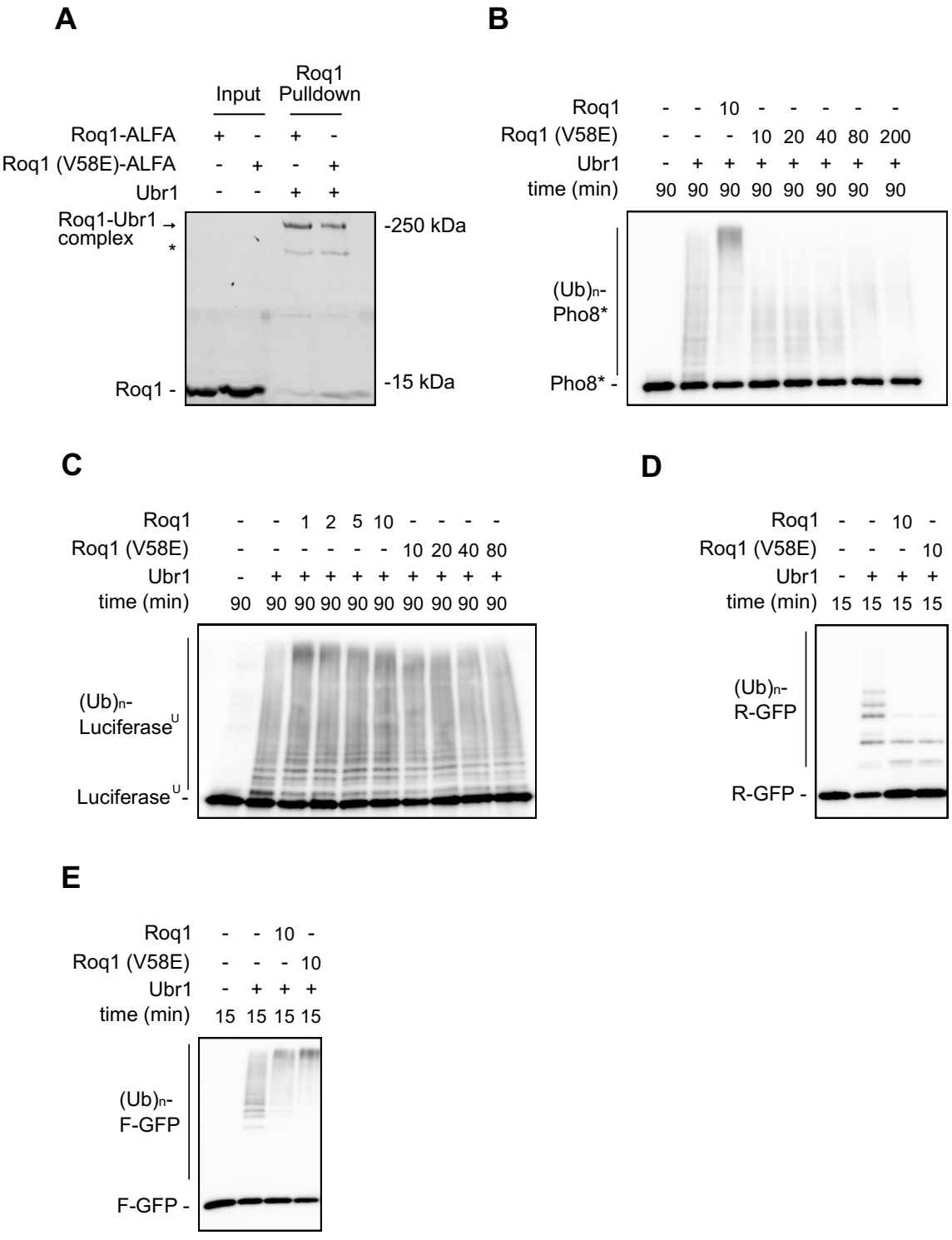

Figure 13. Roq1 requires the hydrophobic motif to distinctively enhance the ubiquitination efficiency of misfolded substrates.

(A) Coomassie-stained SDS-PAGE gel of Roq1-Ubr1 pulldowns with different Roq1 variants. Roq1 (22-104)-ALFA or Roq1 (22-104) (V58E)-ALFA were mixed with FLAG-Ubr1 in a molar ratio of 10:1. The complex was immobilized on ALFA beads and eluted with ALFA peptide. 3.6 µg of each Roq1 variant was loaded as input and used in pulldowns, whereas 6.9 µg FLAG-Ubr1 was used. Note that a Ubr1 input is missing on the gel. The asterisk indicates a degradation product from the Ubr1 purification. The experiment was designed and performed by me.

(B) Pho8 immunoblot from Pho8* ubiquitination assays in presence of Roq1 (22-60)-HA or with increasing amounts of Roq1 (22-60) (V58E)-HA. While Roq1 (22-60)-HA was added at 10-fold molar excess over Ubr1, Roq1 (22-60) (V58E)-HA was added at 10, 20, 40, 80 or 200-fold molar excess. Ubiquitination reactions were incubated at 30°C for 90 minutes. Conceptualization of the experiment was done by Sebastian Schuck, Sibylle Kanngießer and me. I performed the experiment and adapted the figure from (Peters *et al.*, 2024).
(C) Luciferase immunoblot from Luciferase^{U} ubiquitination assays with different concentrations of Roq1 (22-60)-HA or Roq1 (22-60) (V58E)-HA. While Roq1 (22-60)-HA was added at 1, 2, 5 or 10-fold molar excess over Ubr1, Roq1 (22-60) (V58E)-HA was added at 10, 20, 40 or 80-fold molar excess. Ubiquitination reactions were incubated at 30°C for 90 minutes. Note that while Roq1 (22-60)-HA promotes Pho8* ubiquitination, addition of Roq1 (22-60) (V58E)-HA appears to have no prominent effect. Conceptualization of the experiment was done by Sebastian Schuck, Sibylle Kanngießer and me. I performed the experiment.
(D) GFP immunoblot from R-GFP ubiquitination assays in presence of Roq1 (22-60)-HA or Roq1 (22-60) (V58E)-HA. Roq1 variants were added at 10-fold molar excess over Ubr1. Ubiquitination reactions were incubated at 30°C for 15 minutes. The experiment was conceptualized by Sebastian Schuck, Sibylle Kanngießer and me and performed by me. The figure was adapted from (Peters *et al.*, 2024).
(E) As in panel (D), but with F-GFP.

Next, I tested collaboratively with Sibylle Kanngießer how Roq1 (V58E) influences the ubiquitination of Ubr1 substrates with internal degrons. Both Roq1 (V58E) and wild type Roq1 promoted Cup9 ubiquitination (performed by Sibylle Kanngießer, not shown). Mgt1 and Chk1 also contain internal degrons, but in contrast to Cup9, RA and LA dipeptides did not stimulate their ubiquitination (Figures 10B+C; (Hwang *et al.*, 2010a; Oh *et al.*, 2017)). Unexpectedly, Roq1 (V58E) enhanced both Mgt1 and Chk1 ubiquitination (Figure 14A+B). This suggests a regulation by Roq1 independently of R22 and V58.

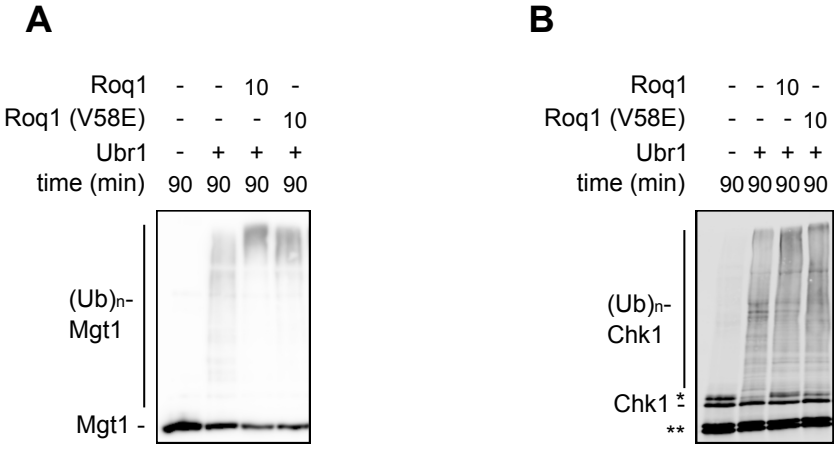

Figure 14. Roq1 does not require the hydrophobic motif to promote the ubiquitination of substrates with internal degrons.

(A) MBP tag immunoblot from Mgt1-MBP ubiquitination assays in presence of Roq1 (22-60)-HA or Roq1 (22-60) (V58E)-HA. Roq1 variants were added at 10-fold molar excess over Ubr1. Ubiquitination reactions were incubated at 30°C for 90 minutes. The experiment was conceptualized and performed by me.
(B) ALFA tag immunoblot from Chk1-ALFA-FLAG ubiquitination assay in presence of Roq1 (22-60)-HA or Roq1 (22-60) (V58E)-HA. While Roq1 (22-60)-HA was added at 10-fold molar excess over Ubr1, Roq1 (22-60) (V58E)-HA was added at 10, 20, 40 or 80-fold molar excess. Ubiquitination reactions were incubated at 30°C for 90 minutes. Note that Roq1 (22-60) (V58E)-HA marginally promoted Chk1 ubiquitination when used at 10-fold excess over Ubr1. The experiment was conceptualized and performed by me. The single asterisk (*) indicates the formation of monoubiquitinated Chk1 in absence of Ubr1. The double asterisk (**) denotes degradation products that appeared during Chk1 expression or purification. The experiment was conceptualized and performed by me.

3.3.2 *Roq1 does not enhance Rad6 or Pho8* recruitment to Ubr1*

How does the hydrophobic motif of Roq1 reprogram Ubr1 on a mechanistic level? First, it could cause conformational re-arrangements within Ubr1 to promote either E2 or substrate recruitment. Alternatively, a combination of the two might facilitate a faster ubiquitin transfer from the E2 to a bound substrate. To test these hypotheses, I first monitored the effect of Roq1 on Rad6 recruitment to Ubr1 using pulldown experiments. Rad6 bound Ubr1 even when unconjugated with ubiquitin, as reported previously (Xie & Varshavsky, 1999). Addition of Roq1 did not stimulate Rad6 recruitment but had rather inhibitory effects at higher concentrations (Figure 15A, compare lanes 4 and 5). Sibylle Kanngießer observed similar effects in her biolayer interferometry experiments (not shown). Strikingly, the inhibitory effect of Roq1 disappeared when I replaced Rad6 with Rad6~Ub, which is charged with ubiquitin, (~ denotes the formation of a thioester bond intermediate between Cys88 of Rad6 and the C-terminal tail of ubiquitin; Figure 15A).
Building on this observation, I further tested the effect of Roq1 on Rad6~Ub recruitment to Ubr1. Ubr1 brings Rad6~Ub and a substrate together in a so-called closed conformation, which orients the Rad6~Ub thioester optimally for ubiquitin transfer (Pan *et al.*, 2021). To assay ubiquitin transfer efficiency, I set up single turnover Rad6~Ub discharge assays (Figure 15B). In brief, Rad6 was first charged with ubiquitin, followed by the addition of EDTA to prevent further charging. Ubr1 was then added to monitor Rad6~Ub discharge. To uncouple Rad6~Ub discharge effects from those that arose during Ubr1 substrate recruitment, I omitted Ubr1 substrates

and used solvent hydroxide ions to discharge Rad6~Ub via hydrolysis. Of note, this approach has been reported previously for other E2 enzymes and Rad6 (Gallego *et al.*, 2016; Keszei & Sicheri, 2017; Ozkan *et al*, 2005). Ubr1 alone barely discharged Rad6~Ub after 15 minutes and the RA dipeptide had no further effect (Figure 15C). Strikingly, adding Roq1 (22-60) accelerated Rad6~Ub discharge (Figures 15C+D). However, whether this effect stems from Roq1 facilitating the closed conformation of Ubr1 or from Roq1 serving as ubiquitin acceptor to some extent remains unclear.

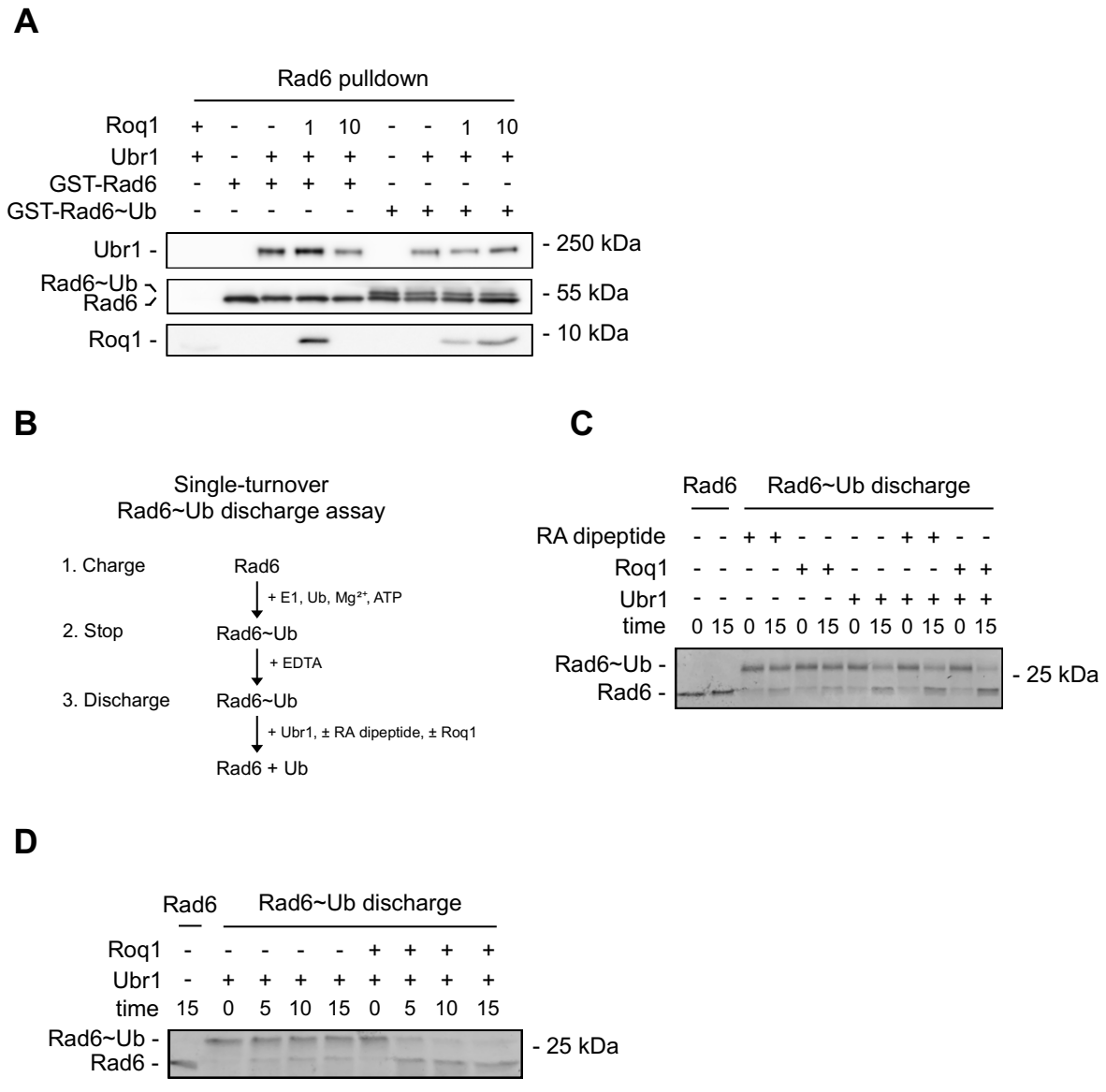

Figure 15. Roq1 does not promote the recruitment of Rad6 to Ubr1 but enhances the Rad6~Ub discharge.

(A) Glutathione S-transferase (GST) tag, FLAG tag and HA tag immunoblots from Ubr1-Rad6 pulldown experiments with GST-Rad6, FLAG-Ubr1 and Roq1 (22-60)-HA. GST-Rad6 was either left uncharged or charged with ubiquitin to generate Rad6~Ub ("~" denotes the formation of a thioester

bond between Rad6 and ubiquitin). GST-Rad6 or GST-Rad6~Ub were mixed in a 2:1 molar ratio with FLAG-Ubr1 and in a 1:1 or 1:10 molar ratio with Roq1 (22-60)-HA. In brief, to pulldown GST-Rad6 or GST-Rad6~Ub-bound protein complexes, glutathione sepharose beads were added and samples were incubated overnight at 4°C, followed by an elution step with 20 mM glutathione. The sample buffer for gel loading was devoid of dithiothreitol to preserve the thioester bond formed between Rad6 and ubiquitin. Note that while Roq1 (22-60)-HA appears to inhibit Ubr1 binding to GST-Rad6 at high concentrations, this effect was not observed for GST-Rad6~Ub. GST-Rad6~Ub undergoes hydrolysis due to the lability of the thioester bond formed between the catalytic cysteine of Rad6 and the C-terminus of ubiquitin. The experiment was conceptualized and performed by me.
(B) Workflow of the single-turnover Rad6~Ub discharge assay. Ubr1 transfers ubiquitin from Rad6~Ub to its substrate in a closed conformation for efficient ubiquitin transfer. To monitor the efficiency of ubiquitin transfer in absence or presence of the RA dipeptide or Roq1 variants, Rad6 was first charged with ubiquitin in presence of an E1 enzyme, ubiquitin, Mg^{2+} and ATP (1). To stop further charging and prevent re-charging of Rad6 with ubiquitin during a single-turnover assay, EDTA was added (2). For Rad6~Ub discharge, Ubr1, RA dipeptide or Roq1 (22-60)-HA were added and Rad6~Ub discharge was monitored over time (3). The protocol was adapted from (Buetow *et al*, 2018). The cartoon was created by me.
(C) Coomassie-stained SDS-PAGE gel of single turnover-discharge Rad6~Ub discharge assay in presence of Ubr1, RA dipeptide or Roq1 (22-60)-HA. Rad6 was first charged with ubiquitin before the reaction was quenched with EDTA. Rad6~Ub discharge was monitored in absence or presence of FLAG-Ubr1, RA dipeptide or Roq1 (22-60)-HA at 30°C for 0 or 15 minutes. Final protein concentrations in the assay are: 2.5 µM Rad6, 2.5 µM ubiquitin, 50 nM FLAG-Ubr1, 200 µM RA dipeptide, 500 nM Roq1 (22-60)-HA. Note that solvent hydroxide ions can discharge Rad6~Ub independently of any substrates, which has also been shown for other E2 enzymes but also Rad6 (Gallego *et al.*, 2016; Keszei & Sicheri, 2017; Ozkan *et al.*, 2005). Note that Roq1 (22-60)-HA discharged Rad6~Ub slightly more efficiently than Ubr1 alone. The experiment was conceptualized and performed by me.
(D) Coomassie-stained SDS-PAGE gel of single turnover-discharge Rad6~Ub discharge assay in presence of Ubr1 or Roq1 (22-60)-HA with shorter time points. Rad6 was charged with ubiquitin and subsequently quenched as in (C). Rad6~Ub discharge was monitored in absence or presence of Roq1 (22-60)-HA over 0, 5, 10 or 15 minutes

To explore the possibility of Roq1 promoting the recruitment of Pho8* or Pho8 to Ubr1, I implemented *in vitro* pulldown assays using Pho8 or Pho8* as bait. While Ubr1 bound better to Pho8* than Pho8, Roq1 had no effect on the Ubr1 recruitment to both (Figure 16).

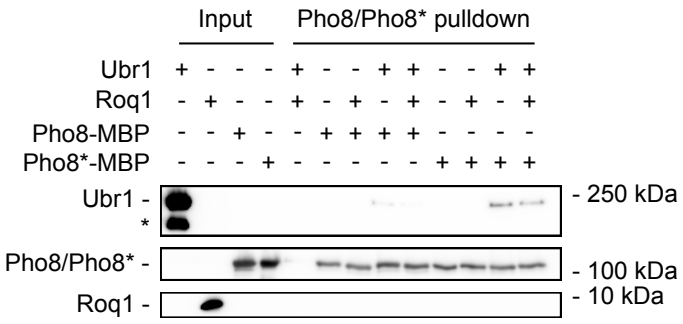

Figure 16. Roq1 does not promote the recruitment of Pho8* to Ubr1.
FLAG tag, Pho8 and HA tag immunoblots from Pho8 and Pho8* pulldowns in absence or presence of FLAG-Ubr1 or Roq1 (22-60)-HA. In brief, Pho8-MBP or Pho8*-MBP were incubated at equimolar concentrations with Ubr1 and a 10-fold molar excess of Roq1 (22-60)-HA at 30°C for 90 minutes to allow complex formation. Pho8-MBP, Pho8*-MBP and bound proteins were precipitated with amylose resin and eluted with maltose-containing buffer. The asterisk (*) indicates a degradation product that originated from FLAG-Ubr1 expression or purification. Note that Roq1 was not detectable in pulldown lanes. The experiment was conceptualized and performed by me. The figure is adapted from (Peters *et al*, 2024).

3.3.3 *The hydrophobic motif improves Ubr1 monoubiquitination efficiency*

Roq1 appears to have no effect on Rad6 or Pho8* recruitment to Ubr1, yet it promotes the ubiquitination of substrates. Substrate ubiquitination is a two-step reaction, consisting of ubiquitin chain initiation followed by chain elongation. Whether Roq1 promotes substrate ubiquitination by catalyzing ubiquitin chain initiation, chain elongation or both is not clear. To solely focus on ubiquitin chain initiation, I sought to uncouple ubiquitin chain initiation from elongation by replacing wild type ubiquitin with a chain elongation-deficient, lysine-free ubiquitin variant, which I termed K(0) Ub (Figure 17A). K(0) Ub still binds to substrate lysine residues via its C-terminus and thereby allows monitoring of substrate monoubiquitination. When employed with Pho8* as substrate in ubiquitination assays, I observed the formation of two distinct bands denoting ubiquitin conjugated to two Pho8* lysines (Figure 17B). Addition of Roq1 increased the number from two to five conjugated ubiquitins. In contrast, the RA dipeptide or Roq1 (V58E) had no effect. Hence, the hydrophobic motif of Roq1 increases the monoubiquitination efficiency of Pho8*. For the type-2 N-degron model substrate F-GFP, Ubr1 glues up to five ubiquitins to substrate lysines in my assays and the RA dipeptide increases it to six (Figure 17C). Addition of Roq1 or Roq1

(V58E) had no effect beyond the RA dipeptide, as expected. Cup9 showed similar effects, as shown in ubiquitination assays originally performed by Sibylle Kanngießer and replicated by me (Figure 17D). For Mgt1, Ubr1 conjugated two ubiquitin molecules in my assays and addition of Roq1 promoted further attachment. Determining the exact number of attached ubiquitins, however, was challenging due to insufficient band separation (Figure 17E).

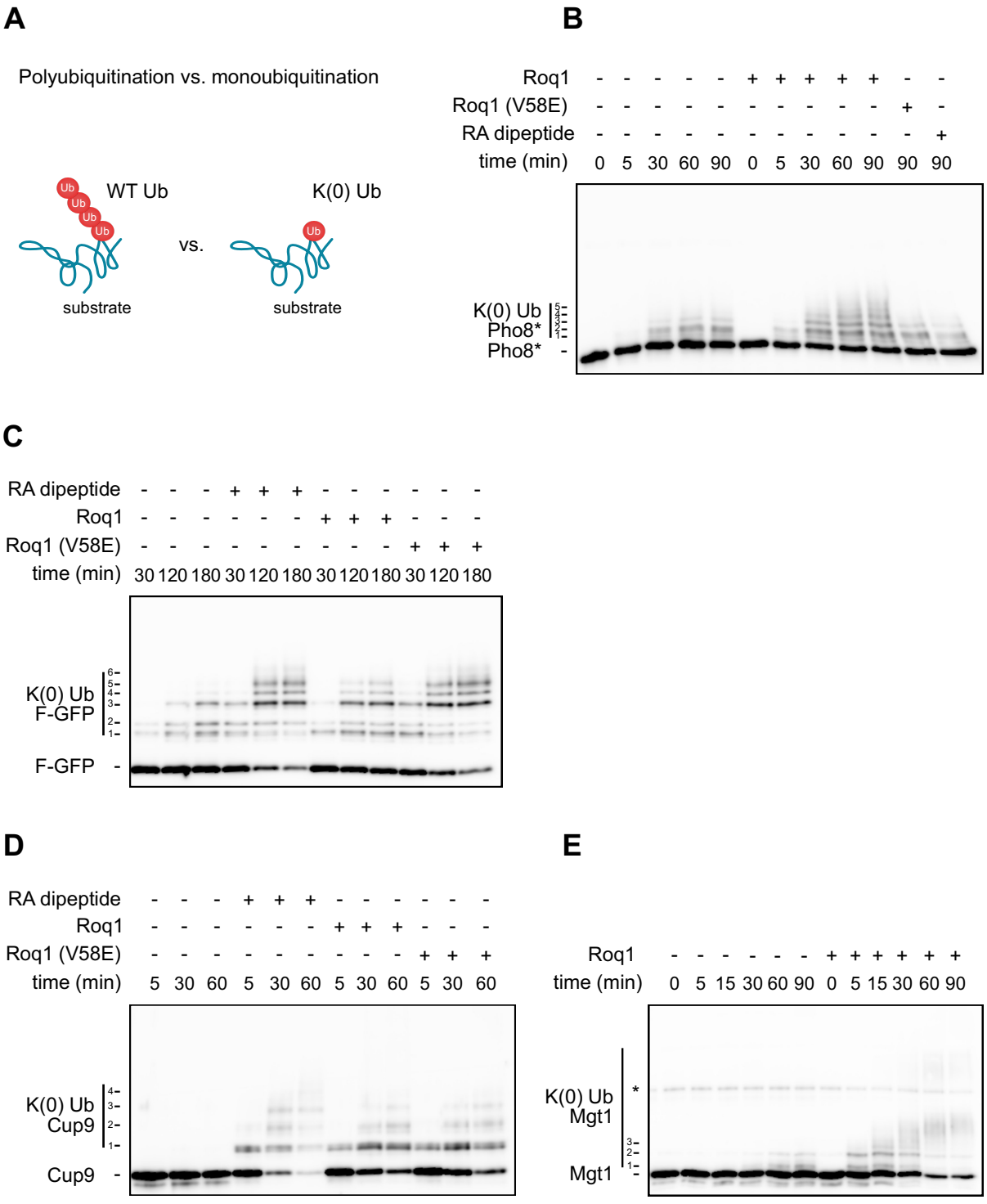

Figure 17. The Roq1 hydrophobic motif improves the Ubr1 monoubiquitination efficiency.
(A) Cartoon representing effects of wild-type (WT) or no-lysine (K(0)) ubiquitin on substrate ubiquitination. The first ubiquitin is covalently linked via its C-terminal carboxyl group to a substrate lysine, cysteine, threonine, or serine residue. Polyubiquitination occurs when additional ubiquitin molecules bind via their C-termini to lysine residues of pre-bound ubiquitins. Mutation of all seven lysine residues within ubiquitin (K(0)) abolishes polyubiquitination and allows the inspection of substrate monoubiquitination.

(B) Pho8 immunoblot from Pho8* ubiquitination assays with K(0) ubiquitin in absence or presence of the RA dipeptide, Roq1 (22-60)-HA or Roq1 (22-60) (V58E)-HA. The RA dipeptide was added at 4000-fold molar excess over Ubr1. Roq1 (22-60)-HA and Roq1 (22-60) (V58E)-HA:Ubr1 molar ratio was 10:1. Ubiquitination reactions were incubated at 30°C for 0, 5, 30, 60 or 90 minutes. Numbers indicate K(0) ubiquitin-Pho8* conjugates. This experiment was initially conceptualized by me, further planned by Sebastian Schuck, Sibylle Kanngießer and me, and subsequently performed by me. The figure was adapted from (Peters *et al.*, 2024).
(C) GFP immunoblot from F-GFP ubiquitination assays with K(0) ubiquitin in absence or presence of the RA dipeptide, Roq1 (22-60)-HA or Roq1 (22-60) (V58E)-HA. The RA dipeptide was added at 4000-fold molar excess over Ubr1. Roq1 (22-60)-HA and Roq1 (22-60) (V58E)-HA:Ubr1 molar ratio was 10:1. Ubiquitination reactions were incubated at 30°C for 30, 120 or 180 minutes. Numbers indicate K(0) ubiquitin-F-GFP conjugates. This experiment was initially conceptualized by me, further planned by Sebastian Schuck, Sibylle Kanngießer and me, and subsequently performed by me. The figure was adapted from (Peters *et al.*, 2024).
(D) Strep tag immunoblot from Cup9-Strep ubiquitination assays with K(0) ubiquitin in absence or presence of the RA dipeptide, Roq1 (22-60)-HA or Roq1 (22-60) (V58E)-HA. The RA dipeptide was added at 4000-fold molar excess over Ubr1. Roq1 (22-60)-HA and Roq1 (22-60) (V58E)-HA:Ubr1 molar ratio was 10:1. Ubiquitination reactions were incubated at 30°C for 5, 30 or 60 minutes. Numbers indicate K(0) ubiquitin-Cup9-Strep conjugates. This experiment was conceptualized by Sebastian Schuck and Sibylle Kanngießer and replicated by me.
(E) MBP tag immunoblot from Mgt1-MBP ubiquitination assays with K(0) ubiquitin in absence or presence of the RA dipeptide, Roq1 (22-60)-HA or Roq1 (22-60) (V58E)-HA. The RA dipeptide was added at 4000-fold molar excess over Ubr1. Roq1 (22-60)-HA and Roq1 (22-60) (V58E)-HA:Ubr1 molar ratio was 10:1. Ubiquitination reactions were incubated at 30°C for 0, 5, 15, 30, 60 or 90 minutes. Numbers indicate K(0) ubiquitin-Mgt1-MBP conjugates. The asterisk (*) indicates an antibody cross-reaction. This experiment was conceptualized and performed by me.

Roq1 accelerates the Ubr1-mediated degradation of a Pho8* reporter construct through proteasomal degradation in yeast (Szoradi *et al*, 2018). Concomitantly, Roq1 increased the ubiquitin chain initiation efficiency of Ubr1. However, whether the subsequent chain elongation builds homotypic or branched ubiquitin chains *in vitro* that could get recognized by the proteasome for degradation is not clear. To test this, I performed *in vitro* ubiquitination assays with Pho8* using various linkage-specific ubiquitin variants. While single mutation of K11, K29 or K63 had no effect on Pho8* ubiquitination, additional mutation of K48 in a (K63R) ubiquitin variant reduced Pho8* ubiquitination (Figure 18A). Interestingly, this variant did not reduce Pho8* ubiquitination to the same extent as lysine-free K(0) ubiquitin, indicating the involvement of at least one other linkage type. Addition of Roq1 generally enhanced Pho8* ubiquitination, as expected, but had no other effect on the ubiquitin linkages (Figure 18B). Whether Ubr1 also builds K-48 linked ubiquitin chains *in vivo* that drive the proteasomal degradation of the Pho8* reporter construct needs to be confirmed.

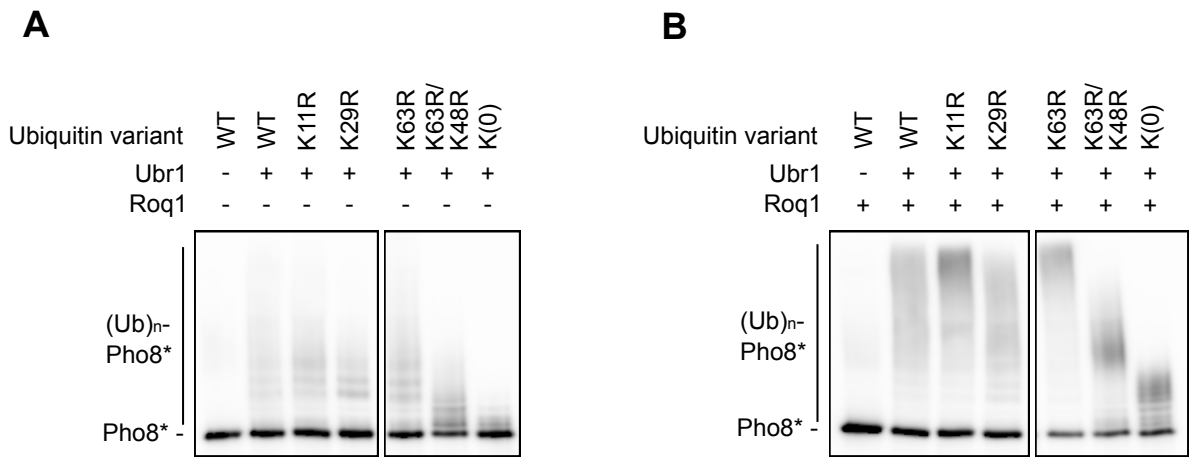

Figure 18. Polyubiquitin chain formation of Pho8* by Ubr1 involves K48-linked ubiquitination.
(A) Pho8 immunoblot from Pho8* ubiquitination assays with different ubiquitin variants in absence of Roq1 22-60)-HA. Ubiquitin variants were added at equimolar concentrations and are wild-type, K11R, K29R, K63R, K63R/K48R or K(0). Ubiquitination reactions were incubated at 30°C for 90 minutes. Note that Pho8* polyubiquitination with K63R/K48R is not completely abolished, suggesting the involvement of an unknown ubiquitin linkage type. The two panels were cropped from the same membrane. This experiment was conceptualized and performed by me.
(B) As in panel (A), but with the addition of Roq1 (22-60)-HA.

Taken together, the Roq1 hydrophobic motif fulfills two distinct purposes: First, it assists Roq1 in interacting with Ubr1, thereby creating avidity effects to support R22 binding to the UBR-Box-1. Enhanced R22 binding subsequently represses or stimulates type-1 and type-2 N-degron substrate ubiquitination, respectively, and promotes the ubiquitination of native substrates such as Cup9. Second, it governs the ubiquitination of misfolded or unfolded Ubr1 substrates such as Pho8* or unfolded Luciferase^{U}. This involves an increased proficiency to monoubiquitinate substrates. Whether the enhanced ubiquitination of Mgt1 and Chk1 requires the Roq1 hydrophobic motif is unclear.

3.4 Structural insights into the Roq1-Ubr1 complex

3.4.1 *Cryo-electron microscopy of the Roq1-Ubr1 complex*

Roq1 profoundly changes Ubr1 activity and substrate specificity. Obtaining a Roq1-Ubr1 structural complex might help to understand 1) which Ubr1 residues contact the Roq1 hydrophobic motif, if 2) Roq1 becomes structured upon Ubr1 binding and 3) whether Ubr1 domains change their conformation. To address these questions, I employed cryo-electron microscopy (cryo-EM) to determine the structure of a Roq1-Ubr1 protein complex.

To isolate the Roq1-Ubr1 complex, I performed pulldown experiments using Roq1 as bait protein, which ensured enrichment of only the Roq1-bound fraction of Ubr1 (Figure 19A). Subsequent sample vitrification, data acquisition and processing were done by Dirk Flemming and Jan Rheinberger of the HDcryoNet facility at the Biochemistry Center. The particles were not evenly distributed throughout the grids after vitrification and formed aggregates to some extent (Figure 19B). The collected dataset was first subjected to particle selection and 2D classification, where alpha helices became visible (Figure 19C). Further 3D classification showed that the Roq1-Ubr1 complex had a sailboat-like structure, as previously described for the Ubr1-Rad6 complex (Figure 19D, Pan *et al,* 2021). The U2BR domain that binds Rad6~Ub was not resolved due to its flexibility, which has been previously described for apo Ubr1 as well (Pan *et al.*, 2021). In addition, there was no apparent EM density that could be attributed to Roq1. The final EM map had a global resolution of 6.3 Å (Figure 19E). The limited number of distinguishable 2D classes and the preferred orientation of particles contributed to imbalances in the local resolution distribution (Figures 19C, F+G). To overcome the local resolution anisotropy, the specimen stage was tilted to an angle of 18°, without much improvement of data quality (not shown).

Overall, the low and locally dispersed resolution of the Roq1-Ubr1 complex made confident assumptions about the underlying mechanism of Ubr1 reprograming impossible.

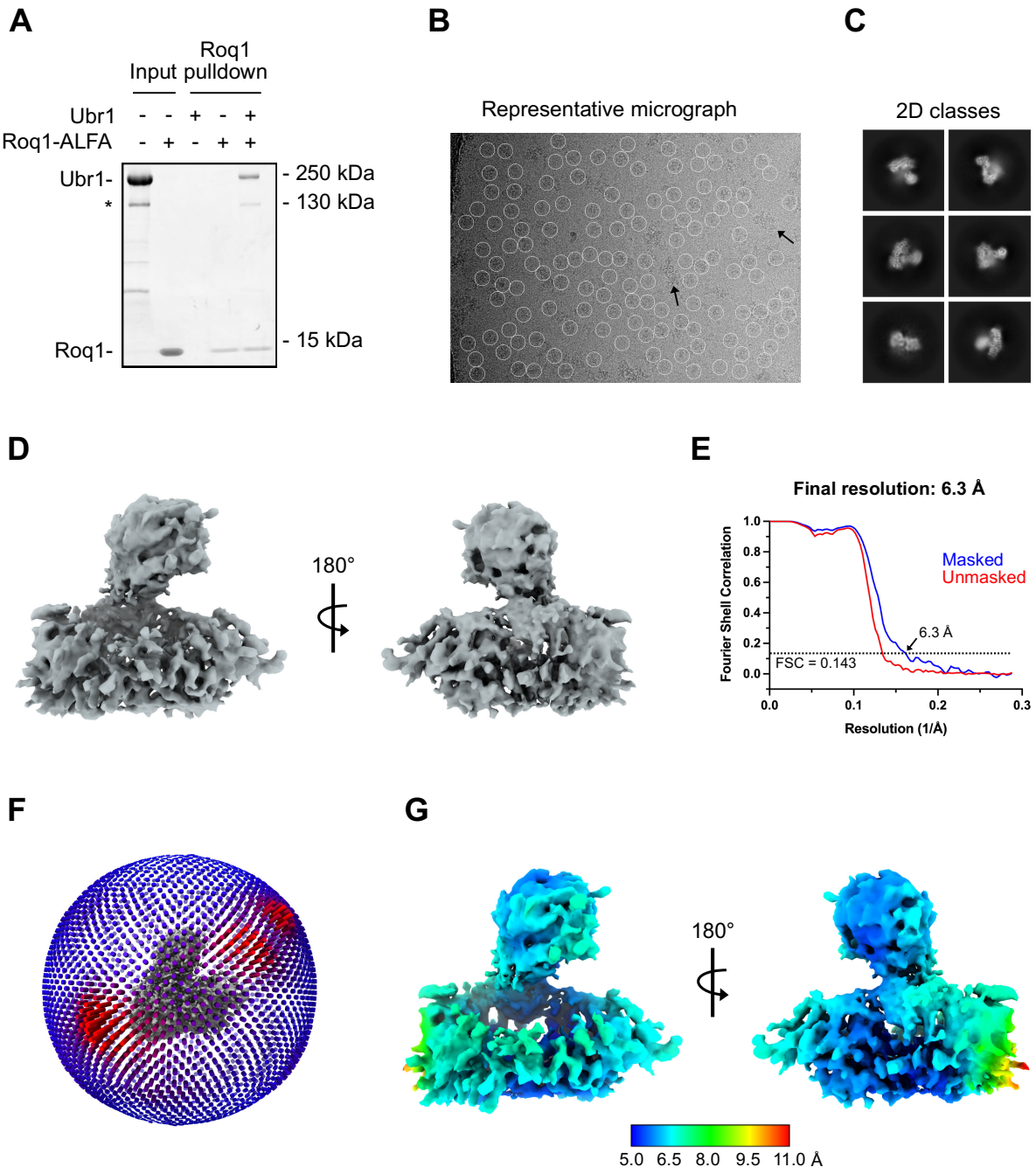

Figure 19. Single particle cryo-electron microscopy (cryo-EM) of the Roq1-Ubr1 complex.
(A) Coomassie-stained SDS-PAGE gel of the isolated Roq1-Ubr1 complex for cryo-EM. Roq1 (22-104)-ALFA was mixed with FLAG-Ubr1 in 10:1 molar ratio. The complex was immobilized on ALFA beads and eluted with ALFA peptide. 2.4 µg Roq1 (22-104)-ALFA and 4.6 µg FLAG-Ubr1 were loaded as input. The asterisk (*) denotes a degradation product from the expression or purification of Ubr1. The experiment was designed and performed by me.
(B) Representative micrograph of the Roq1-Ubr1 complex. In total, 9636 movies that were taken. Roq1-Ubr1 molecules are encircled. Black arrows highlight aggregation products that formed on cryo grids. Data acquisition was performed collaboratively with Dirk Flemming and Jan Rheinberger.
(C) Selected 2D class averages. 972,724 particles were picked in total. Data processing was done by Dirk Flemming and Jan Rheinberger.

(D) Representative 3D class of the Roq1-Ubr1 complex. Data processing was done by Jan Rheinberger and visualized by me.
(E) Fourier shell correlation (FSC) curves of maps before and after masking. The global resolution of 6.3 Ångstrom was specified by the FSC = 0.143 criterion. Data processing was done by Jan Rheinberger and data visualization by me.
(F) Angular distribution of Roq1-Ubr1 particles that are considered for the final resolution map. Red dots indicate a preferred particle orientation. Data processing was done by Jan Rheinberger and visualized by me.
(G) Local resolution map of the Roq1-Ubr1 complex. Data processing was done by Jan Rheinberger and data visualization was performed by me.

3.4.2 *AlphaFold predicts a second Roq1-Ubr1 binding interface*

Roq1 binds Ubr1 through R22 and the hydrophobic motif. While R22 interacts through the UBR-Box-1 with Ubr1, it is unclear where the hydrophobic motif binds. To map binding interface between the hydrophobic motif and Roq1 independently of an empirical structure, Bram Vermeulen and I collaboratively employed an AlphaFold-based strategy. AlphaFold is a powerful tool to predict interactions between folded protein domains but becomes less reliable for intrinsically disordered protein regions. (Ruff & Pappu, 2021). The high disorder tendency (Figures 11A+B) makes confident structure predictions therefore challenging with Roq1. To overcome this hurdle, Rafael Salazar and Sibylle Kanngießer designed a shortened Roq1 variant consisting of only 22 amino acid residues, termed Roq1 (22 aa) (Figure 20A). Roq1 (22 aa) includes N-terminal R22, a 15 amino acid linker and the hydrophobic motif. It reprogramed Ubr1 both *in vivo* and *in vitro* (shown by Sibylle Kanngießer). Using Roq1 (22 aa) and Ubr1, AlphaFold predicted the structure of a Roq1 (22 aa)-Ubr1 complex (Figure 20B). As proof of concept, I anticipated docking of Roq1 R22 to UBR-Box-1 residues. Main UBR-Box-1 residues include but are not limited to D142, T144, D176 and D179 (Choi *et al*, 2010; Matta-Camacho *et al*, 2010; Pan *et al.*, 2021). All of which bound Roq1 R22 (Figure 20C). For the Roq1 hydrophobic motif, AlphaFold docked it into a region within Ubr1 that mainly consists of the hydrophobic amino acid patch I687-L690-Y823 (Figures 20D+E). To test whether these residues mediate Ubr1 reprograming, I generated a Ubr1 (I687D/Y823D) double mutant. L690 is not surface-exposed and was therefore left intact to not disrupt overall Ubr1 structure and function. To probe for Roq1-dependent effects and general Ubr1 activity, I performed standard ubiquitination assays using misfolded Pho8* as

substrate. Ubr1 (I687D/Y823D) ubiquitinated Pho8*, albeit less efficiently than wild type Ubr1. Surprisingly, addition of Roq1 activated Ubr1 (I687D/Y823D) more prominently than wild type Ubr1 (Figure 20F, compare remaining nonubiquitinated Pho8* in lanes 3+4 with lanes 7+8). Concomitantly, biolayer interferometry experiments performed by Sibylle Kanngießer showed a faster and enhanced association between Roq1 and Ubr1 (I687D/Y823D).

These findings reveal that Ubr1 reprograming does not require the I687-L690-Y823 patch but suggests that it competes with the authentic Roq1 hydrophobic motif interaction site for binding.

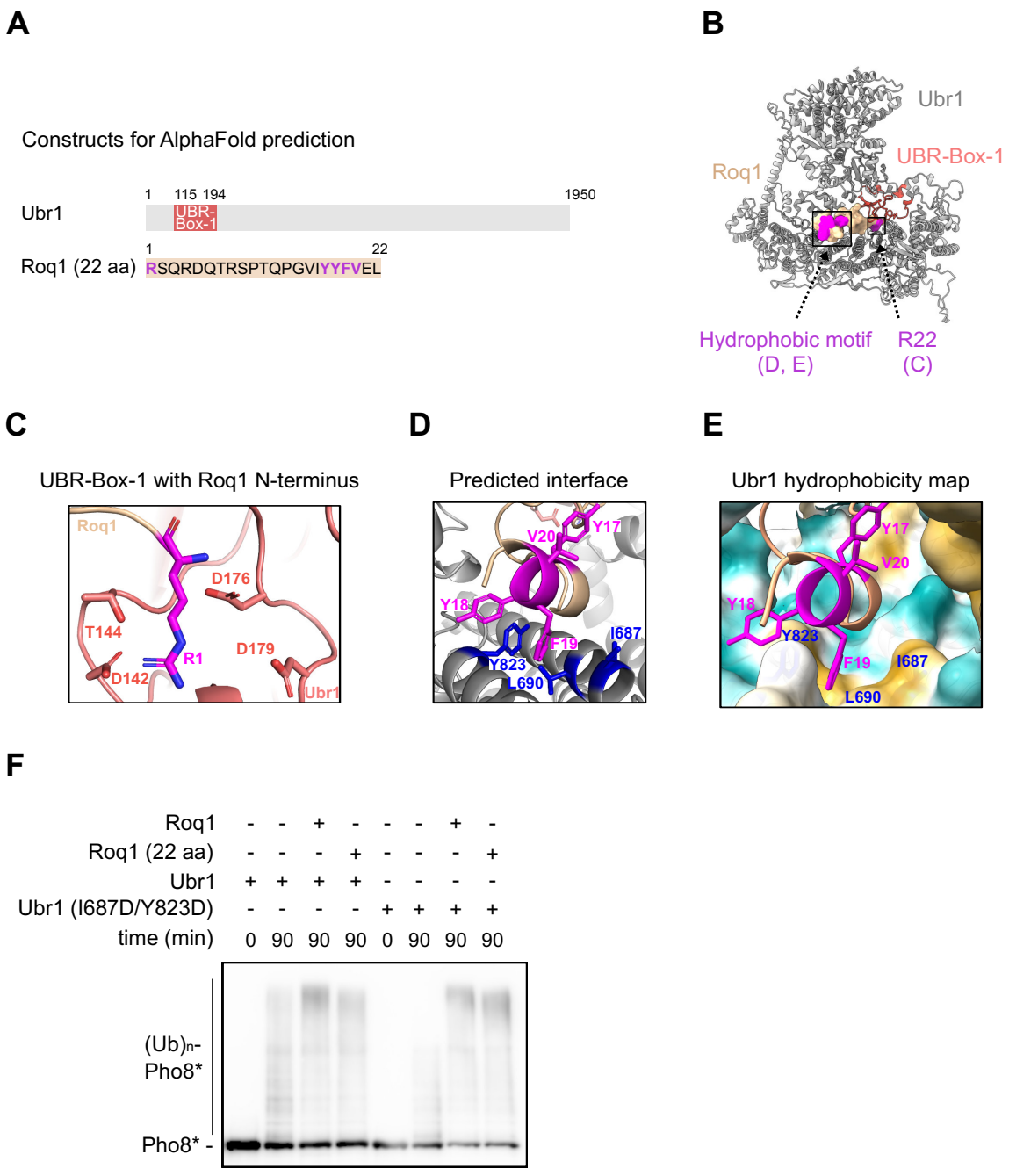

Figure 20. AlphaFold prediction of a Roq1-Ubr1 binding interface.

(A) Cartoon of Ubr1 and Roq1 constructs used for AlphaFold predictions. Full length Ubr1 consists of 1950 amino acids. Its UBR-Box-1 spans amino acid residues 115-194 (Pan *et al*, 2021), binds type-1 N-degron substrates and is highlighted in light red. A shortened but SHRED-active version of Roq1, Roq1 (22 aa), was used for more reliable AlphaFold predictions. Highlighted in purple are the N-terminal arginine and the hydrophobic motif. Roq1 (22 aa) was identified and further characterized by Sibylle Kanngießer.

(B) Global view of the predicted Roq1-Ubr1 structure using AlphaFold Multimer. Boxes refer to close up views of the UBR-Box-1 (panel (C)) and the predicted second binding interface (panels (D+E)). Ubr1 is depicted in grey, Roq1 in beige pink as spheres, its N-terminus and the hydrophobic motif in purple. The disordered Ubr1 C-terminus is not depicted for better visualization. The AlphaFold

Multimer prediction was run by Bram Vermeulen, evaluated by Bram Vermeulen and Stefan Pfeffer and visualized by me.
(C) Predicted architecture of the UBR-Box-1 with the N-terminal arginine of Roq1 (22 aa). Ubr1 residues D142, T144, D176 and D179 (light red), which form the key pocket of the UBR-Box-1 (Choi *et al.*, 2010; Pan *et al.*, 2021), interact with the N-terminal arginine of Roq1 (purple) through hydrogen bonds. Roq1-Ubr1 binding was visualized by me.
(D) Zoomed-in capture of the predicted binding interface between Roq1 YYFV and Ubr1 residues Y823, L690 and I687. Roq1-Ubr1 binding was visualized by me.
(E) As in panel (D), but with Ubr1 hydrophobicity map. Roq1 YYFV docks into a hydrophobic groove (beige) formed by Ubr1 residues Y823, I687 and L690. Note that L690 is buried within the Ubr1 structure and was therefore not used for subsequent mutations. Roq1-Ubr1 binding was visualized by me.
(F) Pho8 immunoblot from Pho8* ubiquitination assays with FLAG-Ubr1 (I687D/Y823D) mutant. Roq1 (22-60)-HA or Roq1 (22 aa) were added at 10-fold molar excess over FLAG-Ubr1 or FLAG-Ubr1 (I687D/Y823D). Pho8* ubiquitination was monitored at 30°C for 90 minutes. Note that while Pho8* ubiquitination is less with FLAG-Ubr1 (I687D/Y823D), Roq1 (22-60)-HA or Roq1 (22 aa) reduce non-ubiquitinated Pho8* levels more efficiently with this Ubr1 variant compared to wild-type. The experiment was conceptualized and performed by me.

3.4.3 *The disordered Ubr1 C-terminus is dispensable for substrate recognition*

Ubr1 as a single subunit RING E3 ligase encompasses a remarkably complex architecture, where many domains fulfil different roles in E2 or substrate recruitment. For example, the UBR-Boxes-1 and 2 bind N-degron substrates, and the UBLC domain regulates Cup9 recognition (Figure 21A; Du *et al.*, 2002; Pane et *al.*, 2021). While being mostly structured, the undefined C-terminus of Ubr1 shows a high disorder tendency and was not resolved in previous cryo-EM structures (Pan *et al.*, 2021). Whether it contains a domain that binds substrates such as misfolded proteins is unclear.

To test this in a systematic manner, I designed Ubr1 truncations lacking parts of the disordered C-terminus and tested their activity in ubiquitination assays (Figure 21B). All of them ubiquitinated R- and F-GFP, including the shortest variant lacking the disordered C-terminus, Ubr1 (1-1812) (Figures 21C+D). Surprisingly, Ubr1 (1-1812) responded to Roq1 and efficiently ubiquitinated Pho8* (Figure 21E). To determine where Pho8* could bind Ubr1, I utilized AlphaFold as a prediction tool. Using Ubr1 (1-1812), Rad6 and Pho8* as template, AlphaFold predicted Pho8* to bind Ubr1 below the RING finger domain (Fig. 21E). The existence of the predicted binding sites still needs to be experimentally confirmed.

In summary, Ubr1 as a complex ubiquitin ligase orchestrates substrate recognition through multiple domains. However, the disordered C-terminus plays no role in the ubiquitination of misfolded proteins such as Pho8*.

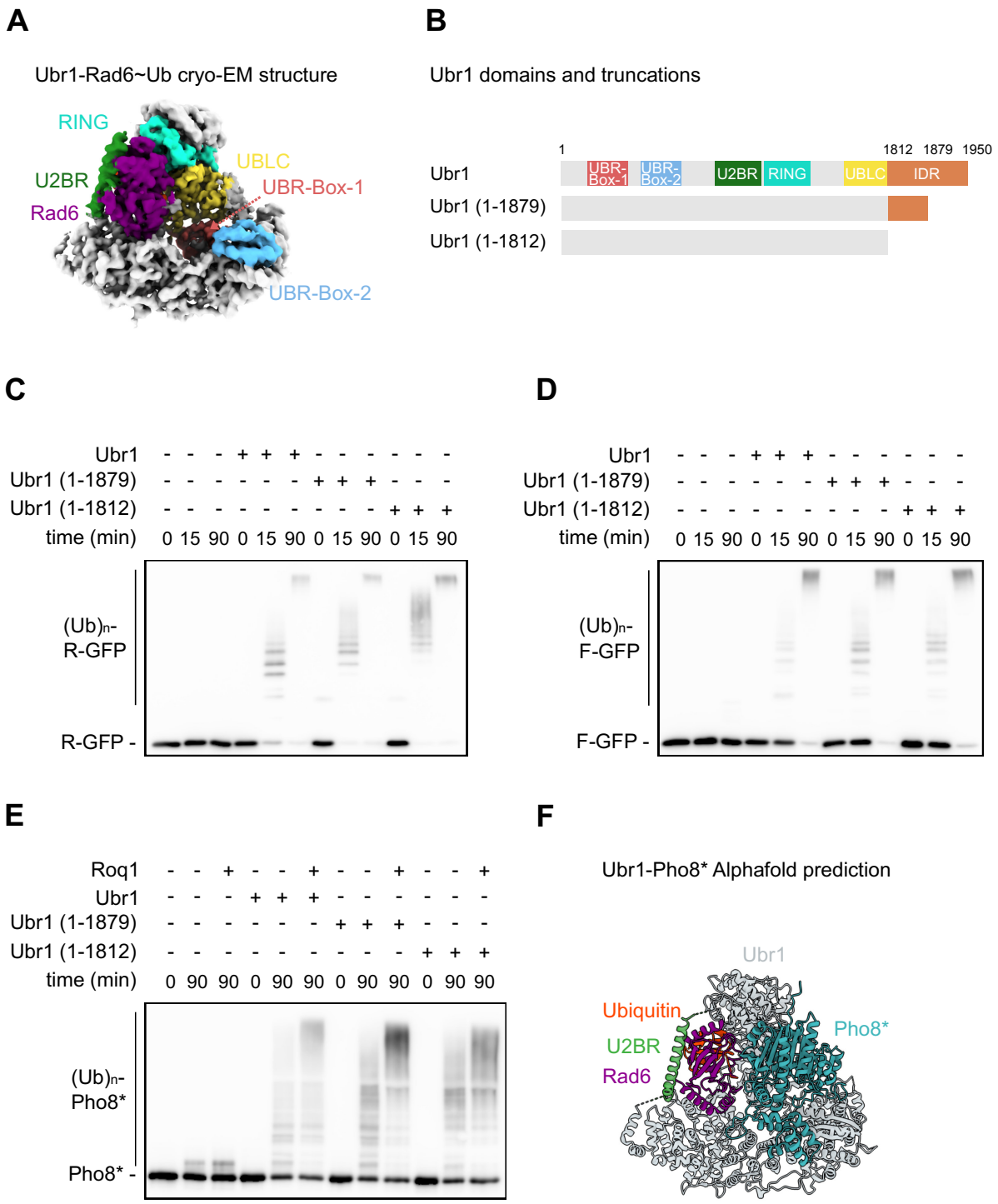

Figure 21. The disordered C-terminus of Ubr1 is dispensable for substrate ubiquitination.
(A) Cryo-EM map of the Ubr1-Rad6~Ub-N-degron complex (EMD: 23806, PDB: 7MEX). Ubr1 domains and Rad6 are highlighted in different colors: UBR1-Box-1 in red, UBR-Box-2 in light blue, UBLC

domain in yellow, RING domain in mint green, U2BR in green, Rad6 in purple. The N-degron substrate and ubiquitin are not visible due to the orientation of the complex in this figure. The EM map was visualized by me.

(B) Cartoon of wild-type Ubr1, its domains and C-terminally truncated Ubr1 variants. Wild-type Ubr1 consists of 1950 amino acid residues. UBR-Box-1 (*red*): residues 115-194, binds type-1 N-degron substrates; UBR-Box-2 (*light blue*): residues 310-382, binds type-2 N-degron substrates; RING domain (*mint green*): residues 1218-1332, interacts with Rad6 and ubiquitin; UBLC (*yellow*): residues 1656-1812, regulates Cup9 binding (Du *et al.*, 2002; Pan *et al.*, 2021; Turner *et al.*, 2000). IDR = intrinsically disordered region, highlighted in orange and with dotted lines. Sequence annotation adapted from (Pan *et al.*, 2021). Ubr1 (1-1879) and Ubr1 (1-1812) represent truncated Ubr1 versions with C-terminal deletions in the disordered region. The cartoon was conceptualized and visualized by me.

(C) GFP immunoblot from R-GFP ubiquitination assays with C-terminally truncated Ubr1 variants. Full-length FLAG-Ubr1, FLAG-Ubr1 (1-1879) and FLAG-Ubr1 (1-1812) were used at equimolar concentrations. R-GFP ubiquitination assays were performed at 30°C for 0, 15 or 90 minutes. The experiment was conceptualized and performed by me.

(D) As in panel (C), but with F-GFP.

(E) Pho8 immunoblot from Pho8* ubiquitination assays with C-terminally truncated Ubr1 variants in absence or presence of Roq1 (22-60)-HA. Full-length FLAG-Ubr1, FLAG-Ubr1 (1-1879) and FLAG-Ubr1 (1-1812) were used at equimolar concentrations. Roq1 (22-60)-HA was added at 10-fold molar excess over Ubr1 variants. Pho8* ubiquitination was monitored at 30°C for 0 or 90 minutes. Note the formation of Pho8* ubiquitination products in absence of Ubr1, which is presumably mediated by Rad6. The experiment was conceptualized and performed by me.

(F) Structural prediction of a Rad6~Ub-Ubr1(1-1812)-Pho8* complex. First, AlphaFold 3 was used to predict the structure of a Rad6-Ubr1 (1-1812)-Pho8* complex in open conformation. Seven zinc ions were added for structural integrity (Pan *et al*, 2021). Next, to bring Ubr1 into the closed conformation and replace Rad6 with Rad6~Ub, I modeled the cryo-EM structure of Ubr1 bound to Rad6~Ub (PDB: 7MEX) into the AlphaFold 3 prediction. Note that Ubr1 residues 1813-1950 are not visible in the 7MEX cryo-EM structure due to the intrinsic disorder of the amino acid residues. The Pho8* binding sites are putative and require experimental validation. Ubr1 is depicted in grey, Rad6 in purple, ubiquitin in orange, and Pho8* in teal. Predictions and modeling were conceptualized and performed by me

4. Discussion

4.1 An updated view on the SHRED pathway

Roq1 profoundly changes Ubr1 activity and substrate specificity during SHRED. The underlying mechanistic principles are not clear. Here, I uncovered through *in vitro* reconstitution experiments the molecular architecture of Roq1 that is needed for Ubr1 reprograming and further identified how Roq1 promotes the ubiquitination of different substrate classes (Figure 22). The simple architecture of Roq1 allows it to engage two gears for efficient communication with Ubr1. First, R22 of Roq1 binds to the UBR-Box-1 as a substrate mimic, in this way blocking type-1 N-degron substrates from binding and activates Ubr1 to effectively ubiquitinate type-2 N-degron substrates and Cup9. Second, binding of the Roq1 hydrophobic motif adds specificity and controls the ubiquitination of misfolded proteins by increasing the Ubr1 ubiquitin chain initiation competence. How Roq1 governs Mgt1 and Chk1 ubiquitination and if this involves the hydrophobic motif or another distinct binding site in Ubr1, is not clear. Altogether, Roq1 comprehensively regulates Ubr1 through its two binding interfaces to achieve maximal SHRED efficacy.

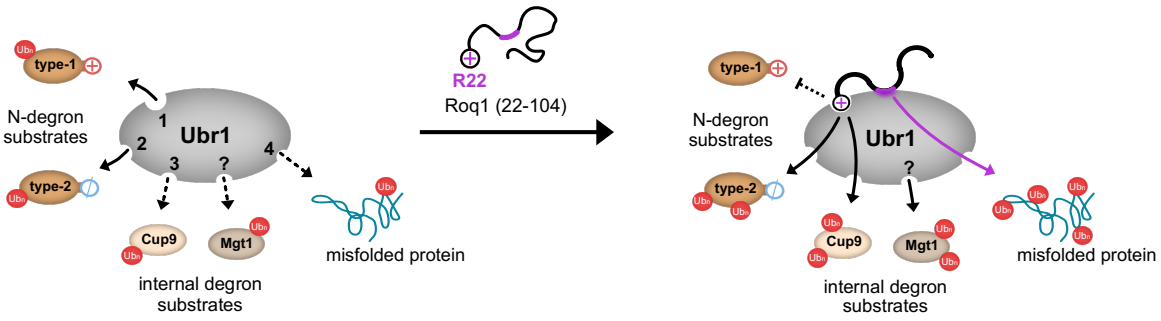

Figure 22. Model how Roq1 reprograms the Ubr1 substrate specificity.
Roq1 (22-104) reprograms the substrate specificity of Ubr1 through heterobivalent binding: It binds with its N-terminal R22 to the UBR-Box-1 and with the hydrophobic YYFV motif to an unknown binding site within Ubr1. R22 binding impairs the ubiquitination of type-1 N-degron substrates but favors type-2 N-degron substrate ubiquitination. Furthermore, R22 stimulates the ubiquitination of native Ubr1 substrates with internal degrons like Cup9. The YYFV motif facilitates the ubiquitin chain initiation of misfolded or unfolded proteins, such as Pho8* or Luciferase^{U}, respectively. Neither R22 nor V58 of the hydrophobic motif promote ubiquitination of endogenous Chk1 and Mgt1, suggesting a different

mechanism by which Roq1 enhances their ubiquitination. Numbers within Ubr1 indicate binding sites for type-1 N-degron substrate (1), type-2 N-degron substrate (2), native substrate Cup9 with internal degron (3) and misfolded or unfolded proteins (4). Note that the binding site for endogenous substrates Chk1 and Mgt1 is not known, and the existence of another binding site is speculative (marked with "?"). $(Ub)_n$ denotes polyubiquitin chains. Conceptualized by Sibylle Kanngießer, Sebastian Schuck and me and further modified by me. Modified from (Peters *et al.*, 2024).

4.2 Translating Roq1-Ubr1 function from *in vitro* to *in vivo*

4.2.1 Roq1 ubiquitination

How can the findings about the *in vitro* Roq1-Ubr1 relationship be translated to its roles *in vivo*? I could demonstrate that Ubr1 ubiquitinates Roq1 *in vitro* (Figure 4). Roq1 ubiquitination, however, is dispensable for reprograming Ubr1, as ubiquitination-deficient Roq1 (22-60) still reprograms Ubr1 (Figure 6A). These observations raise the following two questions: 1) Does Ubr1 ubiquitinate Roq1 *in vivo*? 2) If so, does Ubr1 mediate the subsequent degradation of Roq1? Preliminary experiments performed by Rafael Salazar point towards a ubiquitination of Roq1 *in vivo*, albeit independently of Ubr1 (not shown). A promising candidate ubiquitin ligase to ubiquitinate Roq1 in cells is San1. It shares a similar substrate spectrum with Ubr1 and recognizes stretches of hydrophobic amino acids such as those of the Roq1 hydrophobic motif as degrons (Breckel & Hochstrasser, 2021; Fredrickson *et al.*, 2011). Sibylle Kanngießer, however, could demonstrate that Roq1 stability in yeast cells is unaffected by San1 (not shown).

Which other known yeast E2/E3 pair could, at least in theory, ubiquitinate Roq1? The Rad6/Ubr1 pair ubiquitinates Roq1 on serine or threonine residues (Figure 4). Cleaved Roq1 has been shown to get ubiquitinated independently of Ubr1 *in vivo,* despite having no lysines. Non-lysine ubiquitination is a rapidly growing field of study, that has primarily focused on higher eukaryotes and still lacks insight for lower eukaryotes such as yeast (Dikic & Schulman, 2022). However, one described yeast pair that mediates non-lysine ubiquitination is the Ubc6-Ubc7/Doa10 E2/E3 complex. Its main role lies in the ERAD pathway but has also been shown to ubiquitinate a lysine-free variant of the inner nuclear membrane protein Asi2 (Boban *et al*, 2015; Swanson *et al*, 2001). Additionally, Doa10 targets degrons consisting of amphipathic alpha-helices with hydrophobic residues, making the Roq1 hydrophobic motif a

promising degron candidate (Wu *et al.*, 2024). This is further supported by Sibylle Kanngießer's observation that mutations in the Roq1 hydrophobic motif make the protein more stable (not shown). If Doa10 ubiquitinated Roq1 and thus affected Roq1 degradation, its deletion should prolong SHRED activity *in vivo*. Doa10 deletion, however, did not affect SHRED activity in cells (Szoradi *et al.*, 2018). Thus, it remains enigmatic which ubiquitin ligase mediates Roq1 ubiquitination and its subsequent proteasomal degradation. However, Roq1 ubiquitination seems to be uncoupled from Roq1 function, given that Roq1 (22-60) lacks potential ubiquitination sites but still promotes the degradation of misfolded proteins *in vivo* (demonstrated by Rafael Salazar, not shown).

4.2.2 Ubr1 substrates

Ubr1 recognizes and ubiquitinates three different sets of substrates in my reconstituted *in vitro* system: Misfolded model proteins such as Pho8* or unfolded Luciferase^{U}, N-degron substrates like R- or F-GFP and substrates with internal degrons such as Cup9, Mgt1 or Chk1. I could further demonstrate that Roq1 promotes through Ubr1 the ubiquitination of misfolded proteins, type-2 N-degron substrates and substrates with internal degrons but blocks type-1 N-degron substrate ubiquitination (Figures 5, 7, 8). How can these *in vitro* findings be translated *in vivo* and what role does the Roq1-Ubr1 complex play as a specialized utensil to finetune the degradation of distinct substrate classes during PQC in yeast?

As a first substrate category, Ubr1 binds and ubiquitinates Pho8* and Luciferase^{U} that mimic misfolded and unfolded cytosolic proteins, respectively (Figures 5, 16). Do other ubiquitin ligases contribute to the degradation of such SHRED substrates *in vivo*? In yeast, Doa10, Rsp5, Hul5 and Ubr2 also fulfill dedicated, partially overlapping PQC tasks in ubiquitinating misfolded cytosolic proteins or ER-associated proteins with cytosolic domains (Carvalho *et al*, 2006; Fang *et al.*, 2014; Fang *et al.*, 2011; Nillegoda *et al.*, 2010). In addition, nuclear San1 shares an overlapping substrate spectrum with Ubr1, which also partially resides in the nucleus (Heck *et al.*, 2010; Prasad *et al.*, 2018; Samant *et al.*, 2018). San1 deletion only had mild effects on Pho8* reporter degradation, whereas Ubr2 and Doa10 had no effects, as previously determined (Szoradi *et al.*, 2018). The involvement of Rsp5 or Hul5

was not tested. Despite sharing a significant overlap with other ubiquitin ligases in ubiquitinating misfolded substrates, degradation of Pho8* in yeast seems to be almost entirely specific for Ubr1, underpinning the finetuning of this PQC pathway for substrate-specific demands.

As a second type of substrates, I demonstrated that Ubr1 ubiquitinates type-1/2 N-degron substrates *in vitro*. Roq1 inhibited type-1 N-degron substrate ubiquitination and promoted type-2 N-degron substrate ubiquitination though occupancy of the UBR-Box-1 (Figure 8). These results confirm previous observations in yeast where Roq1 modulated the degradation of ubiquitin-fused model N-degron substrates (Szoradi *et al.*, 2018).

Cup9, which possesses an internal degron, gets ubiquitinated by Ubr1 *in vitro*. Addition of Roq1 promoted further Cup9 ubiquitination (Figure 7A). In contrast, Roq1 restrains Cup9 degradation in yeast (Szoradi *et al.*, 2018). How can these discrepancies be explained? *In vivo*, where multiple potential substrates are present and various cellular conditions apply, Ubr1 might undergo a triage decision and only drive the ubiquitination of a distinct, preferred substrate set. Consequently, my *in vitro* assays could therefore enforce a Roq1-driven enhanced ubiquitination of Cup9, which might not occur *in vivo*. Alternatively, Ubr1 needs to be phosphorylated at position S300 by the YCK1/2 kinases to degrade Cup9 (Hwang & Varshavsky, 2008). Overexpression of Roq1 or application of ER stress might therefore affect the Ubr1 phosphorylation status by changing YCK1/2 activity, perhaps even by stimulating its degradation. *In vitro*, where the Ubr1 phosphorylation status does not change, presence of Roq1 might therefore cause Ubr1 activation towards Cup9, which would not occur *in vivo*. In addition, Cup9 forms a complex with Ssn6 and Tup1 *in vivo,* and each can compensate the loss of the other to retain activity (Xia *et al*, 2008a). As such, degradation of Cup9 alone might therefore be not sufficient to disrupt the activity. This could be an explanation why Ubr1 ubiquitinates Cup9 *in vitro*, since Ssn6-Tup9 alone would compensate for a loss of Cup9 *in vivo*. Altogether, the discrepancies between the Cup9 ubiquitination *in vitro* and its suggested stabilization in cells might be due to the limitations of the *in vitro* assay system, which does not sufficiently reflect cellular conditions.

Similar to Cup9, Ubr1 recognizes Mgt1 through an internal degron (Hwang *et al.*, 2009). I could demonstrate that Ubr1 ubiquitinated Mgt1 *in vitro* and that Roq1 enhanced the ubiquitination (Figure 7B). How could these findings be further

evaluated *in vitro*? Mgt1 protects DNA integrity by restoring damage-induced alkylated DNA through self-alkylation (Hwang *et al.*, 2009). Alkylated Mgt1 gets much faster degraded in yeast than native Mgt1. Thus, I would expect that an alkylated mimic of Mgt1 should get much more rapidly ubiquitinated *in vitro* than wild type. To test this, I could make use of Mgt1 (C151M), which mimics Mgt1 alkylation and that has been used previously to monitor Mgt1 degradation in yeast (Hwang *et al.*, 2009). Alkylated Mgt1 is degraded through synergistic effects of the Ubr1/Ufd4 pathways (Hwang *et al.*, 2010a). Thus, for a comprehensive dissection *in vitro* it will be important to consider contributions of the Ubc4/Ufd4 E2/E3 pair as well. What effect could Roq1 have on Mgt1 degradation in yeast cells? To answer this, I envision a cycloheximide chase experiment to monitor Mgt1 levels in yeast cells treated with the DNA alkylation damage inducer MNNG. If Roq1 directly acts on Ubr1 to degrade alkylated Mgt1, its overexpression should lead to a more rapid Mgt1 decay, and its deletion should slow down the degradation. Together, my *in vitro* data suggest that Roq1 governs the ubiquitination of Mgt1 as an endogenous Ubr1 substrate, which still needs to be further analyzed *in vivo*.

Ubr1 recognizes the mitotic checkpoint kinase Chk1 in a similar manner as Cup9 or Mgt1 through an internal degron. I could demonstrate that Ubr1 ubiquitinates Chk1 *in vitro*, which Roq1 could further enhance (Figure 7C). How are Chk1 levels regulated *in vivo* and what might be the influence of the Roq1 on its stability? *In vivo*, the Chk1 degron is protected from degradation by acetylated Hsp90 (Oh *et al.*, 2017). If acetylation of Hsp90 fails, for instance by deletion of the N-terminal acetyltransferase subunit Naa10, the Chk1 degron is no longer protected. Thus, Ubr1 subsequently targets Chk1 via the accessible degron for proteasomal degradation. It is therefore not surprising that Ubr1 recognizes Chk1 in my *in vitro* assay setup, which lacks chaperones. It is therefore tempting to speculate whether addition of Hsp90 would shield Chk1 from getting ubiquitinated. To probe for any effects of Roq1 on cellular Chk1 levels, I would make use of a previously described Chk1 reporter construct and monitor its stability in *naa10*∆ cells (Oh *et al.*, 2017). If Roq1 promotes Chk1 degradation, inducible overexpression of Roq1 (22-104) should accelerate its breakdown.

Altogether, Roq1 governed the ubiquitination of misfolded proteins and N-degron substrates through Ubr1 *in vitro*, which agrees with the *in vivo* findings of altered substrate stability. In contrast, how Roq1 mediates the degradation of substrates with

internal degrons is not yet fully clear. While *in vivo* experiments suggest that Roq1 stabilizes Cup9, this could not be confirmed *in vitro*. Mgt1 and Chk1, which also possess internal degrons, showed enhanced ubiquitination in presence of Roq1. Whether Roq1 also influences their degradation in cells requires further testing.

4.2.3 The role of chaperones

To degrade cytosolic substrates in yeast, Ubr1 needs the Hsp70 chaperones Ssa1 and Ssa2, the Hsp40 co-chaperones Sis1 and Ydj1, and the Hsp110 nucleotide exchange factor Sse1 (Breckel & Hochstrasser, 2021; Heck *et al.*, 2010; Prasad *et al.*, 2018). Strikingly, Ubr1 did not require chaperones in my reconstituted assays to ubiquitinate its substrates, which is in line with previous observations (Nillegoda *et al.*, 2010). Why are chaperones needed *in vivo* but not *in vitro*? Hsp70 chaperones such as Ssa1 or Ssa2 prevent protein aggregation but promote native protein folding to maintain protein solubility (Kim *et al.*, 2013). Particularly misfolded or unfolded proteins such as Pho8* or Luciferase^{U}, which I employed in my *in vitro* assays, might be prone to form insoluble aggregates. However, both remained soluble throughout the course of my ubiquitination assays and Ubr1 ubiquitinated them efficiently (Figures 6D, E). Intriguingly, ubiquitination reactions using Pho8* or Luciferase^{U}, but not F- or R-GFP, plateaued after 30 to 60 minutes, with nonubiquitinated substrate remaining (Figures 5, 8). The remaining portion could represent a partially aggregated but still soluble substrate species where the degron for Ubr1 recognition is not exposed, explaining why ubiquitination did not go to full completion. Addition of Ssa1 or Ssa2 to ubiquitination assays might increase Pho8* and Luciferase^{U} solubility and degron accessibility by Ubr1, thus intensifying total ubiquitination efficiency. Of note, previous attempts supplying Ubr1 ubiquitination assays with Ssa1, Ydj1 or Ss1 failed due to Ubr1 ubiquitinating them (Chi-Ting Ho, not published).

In contrast to Pho8* or Luciferase^{U}, Chk1 represents a native Ubr1 substrate, whose internal degron is masked by acetylated Hsp90 in yeast and therefore protected from degradation (Oh *et al.*, 2017). In absence of Hsp90, such as in my *in vitro* assays, the internal Chk1 degron is exposed, allowing recognition and subsequent ubiquitination by Ubr1. Conversely, addition of Hsp90 should shield the degron and prevent Ubr1

ubiquitination, assuming Hsp90 would not compete with Chk1 for ubiquitination by Ubr1.

Similar to Chk1, the transcription factor Kar4, the transcriptional regulator Tup1, the glycerol synthesis enzyme Gpd1 and the signal transduction kinase Ste11 are all Hsp90 clients with internal degrons whose degradation by Ubr1 is enhanced in cells lacking Naa10 (Oh *et al.*, 2017). Thus, testing them in my *in vitro* ubiquitination assays will be a promising approach to identify novel endogenous Ubr1 substrates whose ubiquitination status could be governed by Roq1.

Ydj1 and Sis1, as well as the NEF Sse1 assist in protein folding, but also in shuttling misfolded cytosolic substrates to the nucleus, where a significant fraction of Ubr1 and proteasomes reside (Prasad *et al.*, 2018; Wojcik & DeMartino, 2003). Given that Ynm3 and, to some extent, Ubr1 localize in the nucleus, but misfolded SHRED substrates are cytosolic, how are the spatio-temporal events during SHRED orchestrated? Given that the first couple of N-terminal Roq1 residues are conserved (Figure 11C), they might harbor an unconventional nuclear localization signal. Combined with its small size, this might allow Roq1 during proteotoxic stress to freely enter the nucleus, undergo Ynm3 cleavage and bind nuclear Ubr1 for reprograming. Ydj1, Sis1 and Sse1 could keep misfolded substrate soluble, translocate them into the nucleus where they bind reprogramed Ubr1 and get subsequently degraded by the proteasome. In an alternative hypothesis, misfolded cytosolic but ER-associated SHRED substrates could get polyubiquitinated by a cytosolic Ubr1 pool before getting extracted by CDC48 and degraded by cytosolic proteasomes (Ji *et al*, 2022; Szoradi *et al.*, 2018; Wojcik & DeMartino, 2003). Noteworthy, Ubr1 has no attributed role in nuclear PQC in mammals, which raises the question how a mammalian SHRED pathway would degrade its substrates (Breckel & Hochstrasser, 2021).

Hsp70 chaperones bind short peptide sequences enriched with hydrophobic amino acid residues (Mayer & Gierasch, 2019; Rudiger *et al*, 1997a; Rudiger *et al*, 1997b). Hence, the Roq1 hydrophobic motif might be a target of Hsp70 chaperones. To test whether Hsp70 chaperones bind the hydrophobic motif, purified Ssa1 or Ssa2 could be used together with wild type Roq1 or hydrophobic motif mutants in pulldown experiments. If Ssa1/2 bound Roq1 via the hydrophobic motif, I would expect complex formation for wild type Roq1 but not hydrophobic motif mutants. How could this be translated to cellular settings? *ROQ1* transcription is stimulated upon proteotoxic stress. With emerging protein folding stress, there might be a pool of free

Ssa1/2 that can bind newly translated Roq1 and prevent it from activating Ubr1. Under such conditions, substrate-chaperone complexes might facilitate protein refolding rather than degradation. When protein folding stress further continues and the Ssa1/2 demand for misfolded proteins becomes limiting, they might dissociate from Roq1. Free Roq1 could then bind Ubr1 for reprograming to shift the cellular commitment from protein refolding toward protein degradation. Thus, Roq1 could act as a molecular switch in PQC triage decisions and determine whether a damaged protein is refolded or terminally degraded.

4.3 The importance of short linear hydrophobic motifs for Roq1 function

Roq1 extensively regulates Ubr1, despite its simple anatomy. Its main characteristics are the N-terminal R22 and a hydrophobic motif. Both are referred to as short linear hydrophobic motifs (SLiMs). They are short stretches of linear peptide motifs in intrinsically disordered proteins that typically consist of 3-10 amino acid residues (Davey *et al*, 2012). SLiMs are devoid of a three-dimensional structure but can form a stable conformation through binding scaffolding proteins (Van Roey *et al*, 2014), even though they can also remain completely disordered during binding (Heidarsson *et al*, 2022). Their interaction with other proteins ranges from steady over “fuzzy” and includes hydrogen bonding, electrostatic interactions or hydrophobic interfaces (Robustelli *et al*, 2020; Sharma *et al*, 2015; Tompa & Fuxreiter, 2008). SLiMs can be divided into two major groups according to their function: Ligand motifs for protein interactions and modification motifs that are targets for PTMs (Van Roey *et al.*, 2014). Ligand motifs can serve as ligands for protein anchoring but also as degrons for degradation. Modification motifs recruit enzymes for subsequent binding of a PTM moiety such as ubiquitin or proteolytic cleavage. SLiMs functioning as ligand or modification motif is not mutually exclusive. Despite being a small protein, the SLiMs of Roq1 fulfill numerous purposes: Full length Roq1 gets proteolytically processed by the endopeptidase Ynm3 at a conserved IL*RSQR sequence (with * denoting the cleavage location; Figure 11C), leading to an exposed R22 that binds Ubr1 as a ligand. Moreover, mutation of hydrophobic motif residues stabilized Roq1 *in vivo*, indicating that it might serve as a degron for Roq1 degradation. This would allow a cell to quickly adjust Roq1 levels.

R22 and the hydrophobic motif function as ligands for binding Ubr1. The disordered linker region connecting R22 and the hydrophobic motif allows maximum flexibility and therefore robust recognition of each ligand by Ubr1. While each SLiM on its own has low binding affinity to Ubr1, it is the heterobivalent binding mechanism that creates avidity to strongly bind and stimulate Ubr1. Cooperative binding ensures that R22 can outcompete type-1 N-degron substrates for UBR-Box-1 binding (Figure 8A). A similar mechanism has been described for the intrinsically disordered adenovirus protein E1A (Gonzalez-Foutel *et al*, 2022). E1A hijacks the eukaryotic cell cycle by binding the retinoblastoma tumor repressor protein Rb in low picomolar affinity with its two SLiMs that are connected by a disordered linker. This displaces the E2F transcription factor, allows S phase entry and promotes viral genome replication.
Regardless of its plain architecture, the multifunctional SLiMs of Roq1 add the necessary complexity for a comprehensive reprograming of Ubr1.

4.4 How could Roq1 reprogram Ubr1?

4.5.1 Role of the hydrophobic motif for the ubiquitination of Ubr1 substrates

Roq1 R22 and the hydrophobic motif are SLiMs that create avidity for a substrate-specific regulation of Ubr1 via two gears: R22 determines the efficacy for type-1/2 N-degron substrate and Cup9 ubiquitination, and the hydrophobic motif stimulates the ubiquitination of misfolded proteins. Whether the hydrophobic motif is the driving force of Roq1 to enhance Mgt1 and Chk1 ubiquitination is not clear. Mgt1 and Chk1 ubiquitination is not promoted by RA or LA dipeptides that bind to the UBR-Boxes, which highlights the necessity of another functional element in Roq1 that is crucial for Ubr1 reprograming (Figures 10B, C). Roq1 V58, which is part of the hydrophobic motif and required to achieve efficient ubiquitination of misfolded proteins, seems to be dispensable for Mgt1 and Chk1 ubiquitination (Figure 14). Are, to achieve enhanced Mgt1 or Chk1 ubiquitination, other hydrophobic motif residues functionally relevant? To investigate this in a systematic manner, I propose to mutate Y55, Y56, F57 and flanking residues of the hydrophobic motif to single point mutants with charged amino acid residues. By testing these constructs in *in vitro* ubiquitination assays using Mgt1, Chk1 and misfolded protein substrates, I hope to determine 1)

which hydrophobic motif residues are more relevant than others, 2) if amino acids close to the hydrophobic motif are involved in Ubr1 reprograming and 3) if the hydrophobic motif governs Mgt1 and Chk1 ubiquitination. Addressing the last point will further define if Ubr1 reprograming by the hydrophobic motif not also upregulates the ubiquitination of endogenous substrates with internal degrons.

Crucial for a better understanding of Ubr1 reprograming is to identify where the hydrophobic motif binds Ubr1. A further characterization of the Roq1-Ubr1 binding interface represents a valuable proof of concept and enables the deduction of a potential mechanism conservation among higher eukaryotes (see section 4.6). To map the hydrophobic motif-Ubr1 binding interface, I have employed with Bram Vermeulen an AlphaFold Multimer-based prediction strategy, which led to the identification of Ubr1 residues to which Roq1 binds nonspecifically (Figure 20). Elimination of the nonspecific binding interface enhanced Ubr1 association (performed by Sibylle Kanngießer, not shown) and Pho8* ubiquitination. This observation implies that the hydrophobic motif, which is connected with R22 through a dynamic 32-residue long linker, can reach far distances and scans the Ubr1 surface for potential hydrophobic interaction sites. Similar observations have been made for charged patches in intrinsically disordered protein regions that can bind complementary charged regions of folded protein domains (Chen *et al*, 2017a; Martin *et al*, 2021; Mittal *et al*, 2018). In terms of the authentic Roq1-Ubr1 binding site, employing the latest version of AlphaFold and obtaining a low resolution cryo-EM structure of a Roq1-Ubr1 complex did not lead to promising results I could confirm experimentally. However, binding of the Roq1 hydrophobic motif to the UBR-Box-2 seems rather unlikely, given that UBR-Box-2 mutations did not affect SHRED activity *in vivo (*Szoradi *et al., 2018)*.

To gain further insight into the properties of Roq1-Ubr1 binding, I propose a broader biochemical characterization of the Roq1 hydrophobic motif that goes beyond the identification of involved amino acid residues. If the YYFV motif binds Ubr1 through a hydrophobic patch, why does Roq1 possess two tyrosines at position 55 and 56, which are less hydrophobic than phenylalanines, for instance? To test whether exclusively the hydrophobicity of Y55 or Y56 is crucial to bind Ubr1, I propose mutating both to phenylalanines. In contrast to phenylalanines, tryosines can serve through their hydroxyl groups as hydrogen bond acceptor or donor, which could be

relevant for Ubr1 binding. Thus, replacing them with phenylalanines will provide more biochemical information about binding properties.

Altogether, the Roq1 hydrophobic motif binds an unknown binding site in Ubr1, which causes Ubr1 to efficiently ubiquitinate misfolded proteins. Whether the hydrophobic motif also enhances the ubiquitination of substrates with internal degrons, such as Mgt1 or Chk1, could become clearer by a thorough biochemical and structural characterization of the hydrophobic motif and the identification of involved Ubr1 residues.

4.5.2 The importance of a closed Rad6~Ub-Ubr1 conformation

How could Roq1 reprogram the RING ubiquitin ligase Ubr1 on a mechanistic level? RING ubiquitin ligases directly transfer ubiquitin from bound E2s to substrate via a universal mechanism, which involves the adoption of a closed conformation. The binding of proteins or ligands to RING ubiquitin ligases triggers an allosteric switch that promotes the closed conformation and thereby accelerates ubiquitin transfer (DaRosa *et al.*, 2015; Wright *et al*, 2016). According to this, Roq1 binding could uncover a potential non-RING element in Ubr1 that is relevant for ubiquitin binding and achieving the closed Rad6~Ub-Ubr1 conformation, which ultimately stimulates ubiquitin transfer. Similar processes have been described for zinc finger and additional binding domains outside of the RING domain that interact through a second, backside binding event with E2~Ub (Buetow *et al.*, 2015; Das *et al.*, 2009; Dou *et al*, 2013; Middleton *et al.*, 2023). Intriguingly, backside binding to Rad6 has been reported to modulate ubiquitin chain building activity (Hibbert *et al*, 2011; Kumar *et al.*, 2015; Pan *et al.*, 2021; Siepmann *et al*, 2003; Turco *et al.*, 2015). Indeed, Roq1 promoted ubiquitin transfer in single turnover Rad6~Ub discharge assays, which implies a role in achieving the closed Rad6~Ub-Ubr1 conformation (Figures 15B-D). To identify whether the hydrophobic motif favors the closed conformation, it will be crucial to include Roq1 variants with a disrupted hydrophobic motif in my discharge assays as well.

In contrast to the discharge assays, Roq1 had no effect on the recruitment of uncharged Rad6 to Ubr1, as shown in my Rad6-Ubr1 pulldown experiments (Figure 15A) and biolayer interferometry data from by Sibylle Kanngießer. In addition, Roq1

did not stabilize the flexible Rad6-binding UB2R domain of Ubr1 in my Roq1-Ubr1 cryo-EM structure (compare Figures 19D+G with Figure 21A). Both observations might stem from absent Rad6~Ub. Ubiquitin ligases only bind E2s that are charged with ubiquitin to obtain a stable conformation, with few exceptions (Xie & Varshavsky, 1999). Thus, performing cryo-EM and binding experiments with Rad6~Ub will mimic the natural interaction between Ubr1 and its cognate Rad6~Ub enzyme and might reveal whether Roq1 favors a closed Rad6~Ub-Ubr1 conformation. To engineer a E2~Ub thioester mimic that withstands harsh experimental conditions, the active site cysteine of Rad6 could be replaced with a lysine to create a stable amide bond between the introduced lysine and the C-terminus of ubiquitin, as previously described (Plechanovova *et al.*, 2012).

Altogether, the RING ubiquitin ligase Ubr1 acquires with its cognate ubiquitin conjugating enzyme Rad6 a closed conformation that allows efficient ubiquitin transfer. Whether Roq1 promotes the closed conformation assembly by recruiting Rad6~Ub is not clear and requires further optimization of experimental conditions.

4.5.3 Substrate recruitment

Alternatively, or in addition to Rad6~Ub recruitment, Roq1 could also promote substrate recruitment, presumably via allosteric changes within Ubr1. This could be facilitated through an autoinhibitory release of a binding site similar to that of Cup9, which could explain the accelerated substrate ubiquitination once Roq1 binds. Substrate recruitment assays aiming to test this hypothesis showed that misfolded Pho8* bound stronger to Ubr1 than Pho8 (Figure 16), which was expected given that Ubr1 preferentially ubiquitinates Pho8*. However, Roq1 had no effect on Pho8* or Pho8 recruitment in my pulldowns and biolayer interferometry experiments done by Sibylle Kanngießer remained inconclusive. Taken together, a role of Roq1 in substrate recruitment seems unlikely, given that Roq1 activates, apart from type-1 N-degron substrates that directly compete with Roq1 for binding, the ubiquitination of all other tested Ubr1 substrates. This points rather toward generic effects on Rad6 recruitment or ubiquitin transfer than substrate-specific recruitment.

Where do substrates bind Ubr1? While the UBR-Box-1/2 domains are well mapped, it is unknown where misfolded proteins such as Pho8* or substrates with internal

degrons like Mgt1 or Chk1 bind Ubr1. Identifying their binding interface will help understanding 1) if they share overlapping binding sites and 2) whether the Roq1 hydrophobic motif adds substrate specificity. While the intrinsically disordered C-terminal region of Ubr1 plays no role in N-degron or Pho8* ubiquitination (Figures 21C-E), preliminary computational predictions using AlphaFold3 propose a distinct binding interface for Pho8* between the Ubr1 RING and UBR-Box domains (Figure 21F), which still needs to be confirmed experimentally.

Altogether, thorough mapping of Ubr1-substrate binding sites will determine if misfolded proteins and those with internal degrons share overlapping bindings sites. Moreover, it could illuminate how Roq1 stimulates the ubiquitination of both substrate classes.

4.5.4 Ubiquitin chain initiation versus chain elongation

How does Roq1 stimulate substrate ubiquitination, given that both Rad6 and substrate recruitment appear to be unaffected? Rather than changing Rad6 or substrate affinities, Roq1 promotes ubiquitin chain initiation and possibly chain elongation of misfolded proteins, type-2 N-degron substrates and substrates with internal degrons (Figure 17). How can these findings be compared with the ubiquitination features of other ubiquitin ligases?

Ubiquitin chain initiation at multiple substrate lysine residues appears to happen with little sequence dependency for ubiquitin ligases (Fischer *et al.*, 2011; Petroski & Deshaies, 2003; Tang *et al.*, 2007), with recent exceptions (Li *et al*, 2024). In contrast, the processivity of polyubiquitin chain building is more specific due to the spatial monoubiquitin arrangement (Nakasone *et al.*, 2022). In terms of the Roq1-Ubr1 pair, the enhanced efficacy for multi-monoubiquitination could result in more spatially directed ubiquitin priming in the closed conformation, resulting in faster ubiquitin chain building and enhanced solubility of misfolded protein substrates. For a better understanding of the underlying chain initiation processes, it is therefore essential to identify the substrate lysine residues that Ubr1 ubiquitinates.

The hypothesis that Roq1 spatially directs ubiquitin chain initiation further raises the question whether a substrate binds Ubr1 in a single or via multiple encounters. Most substrate-E3 encounters are not fruitful, but once bound multiple ubiquitin molecules

can be transferred to a substrate in a single encounter, which increases overall ubiquitination efficiency (Pierce *et al.*, 2009; Saha & Deshaies, 2008). Thus, probing the effect of Roq1 on Ubr1-substrate encounters will not only be informative with regards to the number of binding events, but also in terms of ubiquitination efficiency.

Attaching the first ubiquitin to a substrate is the slowest stride during ubiquitin chain building (Pierce *et al.*, 2009). Once ubiquitin priming is achieved, the polyubiquitination efficiency is determined by the ratio of chain building vs. substrate dissociation rates, which typically results in fast ubiquitin chain elongation. In contrast to other ubiquitin ligases, Ubr1 displays slightly faster chain initiation than elongation kinetics (Pan *et al.*, 2021; Petroski & Deshaies, 2005; Saha & Deshaies, 2008). Roq1 binding to Ubr1 further accelerated the ubiquitin priming step similarly as neddylation of $CRL1^{ß\text{-}TRP}$ (Baek *et al.*, 2020). However, it remains unclear whether Roq1 also affects Ubr1 substrate chain elongation. To probe for Roq1 effects exclusively on chain building activity ubiquitin chain initiation needs to be uncoupled from elongation. This is particularly challenging since there is no Ubr1 model substrate that would allow uncoupling. To generate such a model substrate, all but one potential substrate ubiquitination site need to be replaced to solely focus on one spatial ubiquitination event. A promising candidate protein is Chk1, whose degron and ubiquitination sites were previously mapped using *in vitro* ubiquitination assays (Oh *et al.*, 2017). While the previously described K(0) ubiquitin variant can be used to monitor monoubiquitination, a ubiquitin-primed substrate variant is required to study polyubiquitination. A recent purification strategy demonstrated a successful generation of monoubiquitinated substrates using a modified N-terminally twin-Strep tagged ubiquitin variant that allowed chromatographic separation of monoubiquitinated from polyubiquitinated substrate species due to avidity effects (Nelson *et al*, 2023). Such a purified monoubiquitinated substrate could then be used in subsequent ubiquitination assays to determine if Roq1 controls ubiquitin chain elongation as well.

With growing ubiquitin chain length, there is an increased demand to limit the conformational freedom of the chain to ideally position the distal acceptor ubiquitin for further chain elongation. In Ubr1, this is mediated through the ubiquitin binding loop motif (UBLM), which binds the acceptor ubiquitin and orients it for polyubiquitination (Pan *et al.*, 2021). If Roq1 also affects chain elongation, could this be achieved through the UBLM? Preliminary attempts by me to mutate the UBLM to impair

polyubiquitination were inconclusive (not shown) and await further investigation. However, future experiments could provide valuable information whether Roq1 controls ubiquitin chain elongation via the UBLM.

Alternatively, or in addition to re-positioning of the distal ubiquitin acceptor, ubiquitin chain specificity can also be met by different E2/E3 pairs for substrate priming and elongation (Bodrug *et al*, 2023; Martinez-Chacin *et al*, 2020; Scott *et al*, 2016). The Rad6/Ubr1 complex physically interacts in physiological settings with the Ubc4/Ufd4 pair to increase the efficacy of N-degron substrate, Cup9 and Mgt1 polyubiquitination (Hwang *et al.*, 2010a). Despite the unlikelihood of a direct physical interaction, Roq1 could allosterically manipulate Ubc4/Ufd4 through Ubr1. Thus, it is required to test via *in vitro* ubiquitination and substrate binding assays whether Roq1 governs through Ubr1 the Ubc4/Ufd4 complex to stimulate further ubiquitin chain elongation.

Polyubiquitination results in distinct ubiquitin chain linkage types, which are hallmark signals for the physiological fate of a substrate. Ubr1 mainly generates K48-linked polyubiquitination that encode for proteasomal degradation, which was unaffected by Roq1 (Figure 18; Pan *et al*, 2021). Strikingly, despite using elongation-deficient K(0) ubiquitin, Ubr1 polyubiquitinated Mgt1 (Figure 17D). The reason for this unusual behavior is not clear. According to one hypothesis, Ubr1 could also form polyubiquitin chains by connecting the C-terminus of an ubiquitin donor with the N-terminal methionine of the ubiquitin acceptor, similar to the LUBAC E3 ligase complex (Kirisako *et al.*, 2006). Testing this hypothesis requires a K(0) ubiquitin variant with a masked N-terminus to prevent M1-ubiquitination, such as methylated K(0) ubiquitin. Using such a ubiquitin variant in my *in vitro* ubiquitination assays will determine whether Ubr1 also forms linear M1-ubiquitin chains that could be an explanation for the unusual Mgt1 polyubiquitination pattern.

Altogether, Roq1 regulates Ubr1 activity and substrate specificity by promoting ubiquitin chain initiation. Whether Roq1 also promotes ubiquitin chain elongation remains unclear. Addressing this requires uncoupling of ubiquitin priming from chain elongation and further biochemical and structural dissection of Ubr1.

4.5.5 Structural insights via cryo-EM

Gaining structural insight into the Roq1-Ubr1 complex could reveal how the hydrophobic motif regulates Ubr1, where it binds and whether Roq1 obtains a constraint 3D structure upon binding. The cryo-EM based strategy I implemented to address these questions led to a low resolution cryo-EM map of the Roq1-Ubr1 complex. In comparison with the previously Rad6~Ub-Ubr1-N-degron cryo-EM structure (PDB: 7MEX), the Roq1-Ubr1 structure had a similar sailboat-like shape but lacked EM density of the Rad6-binding domain UB2R (Figure 19E). Additionally, no prominent EM density for bound Roq1 could be obtained, which could be attributed either to the intrinsic disorder of Roq1 or to a lack of a high-resolution structure. In general, global resolution of the Roq1-Ubr1 complex was limited to particle aggregation and the orientation bias of particles on the grids. To overcome these limitations and improve data quality, future optimizations will include either a different angle in the tilted dataset, a detergent screen to overcome aggregation or the implementation of a GraFix protocol for sample preparation (Kastner *et al*, 2008). The latter method is particularly suitable to isolate labile protein complexes and is gaining increasing attention, as demonstrated with the recent cryo-EM structures of tetrameric Ubr5~MCRS1 and apo Ubr5 (Mark *et al*, 2023; Tsai *et al.*, 2023).

The challenges I faced to obtain a high-resolution structure of the Roq1-Ubr1 complex were comparable with reported attempts to solve the structure of apo Ubr1 (Pan *et al.*, 2021). To overcome locally dispersed resolution biases and sample aggregation the authors reconstituted a ternary Rad6~Ub-Ubr1-N-degron substrate complex. Comparable approaches have been recently employed to solve the structure of a Bre1-Rad6~Ub complex bound to nucleosomes (Deng *et al.*, 2023). Using a similar approach by reconstituting a Rad6~Ub-Ubr1-Roq1 complex might therefore increase the overall changes to obtain a high-resolution structure that provides mechanistic insight into Roq1-mediated Ubr1 reprograming.

Of note, the three-dimensional structure of the Roq1-Ubr1 complex with its sailboat-like shape resembled an object that was intensively studied during the European Space Agency's Rosetta mission, the comet 67P/Churymumov-Gerasimenko (European Space Agency, 2023). The remarkable similarities in their overall shape underpin the conservation of nature's beauty from microscopic proteins on earth to macroscopic comets in the extraterrestrial space.

4.5 Other Roq1-like ubiquitin ligase regulators

Roq1 acts through multifunctional cooperating motifs to regulate Ubr1. Similar mechanisms of ubiquitin ligase regulation have been described in different contexts. For instance, the human C-terminal to LisH (CTLH) 3 complex, a homolog of the yeast GID complex, binds N-degron substrates through interchangeable N-degron substrate receptors. One such receptor, WDR26, binds bona fide substrates with internal basic degrons, such as the NAD^+ sensor NMNAT1 (Canto *et al*, 2015). To regulate NMNAT1 levels, the N-terminus of YPEL5, a CTLH subunit, binds as a substrate mimic to the WDR26-CTLH complex and antagonizes NMNAT1 binding this way (Gottemukkala *et al*, 2024). YPEL5 forms a second binding interface with an adjacent WDR26 receptor domain to create avidity for competitive binding. The multifunctional motifs of YPEL5 are similar to those of Roq1.

Caspases in apoptotic pathways are regulated in a similar manner through a tight interplay between ubiquitin ligases and their modulators. The serine protease HtrA2, a human homolog of yeast Ynm3 and *E. coli* heat shock proteins DegP, DegQ and DegS, resides in the mitochondrial inner membrane but undergoes auto-proteolytic cleavage upon apoptotic stress (Suzuki *et al*, 2001). Its membrane-dissociated form binds with its new N-terminus to the BIR domain of the inhibitor of apoptosis (IAP) RING E3 ligase XIAP, inhibits it and stabilizes this way apoptosis-inducing caspases (Eckelman *et al*, 2008; Martins *et al*, 2002). More mechanistic and structural insight into IAP inhibition and caspase stabilization through degron mimics was recently discovered by cryo-EM structures of the mitochondrial proapoptotic inducer protein SMAC (also known as DIABLO) bound to the hybrid E2/E3 IAP enzyme BIRC6 (Dietz *et al*, 2023; Ehrmann *et al*, 2023; Hunkeler *et al*, 2023; Mace & Day, 2023). Similar to HtrA2 and Roq1, SMAC undergoes proteolytic cleavage upon cellular stress and binds with its new N-terminus the IAPs XIAP and BIRC6 (Ehrmann *et al.*, 2023; Saita *et al*, 2017). BIRC6 inhibition by SMAC, in contrast to XIAP, requires a tripartite binding mode: This involves the SMAC N-degron that binds to the BIR domain, and further interactions between SMAC and CBD-3/CC1 domains of homodimerized BIRC6. This makes SMAC binding nearly irreversible (Ehrmann *et al.*, 2023). In absence of apoptotic stressors, BIRC6 mediates the degradation of N-degron proteases (Bartke *et al*, 2004). The mechanism underlying SMAC-BIRC6 binding therefore shows surprising similarity with a proteolytic processing of Roq1 and how multifunctional binding motifs can regulate a ubiquitin ligase. SMAC, YPEL5, HtrA2

and Roq1 bind their respective ubiquitin ligase through multivalent binding mechanisms. In contrast to Roq1, however, they all inhibit substrate ubiquitination.

A protein that comprehensively governs ubiquitin ligase activity and substrate specificity is the SARS-CoV-2 protein ORF10. It binds via its N-terminus the Cullin-RING ligase $CUL2^{ZYG11B}$, which degrades proteins via the Gln/N-degron pathway (Timms *et al.*, 2019). By mimicking with its N-terminus a Gln/N-degron, ORF10 binds the ZYG11B adaptor and impairs the degradation of Gln/N-degron pathway proteins. In parallel, ORF10 binding promotes the degradation of the intraflagellar transport complex B protein IFT46 (Wang *et al*, 2022; Zhu *et al*, 2024). ORF10, which consists only of 38 amino acids, resembles Roq1 in size and mechanism to effectively reprogram ubiquitin ligases.
Altogether, YPEL5, HtrA2, SMAC and ORF10 act as substrate mimics that establish multivalent binding sites with ubiquitin ligases to control their activity. Thus, they show striking similarities with Roq1.

4.6 Could Roq1 or SHRED be evolutionary conserved?

When yeast is exposed to protein folding stress, the endopeptidase Ynm3 cleaves intrinsically disordered Roq1, which binds with its new N-terminus and a hydrophobic motif the N-degron ubiquitin ligase Ubr1 to comprehensively regulate its activity. Whether the biochemical properties and the underlying SHRED pathway are evolutionary conserved is unclear. The sequential order of stress-activated proteolytic cleavage of a protein followed by its binding to and regulation of a ubiquitin ligase are strikingly similar to the mammalian HtrA2-mediated mitochondrial PQC pathway (see section 4.5). HtrA2 shows remarkable similarity to Roq1 in terms of proteolytic cleavage and ubiquitin ligase regulation, raising the question whether Roq1 could be evolutionary conserved in mammals. Roq1, however, is poorly conserved on a sequence level and the SLiMs required for its function are too short to have identifiable mammalian homologs. Nonetheless, intrinsically disordered proteins can acquire SLiMs *de novo* or *ex nihilo*, the latter of which is often related to human disease mutations (Chhabra *et al*, 2018; Davey *et al*, 2015; Meyer *et al*, 2018). This raises the possibility that the simple architecture of a mammalian Roq1 could evolve

on a functional but not necessarily sequential level. Similarities on a functional level might require (but not strictly depend on) the evolvement of a SLiM that binds Ubr1 in a similar manner as the Roq1 hydrophobic motif. It is therefore crucial to identify the yeast Ubr1 residues that mediate the interaction with the hydrophobic motif for a better understanding if such a binding site is sequentially conserved and might drive regulation of mammalian Ubr1.

While Ubr1 is the only N-recognin is yeast, there are at least four different mammalian ubiquitin ligases involved in the N-degron pathway: Ubr1, 2, 4 and 5. (Tasaki *et al*, 2012). Mammalian Ubr1 and Ubr2 share sequence similarity with each other and with yeast Ubr1. In contrast, Ubr4 and Ubr5 sequence similarity is restricted to the UBR-Box domains (Varshavsky, 2011). Beyond sequence similarity, mammalian Ubr1 and Ubr2 also share functional similarity to ubiquitinate misfolded proteins during ER stress, thereby maintaining protein quality control (Le *et al*, 2024; Singh *et al*, 2020). Moreover, both are predicted to have three-dimensional structures similar to that of yeast Ubr1 (Abramson *et al*, 2024). Thus, if a mammalian Roq1-like regulator with functionally similar SLiMs exists, it might govern both Ubr1 and Ubr2 activity, even though Ubr2 is dispensable for SHRED activity in yeast (Szoradi *et al.*, 2018). Replacing the yeast Rad6/Ubr1 pair with their mammalian counterparts in *in vitro* or *in vivo* experiments might provide a first clue whether they could, in principle, be regulated by Roq1. In case they do not respond to Roq1, however, this could also be attributed to a different sequential and functional design of a mammalian Roq1, which might prevent cross-species interaction.

In short, while there is no direct evidence for a conservation of SHRED in higher eukaryotes, it is conceivable that proteins sequentially unrelated to Roq1 possess functional elements that enable them to reprogram mammalian Ubr1.

Mammalian ubiquitin ligases are linked with various diseases (Cruz Walma *et al.*, 2022; George *et al.*, 2018). The comprehensive mechanistic understanding of their structure-function relationship enabled the rational design of propitious candidates for inhibitors, PROTACs and molecular glue degraders, of which some have already entered late clinical trials (Chirnomas *et al*, 2023; Mato *et al*, 2022; Petrylak *et al*, 2023). The conceptually simple design of Roq1 allows the far-reaching manipulation of the complex ubiquitin ligase Ubr1. This could inspire the design of other E3 regulators, perhaps even of those with therapeutic intentions.

5. Materials and Methods

5.1 Materials

5.1.1 Growth media and plates

Table 1. Growth media for cultivation of bacteria and yeast.

Medium	Composition
2x yeast extract tryptone (YT)	1% (w/v) tryptone 1.0% (w/v) yeast extract 0.5% (w/v) NaCl
Lysogeny Broth (LB)	1% (w/v) tryptone 0.5% (w/v) yeast extract 1% (w/v) NaCl
Yeast extract peptone dextrose (YPD)	1% (w/v) yeast extract 2% (w/v) peptone 2% (w/v) glucose
Synthetic complete dextrose (SCD)	0.69% (w/v) YNB 0.2% (w/v) amino acid mix 2% (w/v) glucose

Table 2. Plates for cultivation of bacteria and yeast. Dropout plates were prepared using an amino acid mix lacking the appropriate amino acid(s).

Plates	Composition
LB ampicillin	LB 2% (w/v) agar 100 µg/ml ampicillin
LB kanamycin	LB 2% (w/v) agar 25 µg/ml kanamycin
SCD	SCD 2% (w/v) agar
YPD	YPD 1% agarose

Table 3. Synthetic complete amino acid mix. Amino acid mixes for dropout media were made with ingredients listed in table 3 but lacking the desired amino acid(s) for selection.

Component	Amount	Component	Amount
Adenine	0.5 g	Isoleucine	2 g
Alanine	2 g	Leucine	4 g
Para-aminobenzoic acid	0.2 g	Lysine	2 g
Arginine	2 g	Methionine	2 g
Asparagine	2 g	Phenylalanine	2 g
Aspartic acid	2 g	Proline	2 g
Cysteine	2 g	Serine	2 g
Glutamic acid	2 g	Threonine	2 g

5.1.2 Buffers and solutions

Table 4. Buffers and solutions. Buffers used for protein purifications are listed separately with the respective protein purification protocol.

Buffer or solution	Composition
Acrylamide mix (30%, 37.5:1)	29.2% (w/v) acrylamide 0.8% (w/v) N,N'-methylenbisacrylamide
ALFA selector CE elution peptide	20 mM in water
Amino acid mix (3.3%)	2% in water
Ammonium persulfate (APS)	10% (w/v) in water
Ampicillin	100 mg/ml in water, filter sterilized
Anode buffer (5x)	1 M Tris-HCl, pH 8.9
Arg-Ala dipeptide	100 mM in DMSO
ATP buffer for ubiquitination reactions (5x)	5x Ubiquitination reaction buffer 25 mM ATP
Betaine	5 M in water containing 0.5% (w/v) Orange

	G
Bis-Tris HCl	1 M in water, pH 6.0
Blocking buffer	25 mM Tris 150 mM NaCl 0.1% (v/v) Tween-20 5% (w/v) nonfat dry milk
Blotting buffer	25 mM Tris 192 mM glycine 20% (v/v) ethanol
Cathode buffer (5x)	500 mM Tris 500 mM Tricine 0.5% (v/v) SDS
Chloramphenicol	34 µg/ml in EtOH
Colony PCR buffer (10x)	200 mM Tris-HCl, pH 8.8 100 mM $(NH_4)_2SO_4$ 100 mM KCl 25 mM $MgCl_2$
cOmplete protease inhibitors (25x)	1 tablet in 25 ml water
Dithiothreitol (DTT)	1 M in water
DNA loading dye (5x)	50% (v/v) glycerol 10% (v/v) 10x TAE buffer 0.05% (w/v) Orange G
dNTPS	10 mM of each in water
Ethanol	20% (v/v) in water, filter-sterilized and degassed
FLAG peptide elution buffer	50 mM HEPES, pH 7.5 0.2 M NaCl 10% (v/v) glycerol 1 mg/ml FLAG peptide
Glucose (10x)	20% (w/v) in water, autoclaved
Glycerol (2x)	30% (w/v) in water, autoclaved
HEPES	1 M in water, pH 7.5, filter sterilized
Kanamycin	25 µg/ml in water, filter sterilized

Laemmli buffer (4x)	278 mM Tris-HCl, pH 6.8 44.4% (v/v) glycerol 4.4% (w/v) LDS 0.02% (w/v) bromophenol blue
Leu-Ala dipeptide	100 mM in DMSO
Lithium acetate	1 M in water, filter sterilized
Lysis buffer for yeast cell lysis	50 mM Tris-HCl, pH 7.5 150 mM NaCl 0.5 mM EDTA 1 mM PMSF 1x complete protease inhibitor cocktail
p-Benzyol-L-phenylalanine (Bpa)	100 mM (100x) in 1 M NaOH
Phenylmethylsulfonyl fluoride (PMSF)	1 M in water
Polyethylene glycol (PEG) 3350	50% (w/v) in water, filter sterilized
Ponceau S	0.1 % Ponceau S 5% (v/v) acetic acid
Salmon sperm DNA	10 mg/ml in water
SDS-PAGE running buffer	25 mM Tris 0.1% (w/v) SDS 192 mM glycine
SDS-PAGE sample buffer (5x)	250 mM Tris pH 6.8 5% SDS 50% (v/v) glycerol 500 mM DTT
Separating gel buffer	2 M Tris, pH 8.8
Sodium dodecyl sulfate (SDS)	15% (w/v) in water
Sodium hydroxide	0.5 M, filter-sterilized
Solution B (3x)	3 M Tris-HCl, pH 8.5 0.3% SDS
Stacking gel buffer	0.5 M Tris, pH 6.8
TAE buffer	2 M Tris

	1 M acetic acid 50 mM EDTA
TBS/Tween (TBST)	10 mM Tris, pH 7.4 150 mM NaCl 0.1% (v/v) Tween
Transformation mix	33% (w/v) polyethylene glycol (PEG) 3350 100 mM lithium acetate 0.28 µg/ml freshly boiled salmon sperm DNA
Ubiquitination reaction buffer (10x)	500 mM HEPES, pH 7.5 1.5 M NaCl 100 mM $MgCl_2$
Yeast nitrogen base w/o ammonium sulfate (YNB)	6.9 % (w/v) in water, autoclaved

Table 5. Chemical compounds. Chemical compounds, antibiotics, and reagents for buffer stocks and media.

Compound	Supplier	Catalogue number
Adenosine triphosphate (ATP)	Sigma-Aldrich	A2383-5G
Agarose	VWR Life Science	443666A
Agar for bacteriology	NeoFroxx GmbH	2235GR100
ALFA elution peptide	NanoTag Biotechnologies	N1520
Ampicillin	AppliChem	A0839
L-Arabinose	Sigma-Aldrich	A3256-100G
Arg-Ala dipeptide (H-RA-OH)	Peptides & Elephants	EP06653/1809W16
Bio-Rad Protein Assay Dye Reagent Concentrate	Bio-Rad	5000006
Bis-Tris	Sigma-Aldrich	B9754-500G
Brij-58	Sigma-Aldrich	P5889-100G
CHAPS hydrate	Merck	C3023-1G

Chloramphenicol	Merck	220551-25GM
cOmplete protease inhibitors	Roche	04693116001
cOmplete protease inhibitors (EDTA free)	Roche	04693132001
D-desthiobiotin	Sigma-Aldrich	D1411-500MG
DNA stain G	Serva	39803.01
dNTPS	Thermo Fisher Scientific	R0181
DTT	Roche	58615530
DYKDDDDK (FLAG) peptide	Thermo Fisher Scientific	A36806
Ethylenediaminetetraacetic acid (EDTA)	AppliChem	A3553, 1000
Guanidinium hydrochloride	Sigma-Aldrich	50950-1KG
L-Glutathione, reduced	Sigma-Aldrich	G4251-10G
Glycine	Thermo Fisher Scientific	220910010
Glycerol	Riedel-de Haen	15523-1L
HEPES	Roth	9150.4
Imidazole	Merck	1.04716.0250
InstandBlue Coomassie Stain	Abcam	Ab119211
isopropyl β-D-1-thiogalactopyranoside (IPTG)	ZellX Biochem	ZXB-06-100-100
Kanamycin sulfate	Sigma-Aldrich	K400-5G
KCl	Merck	1.04937.1000
Leu-Ala dipeptide (H-LA-OH)	Peptides & Elephants	EP06553/1809W17
Maltose	Calbiochem	443111
2-mercaptoethanol	Sigma-Aldrich	M6250-250ML
Milk powder	Roth	T145.2

$MgCl_2$	Merck	1.05833.0250
NaCl	Fisher Scientific	231-598-3
NaOH	Sigma-Aldrich	30620-1KG-R
$NiSO_4$	Sigma-Aldrich	31483-250G
Nonidet P-40 (NP-40)	Sigma-Aldrich	74385-L
p-benzyol-L-phenylalanine (Bpa)	Bachem	40.176.460.005
Phenylmethylsulfonyl fluoride (PMSF)	Applichem	A0999
SDS	Roth	2326.2
Sodium dihydrogen phosphate	AppliChem	A3559, 1000
Di-sodium hydrogen phosphate	AppliChem	A3567, 1000
D-(+)-Trehalose dihydrate	Sigma-Aldrich	T9531-10G
Tris base	Roth	4855.2
Tryptone/Peptone ex casein	Roth	8952.3
Tween-20	AppliChem	A1389, 1000
Urea	Sigma-Aldrich	33247-1KG
Yeast extract	Roth	2363.3

5.1.3 Chromatography columns and resins

Table 6. Chromatography columns and resins used for protein purifications.

Chromatography column or resin	Supplier	Catalogue number
ALFA selector CE resin	NanoTag Biotechnologies	N1512
Amylose resin	New England Biolabs (NEB)	E8021L
Anti-DYKDDDDK (FLAG) affinity	Thermo Fisher Scientific	A36803

resin		
Glutathione Sepharose 4B	Amersham	17075601
Hiload 16/600 Superdex S30 prep grade	Cytiva	28989331
Hiload 16/60 Superdex S75 prep grade	GE Healthcare	28-9893-33
Hiload 16/60 Superdex S200 size-exclusion prep grade resin	GE Healthcare	17-1043-01
HisTrap FF crude column, 1ml	Cytiva	17-5319-01
MBPTrap HP column, 1 ml	Cytiva	29048641
GSTrap4B column, 1 ml	Cytiva	29-0486-09
Resource S column	Cytiva	17117801
Protino Ni-IDA beads	Macherey-Nagel	745210.30
StrepTrap HP column, 1ml	Cytiva	29-0486-53

5.1.4 Proteins, enzymes, standards and kits

Table 7. Commercial proteins.

Protein	Supplier	Catalogue number
Recombinant Human Ubiquitin Activating Enzyme (UBE1)	R&D Systems (Bio-Techne)	E-305-025
Recombinant human ubiquitin (K0)	R&D Systems (Bio-Techne)	UM-NOK-01M
Recombinant human ubiquitin (K0)	MoBiTec	E1610-UBP
Recombinant human ubiquitin (WT)	R&D Systems (Bio-Techne)	U-100H-10M
Recombinant human ubiquitin (K11R)	R&D Systems (Bio-Techne)	UM-K11R-01M
Recombinant human ubiquitin (K29R)	R&D Systems (Bio-Techne)	UM-K29R-01M
Recombinant human ubiquitin	R&D Systems (Bio-Techne)	UM-K48R-01M

(K48R)		
Recombinant human ubiquitin (K63R)	R&D Systems (Bio-Techne)	UM-K63R-01M
Recombinant human ubiquitin (K48R/K63R)	R&D Systems (Bio-Techne)	UM-K4863R-01M
Recombinant luciferase	Promega	E1702

Table 8. Enzymes.

Enzyme	Supplier	Catalogue number
Alkaline phosphatase (FastAP)	Thermo Scientific	EF0651
ALLin™ HiFi DNA Polymerase	highQu	HLE401c1
BamHI-HF	NEB	R3136S
DNase	Sigma	DN25-1G
DpnI	NEB	R0176L
Phusion DNA polymerase	NEB	M0530S
Opti Taq DNA polymerase	Roboklon	E2600-02
Q5 High-Fidelity polymerase	NEB	M0491S
SalI-HF	NEB	R3138S
SpeI-HF	NEB	R0133S
SphI	NEB	R3182S
Taq DNA ligase	NEB	M0208L
Taq polymerase	Sigma-Aldrich	D1806
T4 DNA ligase	Thermo Scientific	EL011
T5 exonuclease	NEB	M0663S
XhoI	NEB	R0146S

Table 9. Standards.

Standard	Supplier	Catalogue number
GeneRuler 1kb Plus DNA ladder	Thermo Fisher Scientific	SM1331
PageRuler Plus Prestained Protein ladder	Thermo Fisher Scientific	26619
Gel filtration standard	Bio-Rad	1511901

Table 10. Kits.

Kit	Supplier	Catalogue number
miniBio Column Plasmid Mini-Preps Kit	miniBio Life Science Products	mB001
miniBio Column DNA Gel Extraction Kit	miniBio Life Science Products	mB003
Pierce™ Rapid Gold BCA Protein Assay Kit	Thermo Scientific	A53225
SuperSignal™ West Pico PLUS Chemiluminescent Substrate	Thermo Scientific	34577

5.1.5 Antibodies

Table 11. Antibodies.

Antibody	Dilution for immunoblot	Supplier	Catalogue number
Primary antibodies			
Mouse monoclonal anti-GFP (clones 7.1/13.1)	1:5000	Roche	11814460001
Mouse monoclonal anti-Pho8 (clone 1D3A10)	1:1000	Abcam	Ab113688
Mouse monoclonal anti-FLAG (clone M2)	1:5000	Sigma-Aldrich	F1804
Rat monoclonal anti-HA	1:5000	Roche	11867423001

(clone 3F10)			
Goat polyclonal anti-Luciferase	1:2500	Merck	3256
Mouse monoclonal anti-MBP (clone MBP-17)	1:3000	Sigma-Aldrich	M6295
Strep-Tactin HRP conjugate	1:100,000	IBA Lifesciences	2-1502-001
Mouse monoclonal anti-polyhistidine (clone HIS-1)	1:3000	Merck	H1029
Anti-ALFA-Li800 (clone1G5)	1:500	Nanotag	N1502-Li800-L
Secondary antibodies			
Donkey polyclonal anti-rat HRP	1:10,000	Jackson ImmunoResearch	712-035-153
Goat polyclonal anti-mouse HRP	1:10,000	Pierce (Thermo Fisher Scientific)	31432
Rabbit polyclonal anti-goat HRP	1:10,000	Jackson ImmunoResearch	305-035-045

5.1.6 SDS-PAGE gel recipes

Table 12. Recipes for Tris-Glycine SDS-PAGE gels.

Separating gel					
	5.5%	**7.5%**	**10%**	**12%**	**15%**
H_2O	3.6 ml	3.2 ml	2.7 ml	2.3 ml	1.7 ml
Separating gel buffer	1.2 ml	1.2 ml	1.2 ml	1.2 ml	1.2 ml
30% acrylamide mix (37.5:1)	1.1 ml	1.5 ml	2.0 ml	2.4 ml	3.0 ml
15% SDS	40 µl	40 µl	40 µl	40 µl	40 µl
10% APS	60 µl	60 µl	60 µl	60 µl	60 µl
TEMED	6 µl	6 µl	6 µl	6 µl	6 µl

Stacking gel	
	4%
H_2O	1.2 ml
Separating gel buffer	0.5 ml
30% acrylamide mix (37.5:1)	0.27 ml
15% SDS	13 µl
10% APS	20 µl
TEMED	2 µl

Table 13. Recipes for Tris-Tricine SDS-PAGE gels.

Separating gel		
	10%	**16%**
H_2O	2.49 ml	1.58 ml
3x Solution B	2.0 ml	2.0 ml
40% acrylamide mix	1.51 ml	2.41 ml
10% APS	30 µl	30 µl
TEMED	3 µl	3 µl
Stacking gel		
	4%	
H_2O	1.13 ml	
3x Solution B	0.67 ml	
40% acrylamide mix	0.20 ml	
10% APS	20 µl	
TEMED	2 µl	

5.1.7 Equipment and software

Table 14. Equipment.

Equipment	Manufacturer
Äkta Pure 25	Cytiva
Amersham Imager 600	GE Healthcare
Avanti JXN-26 centrifuge	Beckman Coulter
Centrifuge 5417 R	Eppendorf
Energy-filtered K3 camera	Gatan
FastPrep-24	MP
Glacios 2 Cryo-TEM	Thermo Fisher Scientific
Heraeus Pico 17 centrifuge	Thermo Scientific
Imager BLstar 16	Biometra
Infini pro plate reader	Tecan
Infors HT Multitron incubator shaker	Infors
Krios G4 cryo-TEM	Thermo Fisher Scientific
Magnetic stirrer MR 3001 K	Heidolph
Megafuge 16R	Thermo Scientific
Microfluidizer M110L	Microfluidics
Mini-PROTEAN Glass Plates	Bio-Rad
Mini-PROTEAN Short Plates	Bio-Rad
NanoDrop ND-1000 Spectrophotometer	Thermo Scientific
Odyssey CLx LI-COR imager	LI-COR
PowerPac Basic power supply	Bio-Rad
Refrigerated Incubator shaker innova 4330	New Brunswick Scientific
Roller mixer RM5	CAT

Spark plate reader	Tecan
Talos L120C G2 TEM	Thermo Fisher Scientific
Thermomixer comfort	Eppendorf
Thermocycler T Professional Trio	Biometra
Ultra low freezer	Sanyo
UV LED lamp	Opsytec Dr. Gröbel GmbH
Vitrobot Mark IV System	Thermo Fisher Scientific

Table 15. Software.

Software	Version	Company
Affinity Designer	1.10.4	Serif
Affinity Photo	1.10.4	Serif
AlphaFold	3	DeepMind
ChimeraX	1.6.1	University of California
ColabFold	1.5.5	DeepMind
Endnote	21.2	Endnote
EPU software	3	Thermo Fisher Scientific
Gatan Microscopy Suite	3.32	Gatan
GraphPad Prism	9.0	GraphPad Software, Inc.
ImageJ	2.0.0-rc-69/1.52n	National Institute of Health
Image Studio	5.2.5	LI-COR
Microsoft Office Package	16.78	Microsoft
PyMOL	2.5.1	Schrödinger, LLC.
RELION	5.0 beta	Sjors Scheres

Unicorn	7.6	Cytiva
SnapGene Viewer	7.2	GSL Biotech LLC

Table 16. Protein disorder prediction servers.

Predictor	Link	Source
IUPred3	https://iupred3.elte.hu/ (01.05.2024, 17:00)	(Erdos *et al*, 2021)
VSL2	http://www.pondr.com/ (01.05.2024, 17:00)	(Romero *et al*, 1997)
PrDOS	https://prdos.hgc.jp/cgi-bin/top.cgi (01.05.2024, 17:00)	(Ishida & Kinoshita, 2007)
DisEMBL	http://dis.embl.de/ (01.05.2024, 17:10)	(Linding *et al*, 2003)
Metapredict	https://metapredict.net/ (01.05.2024, 17:10)	(Emenecker *et al*, 2021)
ESpritz N	http://old.protein.bio.unipd.it/espritz/ (01.05.2024, 17:15)	(Walsh *et al*, 2012)
RONN	https://www.strubi.ox.ac.uk/RONN (01.05.2024, 17:15)	(Yang *et al*, 2005)
CAID	https://caid.idpcentral.org/portal (01.05.2024, 17:20)	(Del Conte *et al*, 2023)
Dispro	https://scratch.proteomics.ics.uci.edu/ (01.05.2024, 17:20)	(Cheng *et al*, 2005)
MFDp2	http://biomine.cs.vcu.edu/servers/MFDp2/ (01.05.2024, 17:25)	(Mizianty *et al*, 2013)
NetsurfP-3.0	https://services.healthtech.dtu.dk/services/NetSurfP-	(Hoie *et al*, 2022)

3.0/
(01.05.2024, 17:25)

5.2 Methods

5.2.1 Molecular biology methods

Table 17. Plasmids.

Plasmid	Alias	Source
pCA528-His$_6$-SUMO-Roq1 (22-60) (R22A)-HA	pSS1412	This study
pCA528-His$_6$-SUMO-GFP	pSS841	Axel Mogk (Schmidt *et al*, 2009)
pCA528-Arg-Linker-GFP	pSS1126	This study
pCA528-Phe-Linker-GFP	pSS1231	This study
pCA528-His$_6$-SUMO-Cup9-StrepII	pSS1179	This study
pCA528	pSS685	(Andreasson *et al*, 2008)
pCA528-Pho8*	pSS1233	This study
pMAl-c2E-PreScission-Hsp42-FLAG	pSS840	Axel Mogk (Ungelenk *et al*, 2016)
pRS305-PADH-Rtn1-Pho8*-FLAG-GFP	pSS174	Szoradi et al, 2018
pCA528-His$_6$-SUMO-Pho8star-MBP	pSS1240	This study
pCA528-His$_6$-SUMO-Pho8-MBP	pSS1250	This study
pCA528-His$_6$-SUMO-Mgt1-MBP	pSS1260	This study
pCA528-Roq1	pSS687	Sebastian Schuck
pCA528-His$_6$-SUMO-Roq1 (22-104)	pSS850	Tamas Szoradi
pCA528-His$_6$-SUMO-Roq1 (22-60)-HA	pSS1340	This study

YEplac-P_{ADH}-181-FLAG-Ubr1	pSS1478	This study
pCA528-Ubc2	pSS1211	Axel Mogk (unpublished)
pCA528-His_6-SUMO-Roq1(22-104)-HA	pSS1298	Rafael Salazar
pET3a-Ubiquitin	pSS1209	Frauke Melchior
pET24a-Ulp1-His6	pSS686	Matthias Mayer (Andreasson *et al.*, 2008)
pGEX-4T-1 GST-Rad6	pSS1373	This study
pCA528-Roq1 (22-104)-ALFA	pSS1375	This study
YEplac181-P_{ADH}-Chk1-ALFA-FLAG	pSS1480	This study
YEplac181-P_{ADH}-FLAG-Ubr1 (UBLM)	pSS1479	This study
YEplac181-P_{ADH}-FLAG-Ubr1 (1-1812)	pSS1481	This study
YEplac181-P_{ADH}-FLAG-Ubr1 (1-1879)	pSS1482	This study
YEplac181-P_{ADH}-FLAG-Ubr1 (I687D/Y823D)	pSS1501	This study
pCA528 Roq1 (22-104)-ALFA Y55amber	pSS1496	Sibylle Kanngießer
pCA528 Roq1 (22-104)-ALFA Y56amber	pSS1497	Sibylle Kanngießer

Table 18. Oligonucleotides. Oligonucleotides were purchased either from Integrated DNA Technologies (IDT) or Sigma-Aldrich and stored in water at final 100 µM stock solutions.

Oligo	Sequence	Source
Pho8* fw	tttaagaaggagatatacatatgTCTGCATCACACAAGAA GAAG	This study
Pho8* rev	ctcagtggtggtggtggtggtgTATTTCTGTAGCATCAAAA TCTG	This study
His_6-SUMO-Roq1(22-104)(R22A) fw	tggtcccgctggctCGCaccaccaatctgttc	This study
His_6-SUMO-Roq1(22-104)(R22A) rev	gaacagattggtggtGCGagccagcgggacca	This study
KGEQ replacement fw	tcacagagaacagattggtggtaggagcaaggggaagaactgtt	This study

	cacgggtg	
KGEQ replacement rev Phe-L-GFP rev	cacccgtgaacagttcttccccttgctcctaccaccaatctgttctctgtga	This study
Phe-L-GFP rev	tcttccccttgctgaaaccaccaatctgttctctgtgagcc	
Phe-L-GFP fw	ggctcacagagaacagattggtggtttcagcaaggggaaga	This study
Cup9 fw	GTTCCTGACTATGCGaattataactgcgaaatacaaaacagg	This study
Cup9 rev	GTGGTGGTGGTGGTGattcatatcagggttggatagc	This study
pCA528 Pho8* fw	ggctcacagagaacagattggtgggATGTCTGCATCACACAAGAAGAAGAATG	This study
pCA528 Pho8* rev	ggagctcgaattcggatccGGTCTtcaTATTTCTGTAGCATCAAAATCTGATGTGTG	This study
pCA528 open fw	AGACCGGATCCGAATTCG	This study
pCA528 open rev	Cccaccaatctgttctctg	This study
Pho8* MBP fw	ATCAGATTTTGATGCTACAGAAATAatgaaaatcgaagaaggtaaactgg	This study
Pho8* MBP rev	agctcgaattcggatccGGTCTTCAAGTCTGCGCGTCTTTTCAG	This study
Pho8* MBP open fw	TGAAGACCGGATCCGAATTC	This study
Pho8* MBP open rev	TATTTCTGTAGCATCAAAATCTGATG	This study
Pho8* fw seq.	CCAATACGTTTTGGAGTTTGCTG	This study
Pho8* intern seq fw	AAGTCAAGGTGGCTTTGGG	This study
MBP intern seq. rev	ttgtaacgtacggcatccc	This study
MBP intern seq. fw.	aaatcatgccgaacatccc	This study
Pho8 fw	GTTGGCTTTCGATGAAGCATTTCAATACGTTTTGGAG	This study
Pho8 rev	CTCCAAAACGTATTGAAATGCTTCATCGAAAGCCAAC	This study
Mgt1 fw	ggctcacagagaacagattggtggGATGAAGGAACTGCTTTACTATACATTC	This study
Mgt1 rev	CACCCGAACCACCACCCGAACCACCCAATCTACTAAGGCTTAAGCTATTTTCC	This study

pCA528 Mgt1 open rev	CCCACCAATCTGTTCTCTGTGAGC	This study
pCA528 Mgt1 open fw	GGTGGTTCGGGTGGTGGT	This study
Ubr1 -102 bp	TCGTCATTGTTCTCGTTCC	This study
Ubr1 0 bp	ATGTGGTCTCATCCGCAGTTTG	This study
Ubr1 +928 bp	AGACGAGCCCCTCTAATAGC	This study
Ubr1 +1880 bp	AGGTGGTGTATTGATCTGG	This study
Ubr1 + 2863 bp	AGCTACTAAGATCAGTTCC	This study
Ubr1 +3819 bp	GAATTTATGCCCATGTGGGATGG	This study
Ubr1 +4844 bp	AGATTCTGAAAATGAAACGC	This study
Roq1(22-60)-HA fw	TACCCATACGATGTTCCTGACTATGCGTGA ACTAATTTAGGCATACAGGAAAACACAAGC	This study
Roq1(22-60)-HA rev	CAGCTCTACAAAGTAGTATATCACGCC	This study
pho-HA-tag fw	TACCCATACGATGTTCCTGACTATGCGTGAGGA TCCGAATTCGAGCT	This study
FLAG-Ubr1 His removal fw	TAACTCGAGATCATGTAATTAGTTATGTCACGC	This study
FLAG-Ubr1 His removal rev	CCAAATCTCTCGCTCATCAGAGTC	This study
Ubr1 (I687D) rev	ggaggtggtatattctaaataggagtcgaaattttgatcttcgtgaaga aca	This study
Ubr1 (I687D) fw	tgttcttcacgaagatcaaaatttcgactcctatttagaatataccacct cc	This study
Ubr1 (Y823D) rev	taattcgggattgtttttataatccgatgcttgatgtaacacagaca	This study
Ubr1 (Y823D) fw	tgtctgtgttacatcaagcatcggattataaaaacaatcccgaatta	This study
MBP intern seq. rev	ttgtaacgtacggcatccc	This study
HA-term fw	TACCCATACGATGTTCCTGACTATGCGTGAGGA TCCGAATTCGAGCT	Rafael Salazar
Roq1-HA rev	CGCATAGTCAGGAACATCGTATGGGTATGAAC AACGGCGAGAGTGAA	Rafael Salazar
His-SUMO-Roq1 fw	TGAGGATCCGAATTCGAGCT	Rafael

His-SUMO-Roq1 rev	TGAACAACGGCGAGAGTGAA	Salazar Rafael
Open FLAG-Ubr1 Chk1 rev	GTCGACTAGAGGATCCCCG	Salazar This study
Open FLAG-Ubr1 Chk1 fw	TAACTCGAGATCATGTAATTAGTTATGTCACGC	This study
Chk1-ALFA-FLAG fw	ATGAGTCTCTCGCAGGTGTCACCTTTACCCC	This study
Chk1-ALFA-FLAG rev	CTTGTCATCGTCGTCCTTGTAGTCACCCGAACC CGGCTCGGTCAATCTTCTCC	This study

5.2.1.1 Molecular cloning

Plasmids used in this study can be found in Table 17. To generate the plasmids needed for this study, plasmid linearization and amplification of DNA were conducted using the Q5 High-Fidelity Polymerase or ALLIn^{TM} HiFi DNA Polymerase (Table 8). Site-directed mutagenesis, DNA insertions and deletions were performed using Stratagene's Quikchange PCR, Gibson assembly (Gibson *et al*, 2009) or round the horn PCR protocols (Moore & Prevelige, 2002). To degrade parental DNA templates after PCR, DpnI was added to each reaction and samples were incubated for at least 1 h at 37°C. Digested parental DNA was separated via agarose gel electrophoresis using a 1% agarose gel and 2x TAE buffer. Separated PCR products were purified by gel extraction and linearized vectors were either re-ligated or ligated with amplified DNA inserts using the T4 DNA ligase or Gibson assembly. Competent *Escherichia coli* (*E. coli*) DH5α cells were then transformed with the generated DNA plasmid for amplification. LB medium containing the appropriate antibiotic was inoculated with a single bacterial colony for overnight growth at 37°C. Plasmids were subsequently isolated using the miniBio Column Plasmid Mini-Preps Kit and verified by Microsynth GmbH via Sanger sequencing.

To generate pSS1240 (His_6-SUMO-Pho8*-MBP), the Pho8* sequence encoding for cytosolic residues 61-550 was amplified from pSS174 (pRS305ADH-Rtn1Pho8*FLAG-GFP). Pho8* bears two point mutations (F352 and N247D) as previously described (Szoradi et al, 2018). Pho8* was integrated into pCA528 (Andreasson *et al.*, 2008), yielding pCA-Pho8* (pSS1233). To generate pCA528-

Pho8*-MBP (pSS1240), the MBP tag sequence harboring an upstream GGSGGGSGG linker was amplified from pMAl-c2E-PreScission-Hsp42-FLAG (Ungelenk *et al.*, 2016) and integrated into linearized pSS1233 via Gibson Assembly. PCA528-Pho8-MBP was subsequently generated by mutating F352D and N247D back to wild type.

pCA528-Roq1 (22-104) was previously generated by Tamas Szoradi. To generate pSS1375, His_6-SUMO-Roq1 (22-104)-ALFA, the ALFA was integrated via round the horn PCR using pSS852 (His_6-SUMO-Roq1 (22-104)) as template. pSS1298 (His_6-SUMO-Roq1 (22-104)-HA) was created in a similar manner by Rafael Salazar under my supervision using oligonucleotides harboring the HA tag sequence. Truncated Roq1 variants such as pSS1412 (His_6-SUMO-Roq1 (22-60)-HA) or pSS1340 (His_6-SUMO-Roq1 (22-60) (R22A)-HA) were created via round the horn PCR. Roq1 variants harboring the (TAG) amber stop codon at position Y55 or Y56 were generated via site-directed mutagenesis.

To generate Ubr1 variants such as pSS1479 (FLAG-Ubr1 (UBLM), pSS1481 (FLAG-Ubr1 (1-1812)), pSS1482 (FLAG-Ubr1 (1-1879)) and pSS1591 (FLAG-Ubr1 (I687D/Y823D)) were generated via site-directed mutagenesis or round the horn PCR using pSS1478 (YEplac181-P_{ADH}-FLAG-Ubr1, (Xia *et al.*, 2008b)) as template.

The N-degron substrates were generated using the expression plasmid pCA528 encoding His_6-SUMO-GFP (Schmidt *et al.*, 2009) as template. To generate pSS1126 (Arg-linker-GFP) and pSS1231 (Phe-linker-GFP), the N-terminal degron amino acids were introduced together with a ten amino acid GFP linker sequence (X-SKGEELFYGV, X=R/F) upstream of the GFP sequence via Gibson assembly. Both N-degron substrates contain an N-terminal His_6-SUMO tag.

Sequences of Cup9, Mgt1 and Chk1 were amplified from yeast W303 genomic DNA. Amplified Cup9 and Mgt1 were inserted into linearized pCA528 downstream of the His_6-SUMO sequence via Gibson assembly. Cup9 was subsequently C-terminally StrepII-tagged and Mgt1 MBP-tagged, yielding pSS1179 (His_6-SUMO-Cup9-StrepII) and pSS1260 (His_6-SUMO-Mgt1-MBP). Chk1 was amplified with a C-terminal ALFA-FLAG overhang and integrated into linearized YEplac181, yielding pSS1480 (Chk1-ALFA-FLAG).

pSS1209 (pET3a-Ubiquitin) was a gift from Jörg Schweiggert (Melchior lab). pSS686 (pET24a-Ulp1-His_6) was obtained from Matthias Mayer. pSS1211 (pCA528-His_6-SUMO-Ubc2) and pCA528-His_6-SUMO-GFP were gifts from Axel Mogk.

5.2.2 Yeast methods

Table 19. Yeast strains.

Strain genotype	Alias	Source
ubr1::nat-P_{GPD}-FLAG-UBR1 pep4Δ	SSY2908	Ilia Kats
Δpep4::TRP1	PWY0005	Peter Walter

5.2.2.1 Growth conditions and transformation of yeast strains

Yeast cells were incubated at 30°C in YPD, SCD or SCD deprived of the relevant amino acid for selection. Detailed growth conditions that were implemented for protein expression, can be found in section 5.2.4.

To transform yeast cells, 5 ml YPD medium were inoculated with cells and grown until next morning. Cells were back-diluted next day to an OD_{600} of 0.4 in 5 ml YPD. They were subsequently grown for 4 h at 30°C, then pelleted at 3,000 xg for 5 minutes and the supernatant was removed. The cells were then washed with room-temperature water, pelleted and 0.1 – 0.5 µg centromeric DNA was added. After resuspension in 360 µl transformation mix (Table 4), the mixture was incubated at 42°C for 40 minutes. Last, the pelleted cells were resuspended in 1 ml YPD. 100 µl were directly plated on a selective plate (auxotrophic marker) or incubated at 30°C for 3 h (antibiotic selection) prior plating to allow expression of the antibiotic resistance gene.

5.2.3 Bacteria methods

Table 20. Bacteria strains.

Strain genotype	Alias	Source
F^- *ompT hsdS*$_B$(r_B^- m_B^-) *gal dcm* (DE3) pRARE (Cam^R)	Rosetta™ (DE3)	Lab Collection
pCA528-Yjl144(22-104) + Rosetta™ (DE3) background	pSS852	Tamas Szoradi

pCA528-Yjl144(22-104)(R22A) + Rosetta™ (DE3) background	pSS1108	This study
pCA528 Arg-L-GFP + Rosetta™ (DE3) background	pSS1144	This study
pCA528 Cup9-StrepII + Rosetta™ (DE3) background	pSS1178	This study
pET3a-Ubiquitin + Rosetta™ (DE3) background	pSS1210	Jörg Schweiggert
pCA528-Ubc2 + Rosetta™ (DE3) background	pSS1212	Axel Mogk
pCA528 Phe-L-GFP + Rosetta™ (DE3) background	pSS1232	This study
pCA528 Pho8star-MBP + Rosetta™ (DE3) background	pSS1241	This study
pCA528 Pho8-MBP + Rosetta™ (DE3) background	pSS1251	This study
pCA528 Mgt1-MBP + Rosetta™ (DE3) background	pSS1261	This study
pCA528 Roq1 (22-60)-HA + Rosetta™ (DE3) background	pSS1341	This study
pGEX-4T-1 GST-Rad6 + Rosetta™ (DE3) background	pSS1374	This study
pCA528 Roq1 (22-104)-ALFA + Rosetta™ (DE3) background	pSS1376	This study
pCA528 Roq1 (22-104) (V58E)-ALFA + Rosetta™ (DE3) background	pSS1452	This study
pCA528 Roq1 (22-104)-ALFA (Y55amber) + pEVOL-pBpF + Rosetta™ (DE3) background	pSS1503	Sibylle Kanngießer
pCA528 Roq1 (22-104)-ALFA (Y56amber) + pEVOL-pBpF + Rosetta™ (DE3) background	pSS1504	Sibylle Kanngießer

5.2.3.1 Growth conditions and transformation of bacteria strains

Bacteria cells were grown at 37°C in LB or 2xYT medium. For detailed growth conditions on protein expression, see section 5.2.4.
For transformations, 1-10 µl of transforming DNA were mixed with 100 µl chemically-competent Dh5α bacteria. The mixture was kept on ice for 15 minutes before 1.5-minute incubation at 42°C. Samples were then kept on ice for one minute prior addition of 900 µl LB medium and a 40-minute recovery at 37°C. Cells were then pelleted at 10,000 xg for 2 minutes, 900 µl of supernatant were removed and the remaining supernatant was streaked on a selective plate containing ampicillin or kanamycin. Plates were subsequently incubated overnight at 37°C.

5.2.4 Biochemistry methods

5.2.4.1 Protein expression and purification

5.2.4.1.1 Ubr1

Expression and purification of Ubr1 and its variants was performed as previously described (Du *et al.*, 2002; Pan *et al.*, 2021), with modifications. Wild type Ubr1 was expressed in *Saccharomyces cerevisiae* (*S. cerevisiae*) SSY2908 (Table 19) from the P_{GPD} promoter and chromosomally tagged with an N-terminal FLAG tag. N-terminally FLAG-tagged Ubr1 mutants were also expressed in *S. cerevisiae* but from the P_{ADH} promoter in the high-copy plasmids pSS1479, 1481, 1482 or 1501 (Table 17).
To express Ubr1, a single yeast colony was grown in YPD (wild type Ubr1) or SC-LEU medium (Ubr1 mutants) in the morning and back-diluted in YPD or SC-LEU medium in the evening to reach an OD_{600} of 1.0 – 2.0 the next day. Cells were harvested and washed once with cold phosphate-buffered saline (PBS) before snap freezing in liquid nitrogen. Cells were resuspended in 10 ml lysis buffer (50 mM HEPES 7.5, 0.2 M NaCl, 10% glycerol, 0.5% NP-40, 1 mM PMSF, Roche protease inhibitor cocktail) per 2 L culture and lysed with a microfluidizer (Table 14) by passing them ten times. The lysate was cleared by centrifugation (11,200 x g, 30 minutes) at 4°C and applied on anti-DYKDDDDK resin (Table 6) pre-equilibrated in buffer A (50

mM HEPES 7.5, 1 M NaCl, 10 % glycerol, 0.5% NP-40). The resin was incubated for 2 h at 4°C while rotating before being washed with buffer A and subsequently with buffer B (50 mM HEPES 7.5, 0.2 M NaCl, 10% glycerol). Bound FLAG-Ubr1 was eluted with buffer B containing 1 mg/ml 3x DYKDDDDK peptide (Table 5). Protein-containing fractions were pooled and frozen in liquid nitrogen.

5.2.4.1.2 Roq1

Wild type Roq1 (22-104) and its variants were equipped with an N-terminal His_6-SUMO tag for protein purification and to protect the unstable N-terminal Arg residue. *E. coli* Rosetta™ (DE3) competent cells were transformed with plasmids containing His_6-SUMO-Roq1 (Table 17) for protein expression.

To express Roq1, single colonies were used to grow overnight cultures at 37°C in 2x YT medium containing chloramphenicol and kanamycin at appropriate concentrations (Table 4). Cells were back-diluted next morning in 2x YT medium to a starting OD_{600} of 0.15 and grown at 37°C. At an OD_{600} of 0.7, protein expression was induced by the addition of final 1 mM IPTG. Cells were subsequently grown for 3 h at 37°C prior harvesting and freezing.

To purify Roq1, cells were resuspended in lysis buffer (50 mM Bis Tris 6.0, 500 mM NaCl, 20 mM imidazole, 5 mM $MgCl_2$, 2 mM 2-mercaptoethanol, 1 mM PMSF, Roche EDTA-free protease inhibitor cocktail) and DNase-treated for 20 minutes at 4°C while stirring. Cells were lysed with a microfluidizer by passing them ten times and subsequently centrifuged at 11,200 x g at 4°C to isolate soluble protein fractions. The supernatant was incubated for 60 minutes at 4°C with 2.0 g Protino-IDA beads (Table 6) to isolate His_6-SUMO-Roq1. The bead slurry was added to a gravity flow column and washed thoroughly with lysis buffer. Subsequent wash steps include washing the beads with wash buffer (50 mM Bis Tris 6.0, 500 mM NaCl, 5 mM $MgCl_2$, 50 mM imidazole and 2 mM 2-mercaptoethanol) and wash buffer containing 5 mM ATP or 750 mM NaCl. His_6-SUMO-Roq1 was eluted with elution buffer (50 mM Bis Tris 6.0, 150 mM NaCl, 250 mM imidazole, 2 mM 2-mercaptoethanol) and protein-containing fractions were pooled. For removal of the N-terminal His_6-SUMO tag and exposure of the unstable Arg-terminus of Roq1, 25 µl of the SUMO protease Ulp1 were added. To allow protein cleavage, the mixture was dialyzed overnight against dialysis buffer (50

mM Bis Tris 6.0, 150 mM NaCl, 2 mM 2-mercaptoethanol) at 4°C. Next morning, free His_6-SUMO, uncleaved His_6-SUMO-Roq1 and the 6xHis-tagged protease Ulp1 were removed by another affinity chromatography step. To achieve this, Protino Ni-IDA beads (Table 6) were added to the dialysate and incubated at 4°C for 30 minutes. The slurry was then poured into a gravity flow column and the flow through containing cleaved Roq1 was collected. To further polish Roq1, the flow through was concentrated to less than 3 ml and applied on a Hiload 16/600 Superdex S30 prep grade size-exclusion column (Table 6) pre-equilibrated in SEC buffer (50 mM HEPES pH 7.5, 150 mM NaCl). Roq1-containing fractions were combined, supplemented with 10% glycerol, concentrated and snap frozen in working aliquots.

Expression and purification of Roq1 amber variants was done collaboratively with Sibylle Kanngießer. Roq1 variants harboring photo-reactive p-benzoyl-l-phenylalanine (Bpa) at position Y55 or Y56 were expressed using the pEVOL/pET system (Malsam *et al*, 2020; Young *et al*, 2010). E. coli BL21 (DE3) cells were co-transformed with pSS1503 (pCA528-Roq1(22-104)-ALFA (Y55amber)) or pSS1504 (pCA528-Roq1(22-104)-ALFA (Y55amber)) and the pEVOL-pBpF plasmid. Cells were grown in 2 L 2xYT media containing 25 µg/ml kanamycin, 34 µg/ml chloramphenicol, 50 mM phosphate buffer pH 7.2 and 1 mM Bpa. 0.25% (w/v) final L-arabinose was added at OD_{600}=0.5. At an OD_{600} of 0.8, L-arabinose was added to final 0.5%. To induce protein expression, 1 mM IPTG was simultaneously added, and cells were grown at 37 °C for 5 h. Cells were centrifuged at 1000 x g at 4°C for 15 min for harvesting, washed once with cold water and snap frozen. Roq1 photo-crosslinking variants were purified as described above, with small deviations. A cell pellet from a 2 L expression was resuspended, lysed and purified via IMAC as described above. 16 ml of the IMAC eluate were dialyzed overnight and mixed with 250 µl of 250 µl of a 50% ALFA-selector resin (CE) slurry (Table 6). The mixture was incubated for 2 hours at 4°C. Beads were washed three times with 500 µl of wash buffer (50 mM HEPES, pH 7.5, 0.15 M NaCl, 10 mM $MgCl_2$). Immobilized Roq1 (22-60) (Y55Bpa)-ALFA or Roq1 (22-60) (Y56Bpa)-ALFA were used for subsequent photo-crosslinking experiments (see 5.2.4.8 for experimental details on photo-crosslinking).

5.2.4.1.3 Rad6

Rad6 was expressed and purified similarly to Roq1, with small deviations. Plasmids containing His_6-SUMO-Rad6 (Table 17) were transformed into *E. coli* Rosetta™ (DE3) competent cells (Table 20). The protein was expressed for four hours at 37°C after IPTG induction. Immobilized metal affinity chromatography (IMAC) purification of His_6-SUMO-Rad6 and subsequent His_6-SUMO cleavage was conducted similarly to Roq1, with phosphate buffer (50 mM NaH_2PO_4, pH 8.0, 300 mM NaCl, 5 mM $MgCl_2$ and 2 mM 2-mercaptoethanol) being used for cell lysis, wash steps and dialysis. Cleaved Rad6 was further purified via size exclusion chromatography (SEC) using a Hiload 16/60 Superdex S75 prep grade column (Table 6) equilibrated in SEC buffer (25 mM HEPES pH 7.5, 25 mM KCl, 5 mM $MgCl_2$, 1 mM DTT).
For pulldown experiments, an N-terminally GST-tagged version of Rad6 was used. GST-Rad6 was expressed in *E. coli* Rosetta™ (DE3) competent cells (Table 20) from plasmid pSS1373 (Table 17) and purified as previously described (Turco *et al.*, 2015), with small deviations. To express GST-Rad6, 2x YT medium was inoculated with single *E. coli* colonies and grown overnight at 37°C. Next morning, cells were back-diluted in 2x YT medium to an OD_{600} of 0.15 and grown at 37°C until an OD_{600} of 0.7. GST-Rad6 expression was induced by the addition of 1 mM IPTG, and cells were grown for 16 hours at 20°C. Cells were harvested, resuspend in lysis buffer (50 mM Tris-HCl, pH 7.4, 100 mM NaCl, 10 mM $MgCl_2$, 0.15% Nonidet P-40, 1 mM DTT, 1 mM PMSF, 1x Roche protease inhibitors) and lysed. Insoluble proteins were removed by a centrifugation step (11,200 x g, 4°C) and the soluble protein pool was applied on a GSTrap 4B column (Table 6) pre-equilibrated in 50 mM Tris-HCl, pH 7.4, 100 mM NaCl, 10 mM $MgCl_2$, 0.15% Nonidet P-40, 1 mM DTT). The column was washed with lysis buffer lacking Nonidet P-40 and ATP wash buffer (50 mM Tris-HCl, pH 7.4, 100 mM NaCl, 10 mM $MgCl_2$, 10 mM ATP, 1 mM DTT). GST-Rad6 was eluted in GST elution buffer (50 mM Tris-HCl, pH 7.4, 100 mM NaCl, 10 mM $MgCl_2$, 20 mM glutathione, 1 mM DTT). Protein-containing fractions were pooled, concentrated, and further polished by applying them on a Hiload 16/60 Superdex S200 size-exclusion column (Table 6) equilibrated in 50 mM Tris-HCl, pH 8.0, 50 mM NaCl, 50 mM KCl, 10 mM $MgCl_2$. Pure fractions were pooled and further concentrated for storage.

5.2.4.1.4 Pho8 and Pho8*

Pho8 and Pho8* were equipped with an N-terminal His_6-SUMO tag for protein purification and a C-terminal MBP tag for increasing protein solubility. to *E. coli* Rosetta™ (DE3) competent cells were transformed with plasmids containing His_6-SUMO-Pho8(*)-MBP (Table 17) for protein expression. Proteins were expressed similarly to Roq1, but grown in LB medium and at 30°C. For protein purification, cells were resuspended in lysis buffer (50 mM HEPES pH 7.5, 500 mM NaCl, 5 mM $MgCl_2$, 10 mM imidazole, 10% glycerol , 0.4% CHAPS, 1 mM PMSF, Roche EDTA-free protease inhibitor cocktail) and DNase-treated for 20 minutes at 4°C prior cell lysis. Cells were centrifuged after cell lysis to separate insoluble proteins from soluble. Soluble proteins were applied on a HisTrap FF crude affinity chromatography column (Table 6) pre-equilibrated in IMAC A buffer (50 mM HEPES pH 7.5, 500 mM NaCl, 5 mM $MgCl_2$, 10% glycerol). Subsequently, the HisTrap column was washed with IMAC wash buffer (50 mM HEPES pH 7.5, 500 mM NaCl, 5 mM $MgCl_2$, 10 mM imidazole, 10% glycerol) and with IMAC ATP wash buffer (50 mM HEPES pH 7.5, 500 mM NaCl, 5 mM $MgCl_2$, 10 mM ATP, 10% glycerol). The protein was eluted with IMAC elution buffer buffer (50 mM HEPES pH 7.5, 500 mM NaCl, 5 mM $MgCl_2$, 250 mM imidazole, 10% glycerol). Eluted protein fractions were combined and dialyzed overnight against Pho8 dialysis buffer (50 mM HEPES pH 7.5, 150 mM NaCl, 10 mM $MgCl_2$, 2 mM 2-mercaptoethanol) in presence of 25 µl Ulp1 to allow His_6-SUMO cleavage. To remove free His_6-SUMO and Ulp1, the dialysate containing Pho8(*)-MBP was further purified via batch purification using amylose resin (Table 6) pre-equilibrated in dialysis buffer. The resin was washed with dialysis buffer and bound proteins were eluted with dialysis buffer containing 10 mM maltose. To further purify Pho8(*)-MBP, protein fractions were combined, further concentrated and injected in a Hiload 16/60 Superdex S200 column (Table 6) equilibrated in SEC buffer (50 mM HEPES pH 7.5, 150 mM NaCl, 10 mM $MgCl_2$). Pure fractions as judged by SDS-PAGE and Coomassie-staining were pooled, supplemented with 10% glycerol and flash frozen in aliquots.

5.2.4.1.5 Mgt1

Mgt1 was expressed and purified similarly to Pho8 and Pho8*, with small deviations. Mgt1 harbors an N-terminal His_6-SUMO tag and a C-terminal MBP tag for solubility and affinity tag-based purifications. *E. coli* Rosetta™ (DE3) competent cells (Table 20) were transformed with plasmids containing His_6-SUMO-Mgt1-MBP (Table 17) for protein expression. His_6-SUMO-Mgt1-MBP was expressed for 3 hours at 30°C after IPTG induction. The protein was similarly purified to Pho8 and Pho8*, with the following adaptations: After protein expression, the cells were resuspended in lysis buffer containing 50 mM HEPES pH 7.5, 500 mM NaCl, 5 mM MgCl2, 10 mM imidazole, 10% glycerol, 1 mM PMSF and Roche EDTA-free protease inhibitor cocktail. During IMAC, the HisTrap crude FF column (Table 6) was washed with lysis buffer containing 10 mM ATP and the protein was eluted with final 200 mM imidazole. The His_6-SUMO tag was removed overnight with dialysis buffer (50 mM HEPES pH 7.5, 150 mM NaCl, 10 mM $MgCl_2$, 2 mM 2-mercaptoethanol) via Ulp1 treatment. Next day, Mgt1 was further purified via batch purification with amylose resin (Table 6) and SEC using a Hiload 16/60 Superdex S75 prep grade column (Table 6) equilibrated in 50 mM HEPES, pH 7.5, 150 mM NaCl, 10 mM $MgCl_2$.10% glycerol was added to pooled SEC fractions just before snap freezing in liquid nitrogen.

5.2.4.1.6 Cup9

Cup9 was expressed as His_6-SUMO-Cup9-StrepII (plasmid pSS1179, Table 17) in *E. coli* Rosetta™ (DE3) competent cells for three hours at 37°C post IPTG induction. Cells were resuspended in lysis buffer (20 mM HEPES pH 7.0, 500 mM NaCl, 10 mM imidazole, 5 mM $MgCl_2$, 1 mM PMSF, 2 mM 2-mercaptoethanol and Roche protease inhibitor cocktail) and similarly purified as Pho8 and Pho8*. After IMAC and His_6-SUMO cleavage, the dialysate containing Cup9-StrepII was injected in a StrepTrap HP column (Table 6) pre-equilibrated in Strep buffer (20 mM HEPES pH 7.0, 500 mM NaCl). The column was washed with Strep buffer and bound Cup9-StrepII was eluted with Strep buffer containing 2.5 mM D-desthiobiotin and 2 mM 2-mercaptoethanol. The eluate was further concentrated and injected in a self-packed Hiload 16/60 Superdex S200 size-exclusion prep grade column pre-equilibrated in 20 mM HEPES

pH 7.5, 500 mM NaCl, 1 mM DTT. Protein-containing fractions were combined, supplemented with final 10% glycerol and snap frozen in liquid nitrogen.

5.2.4.1.7 Chk1

Chk1 was expressed as Chk1-ALFA-FLAG in *S. cerevisiae* PWY0005 (Table 19) from the P_{ADH} promoter in the high-copy plasmid pSS1480 (Table 17). To express Chk1-ALFA-FLAG, a single yeast colony was grown in SCD-LEU medium in the morning and back-diluted in SCD-LEU medium in the evening to reach an OD_{600} of 1.0 – 2.0 the next day. Cells were harvested and washed once with cold PBS before snap freezing. Protein purification was achieved using the Ubr1 purification protocol for FLAG tag purification (section 5.2.4.1.1). See also (Oh *et al.*, 2017).

5.2.4.1.8 Ubiquitin

Wild type, untagged ubiquitin (pSS1209, Table 17) was expressed in *E. coli* Rosetta™ (DE3) competent cells in LB medium for four hours at 37°C post IPTG induction. Cells were harvested, resuspended in lysis buffer (50 mM Tris HCl pH 7.6, 10 mM $MgCl_2$, 0.02% (v/v) NP-40, 1 mM DTT, 1 mM PMSF, Roche protease inhibitor cocktail), DNase-treated and lysed. Lysed cells were centrifuged at 11,200 x g for 30 minutes at 4°C to separate soluble from insoluble proteins. To remove protein contaminants, 1-2 ml of 70% perchloric acid was added drop-by-drop to the supernatant while stirring. Protein contaminants were separated by centrifugation and the soluble protein pool was dialyzed against ubiquitin dialysis buffer (50 mM ammonium acetate pH 4.5). Moreover, to achieve higher purity, ubiquitin was purified by cation exchange with a Resource S column (Table 6) equilibrated in dialysis buffer. Ubiquitin was eluted by applying a linear 0 – 0.5 M NaCl gradient in 50 mM ammonium acetate pH 4.5 over 20 column volumes. The protein eluted with approximately 0.2 M NaCl. Fractions were applied on a Hiload 16/60 Superdex S75 prep grade size-exclusion column (Table 6) equilibrated in SEC buffer (50 mM Tris HCl pH 7.6, 150 mM NaCl, 1 mM DTT) for further purification. Fractions containing pure ubiquitin were pooled, concentrated and snap frozen in aliquots.

5.2.4.1.9 Ulp1

The protease Ulp1 was expressed as Ulp1-His (pSS686, Table 17) in *E. coli* Rosetta™ (DE3) competent cells. Single colonies were used to grow overnight cultures at 30°C in 2x YT medium with 100 µg/ml ampicillin and 34 µg/ml chloramphenicol. Cells were back-diluted next morning in 2x YT medium to a starting OD_{600} of 0.15 and grown at 30°C. At an OD_{600} of 0.7, the temperature was lowered to 20°C and protein expression was induced by the addition of final 0.5 mM IPTG. Cells were subsequently grown overnight prior harvesting. To purify Ulp1, cells were resuspended in lysis buffer (20 mM Tris pH 7.9, 100 mM KCl, 5 mM $MgCl_2$, 0.6% Brij-58, 2 mM 2-mercaptoethanol, 1 mM PMSF, Roche EDTA-free protease inhibitor cocktail), DNase-treated, lysed and further purified via IMAC. During IMAC, Ulp1-His was bound to Protino Ni-IDA resin (Table 6) and incubated for 60 minutes at 4°C. The bead slurry was then applied on a gravity flow column and intensely washed with buffer A (20 mM Tris pH 7.9, 0.1% Brij-58, 100 mM KCl, 2 M urea and 2 mM 2-mercaptoethanol), buffer B (20 mM Tris pH 7.9, 0.1% Brij-58, 1 M KCl and 2 mM 2-mercaptoethanol) and buffer C (20 mM Tris pH 7.9, 100 mM KCl and 2 mM 2-mercaptoethanol). The protein was eluted with elution buffer (20 mM Tris pH 7.9, 100 mM KCl, 250 mM imidazole, 2 mM 2-mercaptoethanol) and dialyzed against buffer (40 mM HEPES pH 7.9, 150 mM KCl, 10% glycerol and 2 mM 2-mercaptoethanol). Next morning, the dialysate was briefly centrifuged to remove insoluble protein aggregates, further concentrated to 8 mg/ml and mixed with final 50% glycerol prior snap freezing in liquid nitrogen.

5.2.4.1.10 R-GFP and F-GFP

R-GFP and F-GFP were expressed and purified similarly to Rad6, with small deviations. Plasmids containing His_6-SUMO-X-GFP (X = R/F) (Table 17) were transformed into *E. coli* Rosetta™ (DE3) competent cells (Table 20). His_6-SUMO-X-GFP was expressed for three hours at 37°C after IPTG induction. IMAC purification of His_6-SUMO-X-GFP and subsequent His_6-SUMO cleavage was conducted similarly to Rad6, with phosphate buffer (50 mM NaH_2PO_4, pH 8.0, 300 mM NaCl, 5 mM $MgCl_2$ and 2 mM 2-mercaptoethanol) being used for cell lysis, wash steps and

dialysis. Lysis and wash buffer contained additional 10 mM imidazole. The ATP wash buffer 10 mM imidazole and 5 mM ATP. His_6-SUMO-X-GFP was eluted with phosphate buffer containing 250 mM imidazole and treated overnight with Ulp1 for His_6-SUMO removal. Ulp1, His-SUMO and uncleaved His_6-SUMO-X-GFP were removed next day via a second IMAC. Cleaved X-GFP was further purified using a size exclusion chromatography (SEC) Hiload 16/60 Superdex S200 prep grade column (Table 6) equilibrated in SEC buffer (50 mM NaH_2PO_4/Na_2HPO_4, pH 8.0, 300 mM NaCl, 2 mM 2-mercaptoethanol). Protein-containing fractions were combined, further concentrated and flash-frozen in aliquots after addition of final 10% glycerol.

5.2.4.2 *In vitro* ubiquitination assay

In vitro ubiquitination reactions were performed in presence of 0.1 µM Uba1, 4 µM Rad6, 0.25 µM Ubr1, 0.2 µM substrate and 80 µM ubiquitin in reaction buffer (50 mM HEPES, pH 7.5, 0.15 M NaCl, 10 mM MgCl2, 5 mM ATP). Roq1 was added, unless otherwise indicated, at final 2.5 µM. Arg-Ala and Leu-Ala dipeptides were added at final 1 mM, were applicable. For substrate competition experiments, two substrates were added simultaneously at equimolar amounts to the reactions. Ubiquitination reactions were incubated at 30°C for 0-180 minutes, depending on the substrate and assay type (end-time point vs. ubiquitination kinetics experiment). Reactions were terminated by adding final 1x sample buffer. Samples were boiled at 65°C for 5 minutes and ubiquitination efficiency was subsequently analyzed via SDS-PAGE followed by immunoblotting. The concentrations of ubiquitin, Ubr1, Roq1 and substrate mutants were similar to the respective wild type concentration.

To assess the formation of oxyester bonds between a substrate and ubiquitin, final 0.25 M NaOH was added to ubiquitination reactions that were terminated with 1x sample buffer. A similar volume of water was added to control tubes lacking NaOH. All tubes were incubated at room temperature for ten minutes. Final 0.25 M HCl was added to NaOH-containing tubes for neutralization whereas the same volume of water was added to those lacking NaOH. 14 µl of each reaction were loaded on an SDS-PAGE gel for immunoblotting.

5.2.4.3 Chemical unfolding of Firefly Luciferase

To generate unfolded Firefly Luciferase (Luciferase^{U}) for *in vitro* ubiquitination assays, recombinant Firefly Luciferase (Table 7) first needs to be denatured. Denatured luciferase needs to be further stabilized in its unfolded state to prevent aggregation. To achieve this, Luciferase was first diluted 4-fold in denaturation buffer (30 mM Tris pH 7.4, 50 mM KCl, 5 mM $MgCl_2$, 7.5 M GuHCl, 10 mM DTT), incubated for 30 minutes on ice and then diluted 100-fold with dilution buffer (30 mM Tris pH 7.4, 50 mM KCl, 5 mM $MgCl_2$, 0.2 M Trehalose, 1 mM DTT) for stabilization. To clear soluble from aggregated Luciferase species, diluted samples were centrifuged at 13,200 xg for 30 minutes at 4°C. The supernatant containing soluble, unfolded luciferase was used for subsequent ubiquitination assays. The same protocol was also applied to obtain native Luciferase (Luciferase^{N}), with the exception of GuHCl being replaced by dilution buffer.

5.2.4.4 Single-encounter ubiquitination assay

To assess whether unfolded Luciferase (Luciferase^{U}) binds Ubr1 in a single encounter event and to ask what the effect of Roq1 is on substrate recruitment, I implemented a chase protocol (Brown *et al.*, 2016; Saha & Deshaies, 2008) to observe substrate ubiquitination when Luciferase^{U} rebinding to Ubr1 is impaired. Such a single encounter assay has three mixtures of ubiquitination conditions:
Ubiquitination 1 consisting of tube T1.1 containing 0.1 µM Uba1, 4 µM Rad6, 5 mM ATP, and 20 µM ubiquitin K (0) and a second tube T1.2 (0.25 µM Ubr1, 75 nM Luciferase^{U} (see 5.2.4.3 for generation of Luciferase^{U}), ± 2.5 µM Roq1 (22-60)-HA. This reaction monitors multiple binding encounters.
Ubiquitination 2 consisting of tube T2.1 (0.1 µM Uba1, 4 µM Rad6, 5 mM ATP and 20 µM ubiquitin K (0)) and tube T2.2 (0.25 µM Ubr1, 75 nM Luciferase^{U}, 8.5 µM Pho8*, ± 2.5 µM Roq1 (22-60)-HA). This sample records the effectiveness of the competitor Pho8* (“no encounter”).
Ubiquitination 3 consisting of tube T3.1 (0.1 µM Uba1, 4 µM Rad6, 5 mM ATP, 20 µM ubiquitin K (0) and 8.5 µM Pho8*) and tube T3.2 (0.25 µM Ubr1, 75 nM Luciferase^{U}, ± 2.5 µM Roq1 (22-60)-HA). This measures the progress of ubiquitination for Luciferase^{U} that was prebound to Ubr1.

All tubes were incubated separately at 22°C for five minutes. Tubes T1.1 and T1.2, tubes T2.1 and T2.2 and tubes T3.1 and T3.2 were subsequently mixed and incubated at 30°C for 30 minutes prior addition of final 1x sample buffer. Samples were loaded on a 7.5% Tris-glycine SDS-PAGE gel and single encounters were analyzed subsequently via immunoblotting against luciferase.

5.2.4.5 Luciferase^{U} and Pho8* solubility assay

To assess the solubility of chemically unfolded Firefly Luciferase (Luciferase^{U}) and Pho8* during ubiquitination assays, reactions were set up as described in 5.2.4.2. Protein samples were removed at indicated time points and either saved as total protein or subjected to a high-speed centrifugation step at 4°C at 18,000 xg for 30 minutes. The supernatant was removed, and the pellet was resuspended in an equal volume of ubiquitination buffer (50 mM HEPES, pH 7.5, 150 mM NaCl, 10 mM $MgCl_2$). Final 1x sample buffer was added to each tube and samples were boiled for 5 minutes at 65°C. Equal volumes of total protein, supernatant and pellet samples were loaded on an SDS-PAGE gel and analyzed via immunoblotting to assess solubility.

5.2.4.6 Single-turnover Rad6~Ub discharge assay

To assess the reactivity of the Rad6~Ub- ("~" denotes an thioester bond formed between Rad6 and ubiquitin) Ubr1 complex, single-turnover discharge assays were performed in a pulse-chase-like experiment as previously described (Buetow *et al.*, 2018). The pulse reaction generated Rad6 charged with ubiquitin: 2.5 µM Rad6 were mixed with 125 nM Uba1 and 2.5 µM ubiquitin in ubiquitination buffer (50 mM HEPES pH 7.5, 150 mM NaCl, 10 mM $MgCl_2$, 5 mM ATP) and incubated at 30°C for 1.5 h. Rad6~Ub charging was quenched afterwards by adding final 1x stop buffer (50 mM HEPES pH 7.5, 150 mM NaCl, 50 mM EDTA). A final concentration of 50 nM Ubr1 (and, if applicable, 200 µM RA dipeptide or 500 nM Roq1 (22-60)-HA was added for the chase reaction. The chase reaction was monitored for 0 – 15 minutes at 30°C. Reactions were stopped by adding 4x Laemmli buffer without reducing agents. Samples were directly loaded on a 15% SDS-PAGE gel and visualized via Coomassie-staining.

5.2.4.7 *In vitro* binding assay

To monitor the interaction between Ubr1 and Pho8 or Pho8*, *in vitro* binding assays were set up as follows: 0.25 µM FLAG-Ubr1 were mixed on ice with 0.25 µM Pho8-MBP or Pho8*-MBP in binding buffer (50 mM HEPES pH 7.5, 150 mM NaCl, 10 mM $MgCl_2$, 20 µg BSA) in a total reaction volume of 30 µl. To determine the effect of Roq1 on Pho8 or Pho8* recruitment to Ubr1, Roq1 (22-60)-HA was added at final 2.5 µM to appropriate tubes. All samples were treated at 30°C for 90 minutes. 12 µl of amylose resin slurry (Table 6) pre-equilibrated in binding buffer were added and samples were incubated for 2 h at 4°C while rotating. After washing the beads three times, Pho8-MBP or Pho8*-MBP with bound proteins was eluted by adding 2x 10 µl elution buffer (50 mM HEPES pH 7.5, 150 mM NaCl, 10 mM $MgCl_2$, 10 mM maltose) with a 15-minute incubation step. Eluted fractions were pooled and loaded after boiling on a 7-15% step gradient SDS-PAGE gel for subsequent immunoblotting.
To monitor the interaction between Ubr1 and Rad6, Rad6 was first pre-charged with ubiquitin (denoted as ~Ub) to mimic the natural interaction between an E3 ligase and its cognate E2. To generate Rad6~Ub, 1.4 µM GST-Rad6 were mixed with 70 nM Uba1 and 5.6 µM ubiquitin in ubiquitination buffer (50 mM HEPES pH 7.5, 150 mM NaCl, 10 mM $MgCl_2$, 5 mM ATP) and incubated for 90 minutes at 30°C. Pre-charged GST-Rad6~Ub was added at final 0.4 µM to tubes containing 0.2 µM FLAG-Ubr1, 0.2 or 2.0 µM Roq1 (22-60)-HA (if desired) and 12 µl of pre-equilibrated glutathione resin (Table 6). The mixture was incubated overnight at 4°C while rotating. Beads were then washed three times with ubiquitination buffer. Bound proteins were eluted with ubiquitination buffer containing 20 mM glutathione and 1 mM DTT after a 45-minute incubation step at 4°C. 15 µl of each sample were loaded on a 4-15% gradient SDS-PAGE gel (Bio-Rad) and subjected to immunoblotting.
For *in vitro* binding experiments between Roq1 and Ubr1, see section 5.2.5.1. Roq1 variants were used at equimolar concentrations.

5.2.4.8 Photo-crosslinking (performed together with Sibylle Kanngießer)

Roq1 (22-104)-ALFA, Roq1 (22-104) (Y55Bpa)-ALFA or Roq1 (22-104) (Y56Bpa)-ALFA were immobilized on magnetic ALFA selector (CE) resin (see 5.2.4.1.2 Roq1 purification for detailed Roq1 purification protocol) and incubated with 150 µl ubiquitination buffer (50 mM HEPES, pH 7.5, 0.15 M NaCl, 10 mM $MgCl_2$) and 170 nM FLAG-Ubr1 were indicated. The mixture was incubated at 4°C for 2 h while rotating prior removal of the supernatant. Beads were washed four times with 500 µl ubiquitination reaction buffer. Proteins were eluted in 2x 25 µl ALFA elution buffer (50 mM HEPES, pH 7.5, 0.15 M NaCl, 10 mM $MgCl_2$, 800 µM ALFA peptide). 20 µl were saved as minus UV control and 20 µl were applied for photo-crosslinking. Samples were illuminated with a UV-LED lamp (Table 14) on ice at 365 nm with the following settings: 15 pulses of 1 s at maximum irradiation power (25 W/cm^2) with 2 sec pauses between pulses. Subsequently, 5 µl 5x sample buffer were added, samples were boiled for 5 min at 65°C prior SDS-PAGE using a 7.5-15% step gradient gel and immunoblotting.

5.2.4.9 Protein determination

Protein concentrations were determined using Bradford reagent (Table 5) in 96-well plates. A 1:5 dilution of the Bradford reagent concentrate was prepared in water and let come to room temperature. Using a 96-well plate, a bovine serum albumin (BSA) reference series was pipetted in duplicates with wells containing 0 – 5 µg BSA. 5 µl of a BSA stock solution ranging from 0 to 1 mg/ml was prepared. Samples were prepared in duplicates. 200 µl of diluted Bradford reagent were added to each well and the plate was incubated at room temperature for 5 minutes prior measurement of the absorbance at 595 nm.

5.2.4.10 SDS-PAGE and immunoblotting

Samples for SDS-PAGE or immunoblotting were prepared by adding 5x sample buffer (Table 4) to final 1x. Samples were boiled at 65°C for five minutes, briefly centrifuged and either stored at -20°C or directly loaded equally on SDS-PAGE gels

with appropriate polyacrylamide percentage (Tables 12 and 13). SDS-PAGE gels were run at room temperature at 200 V with a protein-dependent running time (usually between 35 and 80 minutes) to achieve maximum separation. The SDS-PAGE gel was briefly rinsed with water (Coomassie-staining) or 1x Blotting buffer (immunoblot). For Coomassie-staining, the SDS-PAGE gel was stained with InstantBlue Coomassie stain solution (Table 5) overnight and intensely destained the next day with water. For immunoblotting, proteins were blotted from SDS-PAGE gels on nitrocellulose membranes at 4°C at 100 V for 60-90 minutes, depending on protein size. Small and mid-sized proteins up to 50-60 kDa were blotted for 60 minutes whereas larger proteins and samples from ubiquitination assays were blotted for 90 minutes. Depending on the secondary antibody, membranes were briefly washed either with TBS (fluorescent antibody) or TBST (HRP-coupled antibody) (Table 4). Blocking was performed at room temperature for 10-15 minutes in TBS (fluorescent antibody) or TBST (HRP-coupled antibody) containing 5% (w/v) nonfat dry milk (Table 4). Primary antibodies (Table 11) were diluted in TBST containing 5% (w/v) nonfat dry milk and incubated on the membrane overnight at 4°C. The membranes were then washed 3x 5 minutes with TBST at room temperature before incubation with the secondary antibody (Table 4) for 1h at room temperature. Subsequently, the membranes were washed again for 3x 5 minutes with TBST. Membranes that were incubated with fluorescent antibodies were washed again for 2x 1 minute with TBS. Membranes incubated with a fluorescent secondary antibody were directly developed using an Odyssey CLx LI-COR imager (Table 14) to detect fluorescence at 700 or 800 nm. For the development of membranes incubated with HRP-coupled secondary antibodies, SuperSignal™ West Pico PLUS substrate (Table 10) was used. A 1:1 mixture of substrate A and B was incubated with the membranes for 5 minutes in the dark. Chemiluminescence was then detected using an Amersham 600 imager (Table 14).

5.2.5 Single-particle cryo-electron microscopy

5.2.5.1 Sample preparation

To isolate the Roq1-Ubr1 complex for negative stain-EM and cryo-EM, 0.7 µM FLAG-Ubr1 were mixed with 7.7 µM Roq1 (22-104)-ALFA in ubiquitination buffer (50 mM HEPES pH 7.5, 150 mM NaCl, 10 mM $MgCl_2$) and 20 µl of pre-equilibrated ALFA resin slurry in a total reaction volume of 120 µl. The sample was incubated overnight at 4°C while rotating to allow complex formation. Next day, beads were washed four times with ubiquitination buffer to remove unbound proteins. The FLAG-Ubr1:Roq1-ALFA protein complex was eluted in 3x 6 µl elution buffer (50 mM HEPES pH 7.5, 150 mM NaCl, 10 mM $MgCl_2$, 800 µM ALFA peptide). Fractions were pooled and directly used for negative stain EM (5.2.5.2) and the preparation of cryo-EM grids (see 5.2.5.3).

5.2.5.2 Negative stain EM (performed by Dirk Flemming)

The Roq1-Ubr1 complex was isolated as mentioned above (see 5.2.5.1) and negative stain-EM was performed as previously described (Bohl *et al*, 2024; Lutzmann *et al*, 2005). 5 µl of a 1:10 dilution of the complex in ubiquitination buffer (50 mM HEPES pH 7.5, 150 mM NaCl, 10 mM $MgCl_2$) was added to a glow-discharged, 6-8 nm continuous carbon layer-containing grid. The grid was incubated for 5 s before blotting with a Whatman filter paper and washing with water. The grids were incubated with uranyl acetate (3% w/v) and images were obtained using a Thermo Fisher Talos L120C electron microscope (Table 14) that was operated at 120 kV.

5.2.5.3 Grid preparation (performed by Dirk Flemming)

Grids for cryo-EM were prepared utilizing a Vitrobot mark IV (Table 14) that was run at 4°C and 100% humidity. 3 µl of the isolated Roq1-Ubr1 complex was added to a glow-discharged Quantifoil Cu 2.1 grid and blotted for 5 s (blot force: 5, drain time: 1 s, wait: 10 s) before plunge freezing into liquid ethane.

5.2.5.4 Data acquisition (performed by Dirk Flemming, Jan Rheinberger)

Two datasets of the Roq1-Ubr1 complex were obtained implementing the EPU software (Table 15) on a Titan Krios transmission electron microscope (Table 14). Information were obtained at 300 kV using a K3 camera (Table 14). The defocus range was set to −0.5 µm to −1.5 µm with a pixel size of 0.836 Å/pixel with a nominal magnification of 105,000. Micrograph movie stacks consisted of 70 frames with a dose of 60 e^{-}/A^{2}. 9636 movies and 972,724 particles were collected. A tilted dataset of 18°, as determined by cryoEF (Naydenova & Russo, 2017) was collected using similar parameters.

5.2.5.5. Data processing (performed by Dirk Flemming, Jan Rheinberger)

Data processing was conducted with the latest RELION version (Scheres, 2012a, b). First, the Roq1-Ubr1 dataset containing 9636 micrographs were used for two rounds of 2D classification. 972,724 particles were pooled and further classified into 3D classes without using symmetry options. To evaluate the resolution of refined maps, RELION postprocessing and the standard FSC value 0.143 were applied. This resulted in a final resolution of 6.3 Å. Local resolutions and angular distributions were calculated using RELION 5.0 beta.

5.2.6 Computational predictions and bioinformatic analyses

5.2.6.1 Protein disorder prediction

To predict disordered regions within the Roq1 protein, the Roq1 amino acid sequence (Uniprot ID: P47009) was uploaded to eleven different disorder prediction servers (Table 16). Individual scores were averaged and plotted with standard deviations against the respective amino acid residue number.

5.2.6.2 Roq1 and Ubr1 AlphaFold structure prediction

To predict protein structures the AlphaFold protein structure database from DeepMind was used (Jumper *et al*, 2021; Varadi *et al*, 2022). Roq1 structure was predicted using Uniprot ID P47009, whereas the Ubr1 structure was predicted using Uniprot ID P19812.

5.2.6.3 Protein binding interface prediction (collaboratively done with Bram Vermeulen)

To predict binding interfaces between Roq1 and Ubr1, AlphaFold Multimer (version 2.3.1) without relaxation was used by Bram Vermeulen to produce 25 models. Mini Roq1 (amino acid sequence: RSQRDQTRSPTQPGVIYYFVEL) lacking nonessential elements for Ubr1 reprogramming was used as input together with wild type Ubr1. PyMol was used by me for visualization.
To predict binding interfaces between Ubr1 and Pho8* I used the latest version of AlphaFold 3 (Abramson *et al.*, 2024). Truncated, SHRED-active Ubr1 (1-1812) was used together with the Rad6 and Pho8* sequences for the predictions. Seven zinc ions were included for structural integrity as previously described (Pan *et al*, 2021). To bring Ubr1 into the closed conformation, I aligned the highest ranked prediction model with the previously published Ubr1-Rad6~Ub-N-degron structure (7MEX, Pan *et al*, 2021) and visualized the complex using ChimeraX (Table 15).

5.2.6.4 Multiple sequence alignments (performed by Sebastian Schuck, replicated by me)

To search for Roq1 sequence homologs, the Uniprot ID of *Saccharomyces cerevisiae* Roq1 (P47009) was used to carry out a protein BLAST search. Isolated sequences from *Saccharomyces* and *Kazachstania* species were aligned with CLUSTAL Omega.

6. Bibliography

Abramson J, Adler J, Dunger J, Evans R, Green T, Pritzel A, Ronneberger O, Willmore L, Ballard AJ, Bambrick J *et al* (2024) Accurate structure prediction of biomolecular interactions with AlphaFold 3. *Nature*

Aksnes H, Drazic A, Marie M, Arnesen T (2016) First Things First: Vital Protein Marks by N-Terminal Acetyltransferases. *Trends Biochem Sci* 41: 746-760

Andreasson C, Fiaux J, Rampelt H, Druffel-Augustin S, Bukau B (2008) Insights into the structural dynamics of the Hsp110-Hsp70 interaction reveal the mechanism for nucleotide exchange activity. *Proc Natl Acad Sci U S A* 105: 16519-16524

Arhar T, Shkedi A, Nadel CM, Gestwicki JE (2021) The interactions of molecular chaperones with client proteins: why are they so weak? *J Biol Chem* 297: 101282

Ast T, Aviram N, Chuartzman SG, Schuldiner M (2014) A cytosolic degradation pathway, prERAD, monitors pre-inserted secretory pathway proteins. *J Cell Sci* 127: 3017-3023

Bachmair A, Finley D, Varshavsky A (1986) In vivo half-life of a protein is a function of its amino-terminal residue. *Science* 234: 179-186

Baek K, Krist DT, Prabu JR, Hill S, Klugel M, Neumaier LM, von Gronau S, Kleiger G, Schulman BA (2020) NEDD8 nucleates a multivalent cullin-RING-UBE2D ubiquitin ligation assembly. *Nature* 578: 461-466

Baker RT, Varshavsky A (1991) Inhibition of the N-end rule pathway in living cells. *Proc Natl Acad Sci U S A* 88: 1090-1094

Baker RT, Varshavsky A (1995) Yeast N-terminal amidase. A new enzyme and component of the N-end rule pathway. *J Biol Chem* 270: 12065-12074

Balaji V, Muller L, Lorenz R, Kevei E, Zhang WH, Santiago U, Gebauer J, Llamas E, Vilchez D, Camacho CJ *et al* (2022) A dimer-monomer switch controls CHIP-dependent substrate ubiquitylation and processing. *Mol Cell* 82: 3239-3254 e3211

Balzi E, Choder M, Chen WN, Varshavsky A, Goffeau A (1990) Cloning and functional analysis of the arginyl-tRNA-protein transferase gene ATE1 of Saccharomyces cerevisiae. *J Biol Chem* 265: 7464-7471

Bard JAM, Goodall EA, Greene ER, Jonsson E, Dong KC, Martin A (2018) Structure and Function of the 26S Proteasome. *Annu Rev Biochem* 87: 697-724

Bartel B, Wunning I, Varshavsky A (1990) The recognition component of the N-end rule pathway. *EMBO J* 9: 3179-3189

Bartke T, Pohl C, Pyrowolakis G, Jentsch S (2004) Dual role of BRUCE as an antiapoptotic IAP and a chimeric E2/E3 ubiquitin ligase. *Mol Cell* 14: 801-811

Bays NW, Gardner RG, Seelig LP, Joazeiro CA, Hampton RY (2001) Hrd1p/Der3p is a membrane-anchored ubiquitin ligase required for ER-associated degradation. *Nat Cell Biol* 3: 24-29

Bilodeau PS, Urbanowski JL, Winistorfer SC, Piper RC (2002) The Vps27p Hse1p complex binds ubiquitin and mediates endosomal protein sorting. *Nat Cell Biol* 4: 534-539

Boban M, Ljungdahl PO, Foisner R (2015) Atypical ubiquitylation in yeast targets lysine-less Asi2 for proteasomal degradation. *J Biol Chem* 290: 2489-2495

Bodrug T, Welsh KA, Bolhuis DL, Paulsmall a CE, Martinez-Chacin RC, Liu B, Pinkin N, Bonacci T, Cui L, Xu P *et al* (2023) Time-resolved cryo-EM (TR-EM) analysis of substrate polyubiquitination by the RING E3 anaphase-promoting complex/cyclosome (APC/C). *Nat Struct Mol Biol*

Bohl V, Hollmann NM, Melzer T, Katikaridis P, Meins L, Simon B, Flemming D, Sinning I, Hennig J, Mogk A (2024) The Listeria monocytogenes persistence factor ClpL is a potent stand-alone disaggregase. *Elife* 12

Bracher PJ, Snyder PW, Bohall BR, Whitesides GM (2011) The relative rates of thiol-thioester exchange and hydrolysis for alkyl and aryl thioalkanoates in water. *Orig Life Evol Biosph* 41: 399-412

Branigan E, Carlos Penedo J, Hay RT (2020) Ubiquitin transfer by a RING E3 ligase occurs from a closed E2~ubiquitin conformation. *Nat Commun* 11: 2846

Breckel CA, Hochstrasser M (2021) Ubiquitin Ligase Redundancy and Nuclear-Cytoplasmic Localization in Yeast Protein Quality Control. *Biomolecules* 11

Brown NG, VanderLinden R, Watson ER, Weissmann F, Ordureau A, Wu KP, Zhang W, Yu S, Mercredi PY, Harrison JS *et al* (2016) Dual RING E3 Architectures Regulate Multiubiquitination and Ubiquitin Chain Elongation by APC/C. *Cell* 165: 1440-1453

Brzovic PS, Lissounov A, Christensen DE, Hoyt DW, Klevit RE (2006) A UbcH5/ubiquitin noncovalent complex is required for processive BRCA1-directed ubiquitination. *Mol Cell* 21: 873-880

Buetow L, Gabrielsen M, Anthony NG, Dou H, Patel A, Aitkenhead H, Sibbet GJ, Smith BO, Huang DT (2015) Activation of a primed RING E3-E2-ubiquitin complex by non-covalent ubiquitin. *Mol Cell* 58: 297-310

Buetow L, Gabrielsen M, Huang DT (2018) Single-Turnover RING/U-Box E3-Mediated Lysine Discharge Assays. *Methods Mol Biol* 1844: 19-31

Buetow L, Huang DT (2016) Structural insights into the catalysis and regulation of E3 ubiquitin ligases. *Nat Rev Mol Cell Biol* 17: 626-642

Canto C, Menzies KJ, Auwerx J (2015) NAD(+) Metabolism and the Control of Energy Homeostasis: A Balancing Act between Mitochondria and the Nucleus. *Cell Metab* 22: 31-53

Cappadocia L, Lima CD (2018) Ubiquitin-like Protein Conjugation: Structures, Chemistry, and Mechanism. *Chem Rev* 118: 889-918

Carvalho P, Goder V, Rapoport TA (2006) Distinct ubiquitin-ligase complexes define convergent pathways for the degradation of ER proteins. *Cell* 126: 361-373

Chambers LR, Ye Q, Cai J, Gong M, Ledvina HE, Zhou H, Whiteley AT, Suhandynata RT, Corbett KD (2024) A eukaryotic-like ubiquitination system in bacterial antiviral defence. *Nature* 631: 843-849

Chen Q, Yang R, Korolev N, Liu CF, Nordenskiold L (2017a) Regulation of Nucleosome Stacking and Chromatin Compaction by the Histone H4 N-Terminal Tail-H2A Acidic Patch Interaction. *J Mol Biol* 429: 2075-2092

Chen SJ, Wu X, Wadas B, Oh JH, Varshavsky A (2017b) An N-end rule pathway that recognizes proline and destroys gluconeogenic enzymes. *Science* 355

Chen Y, Zhou D, Yao Y, Sun Y, Yao F, Ma L (2022) Monoubiquitination in Homeostasis and Cancer. *Int J Mol Sci* 23

Cheng J, Randall AZ, Sweredoski MJ, Baldi P (2005) SCRATCH: a protein structure and structural feature prediction server. *Nucleic Acids Res* 33: W72-76

Chhabra Y, Wong HY, Nikolajsen LF, Steinocher H, Papadopulos A, Tunny KA, Meunier FA, Smith AG, Kragelund BB, Brooks AJ *et al* (2018) A growth hormone receptor SNP promotes lung cancer by impairment of SOCS2-mediated degradation. *Oncogene* 37: 489-501

Chin JW, Martin AB, King DS, Wang L, Schultz PG (2002) Addition of a photocrosslinking amino acid to the genetic code of Escherichiacoli. *Proc Natl Acad Sci U S A* 99: 11020-11024

Chirnomas D, Hornberger KR, Crews CM (2023) Protein degraders enter the clinic - a new approach to cancer therapy. *Nat Rev Clin Oncol* 20: 265-278

Choi WS, Jeong BC, Joo YJ, Lee MR, Kim J, Eck MJ, Song HK (2010) Structural basis for the recognition of N-end rule substrates by the UBR box of ubiquitin ligases. *Nat Struct Mol Biol* 17: 1175-1181

Christianson JC, Carvalho P (2022) Order through destruction: how ER-associated protein degradation contributes to organelle homeostasis. *EMBO J* 41: e109845

Chrustowicz J, Sherpa D, Teyra J, Loke MS, Popowicz GM, Basquin J, Sattler M, Prabu JR, Sidhu SS, Schulman BA (2022) Multifaceted N-Degron Recognition and Ubiquitylation by GID/CTLH E3 Ligases. *J Mol Biol* 434: 167347

Ciehanover A, Hod Y, Hershko A (1978) A heat-stable polypeptide component of an ATP-dependent proteolytic system from reticulocytes. *Biochem Biophys Res Commun* 81: 1100-1105

Cruz Walma DA, Chen Z, Bullock AN, Yamada KM (2022) Ubiquitin ligases: guardians of mammalian development. *Nat Rev Mol Cell Biol* 23: 350-367

DaRosa PA, Wang Z, Jiang X, Pruneda JN, Cong F, Klevit RE, Xu W (2015) Allosteric activation of the RNF146 ubiquitin ligase by a poly(ADP-ribosyl)ation signal. *Nature* 517: 223-226

Das R, Mariano J, Tsai YC, Kalathur RC, Kostova Z, Li J, Tarasov SG, McFeeters RL, Altieri AS, Ji X *et al* (2009) Allosteric activation of E2-RING finger-mediated ubiquitylation by a structurally defined specific E2-binding region of gp78. *Mol Cell* 34: 674-685

Davey NE, Cyert MS, Moses AM (2015) Short linear motifs - ex nihilo evolution of protein regulation. *Cell Commun Signal* 13: 43

Davey NE, Van Roey K, Weatheritt RJ, Toedt G, Uyar B, Altenberg B, Budd A, Diella F, Dinkel H, Gibson TJ (2012) Attributes of short linear motifs. *Mol Biosyst* 8: 268-281

Del Conte A, Bouhraoua A, Mehdiabadi M, Clementel D, Monzon AM, predictors C, Tosatto SCE, Piovesan D (2023) CAID prediction portal: a comprehensive service for predicting intrinsic disorder and binding regions in proteins. *Nucleic Acids Res* 51: W62-W69

Demir D, Kendir Demirkol Y, Gerenli N, Aktas Karabay E (2022) Johanson-Blizzard's Syndrome with a Novel UBR1 Mutation. *J Pediatr Genet* 11: 147-150

Deng Z, Ai H, Sun M, Tong Z, Du Y, Qu Q, Zhang L, Xu Z, Tao S, Shi Q *et al* (2023) Mechanistic insights into nucleosomal H2B monoubiquitylation mediated by yeast Bre1-Rad6 and its human homolog RNF20/RNF40-hRAD6A. *Mol Cell*

Deol KK, Lorenz S, Strieter ER (2019) Enzymatic Logic of Ubiquitin Chain Assembly. *Front Physiol* 10: 835

Deshaies RJ, Joazeiro CA (2009) RING domain E3 ubiquitin ligases. *Annu Rev Biochem* 78: 399-434

Dietz L, Ellison CJ, Riechmann C, Cassidy CK, Felfoldi FD, Pinto-Fernandez A, Kessler BM, Elliott PR (2023) Structural basis for SMAC-mediated antagonism of caspase inhibition by the giant ubiquitin ligase BIRC6. *Science* 379: 1112-1117

Dikic I, Schulman BA (2022) An expanded lexicon for the ubiquitin code. *Nat Rev Mol Cell Biol*

Dikic I, Wakatsuki S, Walters KJ (2009) Ubiquitin-binding domains - from structures to functions. *Nat Rev Mol Cell Biol* 10: 659-671

Dou H, Buetow L, Hock A, Sibbet GJ, Vousden KH, Huang DT (2012a) Structural basis for autoinhibition and phosphorylation-dependent activation of c-Cbl. *Nat Struct Mol Biol* 19: 184-192

Dou H, Buetow L, Sibbet GJ, Cameron K, Huang DT (2012b) BIRC7-E2 ubiquitin conjugate structure reveals the mechanism of ubiquitin transfer by a RING dimer. *Nat Struct Mol Biol* 19: 876-883

Dou H, Buetow L, Sibbet GJ, Cameron K, Huang DT (2013) Essentiality of a non-RING element in priming donor ubiquitin for catalysis by a monomeric E3. *Nat Struct Mol Biol* 20: 982-986

Du F, Navarro-Garcia F, Xia Z, Tasaki T, Varshavsky A (2002) Pairs of dipeptides synergistically activate the binding of substrate by ubiquitin ligase through dissociation of its autoinhibitory domain. *Proc Natl Acad Sci U S A* 99: 14110-14115

Eckelman BP, Drag M, Snipas SJ, Salvesen GS (2008) The mechanism of peptide-binding specificity of IAP BIR domains. *Cell Death Differ* 15: 920-928

Ehrmann JF, Grabarczyk DB, Heinke M, Deszcz L, Kurzbauer R, Hudecz O, Shulkina A, Gogova R, Meinhart A, Versteeg GA *et al* (2023) Structural basis for regulation of apoptosis and autophagy by the BIRC6/SMAC complex. *Science* 379: 1117-1123

Eisele F, Wolf DH (2008) Degradation of misfolded protein in the cytoplasm is mediated by the ubiquitin ligase Ubr1. *FEBS Lett* 582: 4143-4146

Emenecker RJ, Griffith D, Holehouse AS (2021) Metapredict: a fast, accurate, and easy-to-use predictor of consensus disorder and structure. *Biophys J* 120: 4312-4319

Erdos G, Pajkos M, Dosztanyi Z (2021) IUPred3: prediction of protein disorder enhanced with unambiguous experimental annotation and visualization of evolutionary conservation. *Nucleic Acids Res* 49: W297-W303

Erpapazoglou Z, Walker O, Haguenauer-Tsapis R (2014) Versatile roles of k63-linked ubiquitin chains in trafficking. *Cells* 3: 1027-1088

European Space Agency. 2023. Rosetta Factsheet. https://www.esa.int/Science_Exploration/Space_Science/Rosetta/Rosetta_factsheet (accessed 15th August 2024)

Fang NN, Chan GT, Zhu M, Comyn SA, Persaud A, Deshaies RJ, Rotin D, Gsponer J, Mayor T (2014) Rsp5/Nedd4 is the main ubiquitin ligase that targets cytosolic misfolded proteins following heat stress. *Nat Cell Biol* 16: 1227-1237

Fang NN, Ng AH, Measday V, Mayor T (2011) Hul5 HECT ubiquitin ligase plays a major role in the ubiquitylation and turnover of cytosolic misfolded proteins. *Nat Cell Biol* 13: 1344-1352

Fang S, Chen G, Wang Y, Ganti R, Chernova TA, Zhou L, Jacobs SE, Duong D, Kiyokawa H, Chernoff YO *et al* (2023) Profiling and verifying the substrates of E3 ubiquitin ligase Rsp5 in yeast cells. *STAR Protoc* 4: 102489

Finley D (2009) Recognition and processing of ubiquitin-protein conjugates by the proteasome. *Annu Rev Biochem* 78: 477-513

Finley D, Ulrich HD, Sommer T, Kaiser P (2012) The ubiquitin-proteasome system of Saccharomyces cerevisiae. *Genetics* 192: 319-360

Fischer ES, Scrima A, Bohm K, Matsumoto S, Lingaraju GM, Faty M, Yasuda T, Cavadini S, Wakasugi M, Hanaoka F *et al* (2011) The molecular basis of

CRL4DDB2/CSA ubiquitin ligase architecture, targeting, and activation. *Cell* 147: 1024-1039

Fredrickson EK, Rosenbaum JC, Locke MN, Milac TI, Gardner RG (2011) Exposed hydrophobicity is a key determinant of nuclear quality control degradation. *Mol Biol Cell* 22: 2384-2395

French ME, Klosowiak JL, Aslanian A, Reed SI, Yates JR, 3rd, Hunter T (2017) Mechanism of ubiquitin chain synthesis employed by a HECT domain ubiquitin ligase. *J Biol Chem* 292: 10398-10413

Gallego LD, Ghodgaonkar Steger M, Polyansky AA, Schubert T, Zagrovic B, Zheng N, Clausen T, Herzog F, Kohler A (2016) Structural mechanism for the recognition and ubiquitination of a single nucleosome residue by Rad6-Bre1. *Proc Natl Acad Sci U S A* 113: 10553-10558

Geffen Y, Appleboim A, Gardner RG, Friedman N, Sadeh R, Ravid T (2016) Mapping the Landscape of a Eukaryotic Degronome. *Mol Cell* 63: 1055-1065

George AJ, Hoffiz YC, Charles AJ, Zhu Y, Mabb AM (2018) A Comprehensive Atlas of E3 Ubiquitin Ligase Mutations in Neurological Disorders. *Front Genet* 9: 29

Gibson DG, Young L, Chuang RY, Venter JC, Hutchison CA, 3rd, Smith HO (2009) Enzymatic assembly of DNA molecules up to several hundred kilobases. *Nat Methods* 6: 343-345

Goldstein G, Scheid M, Hammerling U, Schlesinger DH, Niall HD, Boyse EA (1975) Isolation of a polypeptide that has lymphocyte-differentiating properties and is probably represented universally in living cells. *Proc Natl Acad Sci U S A* 72: 11-15

Gonzalez-Foutel NS, Glavina J, Borcherds WM, Safranchik M, Barrera-Vilarmau S, Sagar A, Estana A, Barozet A, Garrone NA, Fernandez-Ballester G *et al* (2022) Conformational buffering underlies functional selection in intrinsically disordered protein regions. *Nat Struct Mol Biol* 29: 781-790

Gottemukkala KV, Chrustowicz J, Sherpa D, Sepic S, Vu DT, Karayel O, Papadopoulou EC, Gross A, Schorpp K, von Gronau S *et al* (2024) Non-canonical substrate recognition by the human WDR26-CTLH E3 ligase regulates prodrug metabolism. *Mol Cell* 84: 1948-1963 e1911

Haakonsen DL, Rape M (2019) Branching Out: Improved Signaling by Heterotypic Ubiquitin Chains. *Trends Cell Biol* 29: 704-716

Heck JW, Cheung SK, Hampton RY (2010) Cytoplasmic protein quality control degradation mediated by parallel actions of the E3 ubiquitin ligases Ubr1 and San1. *Proc Natl Acad Sci U S A* 107: 1106-1111

Heidarsson PO, Mercadante D, Sottini A, Nettels D, Borgia MB, Borgia A, Kilic S, Fierz B, Best RB, Schuler B (2022) Release of linker histone from the nucleosome driven by polyelectrolyte competition with a disordered protein. *Nat Chem* 14: 224-231

Hershko A, Ciechanover A (1998) The ubiquitin system. *Annu Rev Biochem* 67: 425-479

Hershko A, Heller H, Elias S, Ciechanover A (1983) Components of ubiquitin-protein ligase system. Resolution, affinity purification, and role in protein breakdown. *J Biol Chem* 258: 8206-8214

Hibbert RG, Huang A, Boelens R, Sixma TK (2011) E3 ligase Rad18 promotes monoubiquitination rather than ubiquitin chain formation by E2 enzyme Rad6. *Proc Natl Acad Sci U S A* 108: 5590-5595

Hicke L, Dunn R (2003) Regulation of membrane protein transport by ubiquitin and ubiquitin-binding proteins. *Annu Rev Cell Dev Biol* 19: 141-172

Higuchi-Sanabria R, Frankino PA, Paul JW, 3rd, Tronnes SU, Dillin A (2018) A Futile Battle? Protein Quality Control and the Stress of Aging. *Dev Cell* 44: 139-163

Hochstrasser M (1996) Ubiquitin-dependent protein degradation. *Annu Rev Genet* 30: 405-439

Hodakova Z, Grishkovskaya I, Brunner HL, Bolhuis DL, Belacic K, Schleiffer A, Kotisch H, Brown NG, Haselbach D (2023) Cryo-EM structure of the chain-elongating E3 ubiquitin ligase UBR5. *EMBO J* 42: e113348

Hoege C, Pfander B, Moldovan GL, Pyrowolakis G, Jentsch S (2002) RAD6-dependent DNA repair is linked to modification of PCNA by ubiquitin and SUMO. *Nature* 419: 135-141

Hoie MH, Kiehl EN, Petersen B, Nielsen M, Winther O, Nielsen H, Hallgren J, Marcatili P (2022) NetSurfP-3.0: accurate and fast prediction of protein structural features by protein language models and deep learning. *Nucleic Acids Res* 50: W510-W515

Hu RG, Sheng J, Qi X, Xu Z, Takahashi TT, Varshavsky A (2005) The N-end rule pathway as a nitric oxide sensor controlling the levels of multiple regulators. *Nature* 437: 981-986

Hu RG, Wang H, Xia Z, Varshavsky A (2008) The N-end rule pathway is a sensor of heme. *Proc Natl Acad Sci U S A* 105: 76-81

Hunkeler M, Jin CY, Fischer ES (2023) Structures of BIRC6-client complexes provide a mechanism of SMAC-mediated release of caspases. *Science* 379: 1105-1111

Huyer G, Piluek WF, Fansler Z, Kreft SG, Hochstrasser M, Brodsky JL, Michaelis S (2004) Distinct machinery is required in Saccharomyces cerevisiae for the endoplasmic reticulum-associated degradation of a multispanning membrane protein and a soluble luminal protein. *J Biol Chem* 279: 38369-38378

Hwang CS, Shemorry A, Auerbach D, Varshavsky A (2010a) The N-end rule pathway is mediated by a complex of the RING-type Ubr1 and HECT-type Ufd4 ubiquitin ligases. *Nat Cell Biol* 12: 1177-1185

Hwang CS, Shemorry A, Varshavsky A (2009) Two proteolytic pathways regulate DNA repair by cotargeting the Mgt1 alkylguanine transferase. *Proc Natl Acad Sci U S A* 106: 2142-2147

Hwang CS, Shemorry A, Varshavsky A (2010b) N-terminal acetylation of cellular proteins creates specific degradation signals. *Science* 327: 973-977

Hwang CS, Varshavsky A (2008) Regulation of peptide import through phosphorylation of Ubr1, the ubiquitin ligase of the N-end rule pathway. *Proc Natl Acad Sci U S A* 105: 19188-19193

Ibarra R, Borror HR, Hart B, Gardner RG, Kleiger G (2021) The San1 Ubiquitin Ligase Avidly Recognizes Misfolded Proteins through Multiple Substrate Binding Sites. *Biomolecules* 11

Ishida T, Kinoshita K (2007) PrDOS: prediction of disordered protein regions from amino acid sequence. *Nucleic Acids Res* 35: W460-464

Ito F, Alvarez-Cabrera AL, Liu S, Yang H, Shiriaeva A, Zhou ZH, Chen XS (2023) Structural basis for HIV-1 antagonism of host APOBEC3G via Cullin E3 ligase. *Sci Adv* 9: eade3168

Jang HS, Lee Y, Kim Y, Huh WK (2024) The ubiquitin-proteasome system degrades fatty acid synthase under nitrogen starvation when autophagy is dysfunctional in Saccharomyces cerevisiae. *Biochem Biophys Res Commun* 733: 150423

Jevtic P, Haakonsen DL, Rape M (2021) An E3 ligase guide to the galaxy of small-molecule-induced protein degradation. *Cell Chem Biol* 28: 1000-1013

Ji Z, Li H, Peterle D, Paulo JA, Ficarro SB, Wales TE, Marto JA, Gygi SP, Engen JR, Rapoport TA (2022) Translocation of polyubiquitinated protein substrates by the hexameric Cdc48 ATPase. *Mol Cell* 82: 570-584 e578

Jumper J, Evans R, Pritzel A, Green T, Figurnov M, Ronneberger O, Tunyasuvunakool K, Bates R, Zidek A, Potapenko A *et al* (2021) Highly accurate protein structure prediction with AlphaFold. *Nature* 596: 583-589

Kaganovich D, Kopito R, Frydman J (2008) Misfolded proteins partition between two distinct quality control compartments. *Nature* 454: 1088-1095

Kampmeyer C, Larsen-Ledet S, Wagnkilde MR, Michelsen M, Iversen HKM, Nielsen SV, Lindemose S, Caregnato A, Ravid T, Stein A *et al* (2022) Disease-linked mutations cause exposure of a protein quality control degron. *Structure* 30: 1245-1253 e1245

Kannouche PL, Wing J, Lehmann AR (2004) Interaction of human DNA polymerase eta with monoubiquitinated PCNA: a possible mechanism for the polymerase switch in response to DNA damage. *Mol Cell* 14: 491-500

Kastner B, Fischer N, Golas MM, Sander B, Dube P, Boehringer D, Hartmuth K, Deckert J, Hauer F, Wolf E *et al* (2008) GraFix: sample preparation for single-particle electron cryomicroscopy. *Nat Methods* 5: 53-55

Kelsall IR (2022) Non-lysine ubiquitylation: Doing things differently. *Front Mol Biosci* 9: 1008175

Kelsall IR, McCrory EH, Xu Y, Scudamore CL, Nanda SK, Mancebo-Gamella P, Wood NT, Knebel A, Matthews SJ, Cohen P (2022) HOIL-1 ubiquitin ligase activity targets unbranched glucosaccharides and is required to prevent polyglucosan accumulation. *EMBO J* 41: e109700

Keszei AF, Sicheri F (2017) Mechanism of catalysis, E2 recognition, and autoinhibition for the IpaH family of bacterial E3 ubiquitin ligases. *Proc Natl Acad Sci U S A* 114: 1311-1316

Kim YE, Hipp MS, Bracher A, Hayer-Hartl M, Hartl FU (2013) Molecular chaperone functions in protein folding and proteostasis. *Annu Rev Biochem* 82: 323-355

Kirisako T, Kamei K, Murata S, Kato M, Fukumoto H, Kanie M, Sano S, Tokunaga F, Tanaka K, Iwai K (2006) A ubiquitin ligase complex assembles linear polyubiquitin chains. *EMBO J* 25: 4877-4887

Koegl M, Hoppe T, Schlenker S, Ulrich HD, Mayer TU, Jentsch S (1999) A novel ubiquitination factor, E4, is involved in multiubiquitin chain assembly. *Cell* 96: 635-644

Komander D, Rape M (2012) The ubiquitin code. *Annu Rev Biochem* 81: 203-229

Konstantinidou M, Arkin MR (2024) Molecular glues for protein-protein interactions: Progressing toward a new dream. *Cell Chem Biol*

Kumar P, Magala P, Geiger-Schuller KR, Majumdar A, Tolman JR, Wolberger C (2015) Role of a non-canonical surface of Rad6 in ubiquitin conjugating activity. *Nucleic Acids Res* 43: 9039-9050

Labbadia J, Morimoto RI (2015) The biology of proteostasis in aging and disease. *Annu Rev Biochem* 84: 435-464

Le L, Park S, Lee JH, Kim YK, Lee MJ (2024) N-recognins UBR1 and UBR2 as central ER stress sensors in mammals. *Mol Cells* 47: 100001

Li J, Purser N, Liwocha J, Scott DC, Byers HA, Steigenberger B, Hill S, Tripathi-Giesgen I, Hinkle T, Hansen FM *et al* (2024) Cullin-RING ligases employ geometrically optimized catalytic partners for substrate targeting. *Mol Cell* 84: 1304-1320 e1316

Li M, Brooks CL, Wu-Baer F, Chen D, Baer R, Gu W (2003) Mono- versus polyubiquitination: differential control of p53 fate by Mdm2. *Science* 302: 1972-1975

Li W, Tu D, Brunger AT, Ye Y (2007) A ubiquitin ligase transfers preformed polyubiquitin chains from a conjugating enzyme to a substrate. *Nature* 446: 333-337

Li YL, Langley CA, Azumaya CM, Echeverria I, Chesarino NM, Emerman M, Cheng Y, Gross JD (2023) The structural basis for HIV-1 Vif antagonism of human APOBEC3G. *Nature* 615: 728-733

Liao Y, Sumara I, Pangou E (2022) Non-proteolytic ubiquitylation in cellular signaling and human disease. *Commun Biol* 5: 114

Lin HC, Yeh CW, Chen YF, Lee TT, Hsieh PY, Rusnac DV, Lin SY, Elledge SJ, Zheng N, Yen HS (2018) C-Terminal End-Directed Protein Elimination by CRL2 Ubiquitin Ligases. *Mol Cell* 70: 602-613 e603

Linding R, Jensen LJ, Diella F, Bork P, Gibson TJ, Russell RB (2003) Protein disorder prediction: implications for structural proteomics. *Structure* 11: 1453-1459

Liu C, Liu W, Ye Y, Li W (2017) Ufd2p synthesizes branched ubiquitin chains to promote the degradation of substrates modified with atypical chains. *Nat Commun* 8: 14274

Liwocha J, Li J, Purser N, Rattanasopa C, Maiwald S, Krist DT, Scott DC, Steigenberger B, Prabu JR, Schulman BA *et al* (2024) Mechanism of millisecond Lys48-linked poly-ubiquitin chain formation by cullin-RING ligases. *Nat Struct Mol Biol* 31: 378-389

Lutzmann M, Kunze R, Stangl K, Stelter P, Toth KF, Bottcher B, Hurt E (2005) Reconstitution of Nup157 and Nup145N into the Nup84 complex. *J Biol Chem* 280: 18442-18451

Mace PD, Day CL (2023) A massive machine regulates cell death. *Science* 379: 1093-1094

Malsam J, Barfuss S, Trimbuch T, Zarebidaki F, Sonnen AF, Wild K, Scheutzow A, Rohland L, Mayer MP, Sinning I *et al* (2020) Complexin Suppresses Spontaneous Exocytosis by Capturing the Membrane-Proximal Regions of VAMP2 and SNAP25. *Cell Rep* 32: 107926

Maria-Solano M, Lazim R, Choi S (2024) In silico design and binding mechanism od E3 Ligase Ubr1 recruiters. *bioRxiv preprint*

Mark KG, Kolla S, Aguirre JD, Garshott DM, Schmitt S, Haakonsen DL, Xu C, Kater L, Kempf G, Martinez-Gonzalez B *et al* (2023) Orphan quality control shapes network dynamics and gene expression. *Cell* 186: 3460-3475 e3423

Martin EW, Thomasen FE, Milkovic NM, Cuneo MJ, Grace CR, Nourse A, Lindorff-Larsen K, Mittag T (2021) Interplay of folded domains and the disordered low-complexity domain in mediating hnRNPA1 phase separation. *Nucleic Acids Res* 49: 2931-2945

Martinez-Chacin RC, Bodrug T, Bolhuis DL, Kedziora KM, Bonacci T, Ordureau A, Gibbs ME, Weissmann F, Qiao R, Grant GD *et al* (2020) Ubiquitin chain-elongating enzyme UBE2S activates the RING E3 ligase APC/C for substrate priming. *Nat Struct Mol Biol* 27: 550-560

Martinez-Fonts K, Davis C, Tomita T, Elsasser S, Nager AR, Shi Y, Finley D, Matouschek A (2020) The proteasome 19S cap and its ubiquitin receptors provide a versatile recognition platform for substrates. *Nat Commun* 11: 477

Martins LM, Iaccarino I, Tenev T, Gschmeissner S, Totty NF, Lemoine NR, Savopoulos J, Gray CW, Creasy CL, Dingwall C *et al* (2002) The serine protease Omi/HtrA2 regulates apoptosis by binding XIAP through a reaper-like motif. *J Biol Chem* 277: 439-444

Mashahreh B, Armony S, Johansson KE, Chappleboim A, Friedman N, Gardner RG, Hartmann-Petersen R, Lindorff-Larsen K, Ravid T (2022) Conserved degronome features governing quality control associated proteolysis. *Nat Commun* 13: 7588

Masuda Y, Suzuki M, Kawai H, Hishiki A, Hashimoto H, Masutani C, Hishida T, Suzuki F, Kamiya K (2012) En bloc transfer of polyubiquitin chains to PCNA in vitro is mediated by two different human E2-E3 pairs. *Nucleic Acids Res* 40: 10394-10407

Mato AR, Wierda WG, Ai WZ, Flinn IW, Tees M, Patel MR, Patel K, O'Brien S, Bond DA, Roeker LE *et al* (2022) NX-2127-001, a First-in-Human Trial of NX-2127, a Bruton's Tyrosine Kinase-Targeted Protein Degrader, in Patients with Relapsed or Refractory Chronic Lymphocytic Leukemia and B-Cell Malignancies. *Blood* 140: 2329-2332

Matta-Camacho E, Kozlov G, Li FF, Gehring K (2010) Structural basis of substrate recognition and specificity in the N-end rule pathway. *Nat Struct Mol Biol* 17: 1182-1187

Mayer MP, Gierasch LM (2019) Recent advances in the structural and mechanistic aspects of Hsp70 molecular chaperones. *J Biol Chem* 294: 2085-2097

Metzger MB, Liang YH, Das R, Mariano J, Li S, Li J, Kostova Z, Byrd RA, Ji X, Weissman AM (2013) A structurally unique E2-binding domain activates ubiquitination by the ERAD E2, Ubc7p, through multiple mechanisms. *Mol Cell* 50: 516-527

Metzger MB, Scales JL, Dunklebarger MF, Loncarek J, Weissman AM (2020) A protein quality control pathway at the mitochondrial outer membrane. *Elife* 9

Meyer HJ, Rape M (2014) Enhanced protein degradation by branched ubiquitin chains. *Cell* 157: 910-921

Meyer K, Kirchner M, Uyar B, Cheng JY, Russo G, Hernandez-Miranda LR, Szymborska A, Zauber H, Rudolph IM, Willnow TE *et al* (2018) Mutations in Disordered Regions Can Cause Disease by Creating Dileucine Motifs. *Cell* 175: 239-253 e217

Middleton AJ, Barzak FM, Fokkens TJ, Nguyen K, Day CL (2023) Zinc finger 1 of the RING E3 ligase, RNF125, interacts with the E2 to enhance ubiquitylation. *Structure*

Miller SB, Ho CT, Winkler J, Khokhrina M, Neuner A, Mohamed MY, Guilbride DL, Richter K, Lisby M, Schiebel E *et al* (2015) Compartment-specific aggregases direct distinct nuclear and cytoplasmic aggregate deposition. *EMBO J* 34: 778-797

Mittal A, Holehouse AS, Cohan MC, Pappu RV (2018) Sequence-to-Conformation Relationships of Disordered Regions Tethered to Folded Domains of Proteins. *J Mol Biol* 430: 2403-2421

Mizianty MJ, Peng Z, Kurgan L (2013) MFDp2: Accurate predictor of disorder in proteins by fusion of disorder probabilities, content and profiles. *Intrinsically Disord Proteins* 1: e24428

Mizushima N (2024) Ubiquitin in autophagy and non-protein ubiquitination. *Nat Struct Mol Biol* 31: 208-209

Moore SD, Prevelige PE, Jr. (2002) A P22 scaffold protein mutation increases the robustness of head assembly in the presence of excess portal protein. *J Virol* 76: 10245-10255

Mullard A (2021) FDA approves first EGFR exon 20 targeted kinase inhibitor. *Nat Rev Drug Discov* 20: 806

Muller L, Hoppe T (2024) UPS-dependent strategies of protein quality control degradation. *Trends Biochem Sci*

Nakasone MA, Majorek KA, Gabrielsen M, Sibbet GJ, Smith BO, Huang DT (2022) Structure of UBE2K-Ub/E3/polyUb reveals mechanisms of K48-linked Ub chain extension. *Nat Chem Biol* 18: 422-431

Naydenova K, Russo CJ (2017) Measuring the effects of particle orientation to improve the efficiency of electron cryomicroscopy. *Nat Commun* 8: 629

Nelson SL, Li Y, Chen Y, Deshmukh L (2023) Avidity-Based Method for the Efficient Generation of Monoubiquitinated Recombinant Proteins. *J Am Chem Soc* 145: 7748-7752

Nillegoda NB, Theodoraki MA, Mandal AK, Mayo KJ, Ren HY, Sultana R, Wu K, Johnson J, Cyr DM, Caplan AJ (2010) Ubr1 and Ubr2 function in a quality control pathway for degradation of unfolded cytosolic proteins. *Mol Biol Cell* 21: 2102-2116

Oh JH, Hyun JY, Chen SJ, Varshavsky A (2020) Five enzymes of the Arg/N-degron pathway form a targeting complex: The concept of superchanneling. *Proc Natl Acad Sci U S A* 117: 10778-10788

Oh JH, Hyun JY, Varshavsky A (2017) Control of Hsp90 chaperone and its clients by N-terminal acetylation and the N-end rule pathway. *Proc Natl Acad Sci U S A* 114: E4370-E4379

Ohtake F, Saeki Y, Sakamoto K, Ohtake K, Nishikawa H, Tsuchiya H, Ohta T, Tanaka K, Kanno J (2015) Ubiquitin acetylation inhibits polyubiquitin chain elongation. *EMBO Rep* 16: 192-201

Otten EG, Werner E, Crespillo-Casado A, Boyle KB, Dharamdasani V, Pathe C, Santhanam B, Randow F (2021) Ubiquitylation of lipopolysaccharide by RNF213 during bacterial infection. *Nature* 594: 111-116

Ozkan E, Yu H, Deisenhofer J (2005) Mechanistic insight into the allosteric activation of a ubiquitin-conjugating enzyme by RING-type ubiquitin ligases. *Proc Natl Acad Sci U S A* 102: 18890-18895

Pan M, Zheng Q, Wang T, Liang L, Mao J, Zuo C, Ding R, Ai H, Xie Y, Si D *et al* (2021) Structural insights into Ubr1-mediated N-degron polyubiquitination. *Nature*

Pao KC, Wood NT, Knebel A, Rafie K, Stanley M, Mabbitt PD, Sundaramoorthy R, Hofmann K, van Aalten DMF, Virdee S (2018) Activity-based E3 ligase profiling uncovers an E3 ligase with esterification activity. *Nature* 556: 381-385

Peters N, Kanngießer S, Pajonk O, Salazar Claros R, Mogk A, Schuck S (2024) Reprograming of the ubiquitin ligase Ubr1 by intrinsically disordered Roq1 through cooperating multifunctional motifs. *bioRxiv*: 2024.2007.2024.604893

Petroski MD, Deshaies RJ (2003) Context of multiubiquitin chain attachment influences the rate of Sic1 degradation. *Mol Cell* 11: 1435-1444

Petroski MD, Deshaies RJ (2005) Mechanism of lysine 48-linked ubiquitin-chain synthesis by the cullin-RING ubiquitin-ligase complex SCF-Cdc34. *Cell* 123: 1107-1120

Petrylak DP, Stewart TF, Gao X, Berghorn E, Lu H, Chan E, Gedrich R, Lang JM, McKean M (2023) A phase 2 expansion study of ARV-766, a PROTAC androgen receptor (AR) degrader, in metastatic castration-resistant prostate cancer (mCRPC). *Journal of Clinical Oncology* 41: TPS290-TPS290

Piatkov KI, Brower CS, Varshavsky A (2012) The N-end rule pathway counteracts cell death by destroying proapoptotic protein fragments. *Proc Natl Acad Sci U S A* 109: E1839-1847

Pickart CM, Rose IA (1985) Functional heterogeneity of ubiquitin carrier proteins. *J Biol Chem* 260: 1573-1581

Pierce NW, Kleiger G, Shan SO, Deshaies RJ (2009) Detection of sequential polyubiquitylation on a millisecond timescale. *Nature* 462: 615-619

Plechanovova A, Jaffray EG, Tatham MH, Naismith JH, Hay RT (2012) Structure of a RING E3 ligase and ubiquitin-loaded E2 primed for catalysis. *Nature* 489: 115-120

Prasad R, Kawaguchi S, Ng DT (2010) A nucleus-based quality control mechanism for cytosolic proteins. *Mol Biol Cell* 21: 2117-2127

Prasad R, Xu C, Ng DTW (2018) Hsp40/70/110 chaperones adapt nuclear protein quality control to serve cytosolic clients. *J Cell Biol* 217: 2019-2032

Pruneda JN, Littlefield PJ, Soss SE, Nordquist KA, Chazin WJ, Brzovic PS, Klevit RE (2012) Structure of an E3:E2~Ub complex reveals an allosteric mechanism shared among RING/U-box ligases. *Mol Cell* 47: 933-942

Randles L, Walters KJ (2012) Ubiquitin and its binding domains. *Front Biosci (Landmark Ed)* 17: 2140-2157

Rao H, Uhlmann F, Nasmyth K, Varshavsky A (2001) Degradation of a cohesin subunit by the N-end rule pathway is essential for chromosome stability. *Nature* 410: 955-959

Robustelli P, Piana S, Shaw DE (2020) Mechanism of Coupled Folding-upon-Binding of an Intrinsically Disordered Protein. *J Am Chem Soc* 142: 11092-11101

Romero, Obradovic, Dunker K (1997) Sequence Data Analysis for Long Disordered Regions Prediction in the Calcineurin Family. *Genome Inform Ser Workshop Genome Inform* 8: 110-124

Rosenbaum JC, Fredrickson EK, Oeser ML, Garrett-Engele CM, Locke MN, Richardson LA, Nelson ZW, Hetrick ED, Milac TI, Gottschling DE *et al* (2011) Disorder targets misorder in nuclear quality control degradation: a disordered ubiquitin ligase directly recognizes its misfolded substrates. *Mol Cell* 41: 93-106

Rudiger S, Buchberger A, Bukau B (1997a) Interaction of Hsp70 chaperones with substrates. *Nat Struct Biol* 4: 342-349

Rudiger S, Germeroth L, Schneider-Mergener J, Bukau B (1997b) Substrate specificity of the DnaK chaperone determined by screening cellulose-bound peptide libraries. *EMBO J* 16: 1501-1507

Ruff KM, Pappu RV (2021) AlphaFold and Implications for Intrinsically Disordered Proteins. *J Mol Biol* 433: 167208

Ruggiano A, Foresti O, Carvalho P (2014) Quality control: ER-associated degradation: protein quality control and beyond. *J Cell Biol* 204: 869-879

Saha A, Deshaies RJ (2008) Multimodal activation of the ubiquitin ligase SCF by Nedd8 conjugation. *Mol Cell* 32: 21-31

Saita S, Nolte H, Fiedler KU, Kashkar H, Venne AS, Zahedi RP, Kruger M, Langer T (2017) PARL mediates Smac proteolytic maturation in mitochondria to promote apoptosis. *Nat Cell Biol* 19: 318-328

Sakamaki JI, Ode KL, Kurikawa Y, Ueda HR, Yamamoto H, Mizushima N (2022) Ubiquitination of phosphatidylethanolamine in organellar membranes. *Mol Cell* 82: 3677-3692 e3611

Samant RS, Livingston CM, Sontag EM, Frydman J (2018) Distinct proteostasis circuits cooperate in nuclear and cytoplasmic protein quality control. *Nature* 563: 407-411

Scheres SH (2012a) A Bayesian view on cryo-EM structure determination. *J Mol Biol* 415: 406-418

Scheres SH (2012b) RELION: implementation of a Bayesian approach to cryo-EM structure determination. *J Struct Biol* 180: 519-530

Schmidt R, Zahn R, Bukau B, Mogk A (2009) ClpS is the recognition component for Escherichia coli substrates of the N-end rule degradation pathway. *Mol Microbiol* 72: 506-517

Scott DC, King MT, Baek K, Gee CT, Kalathur R, Li J, Purser N, Nourse A, Chai SC, Vaithiyalingam S *et al* (2023) E3 ligase autoinhibition by C-degron mimicry maintains C-degron substrate fidelity. *Mol Cell* 83: 770-786 e779

Scott DC, Monda JK, Bennett EJ, Harper JW, Schulman BA (2011) N-terminal acetylation acts as an avidity enhancer within an interconnected multiprotein complex. *Science* 334: 674-678

Scott DC, Rhee DY, Duda DM, Kelsall IR, Olszewski JL, Paulo JA, de Jong A, Ovaa H, Alpi AF, Harper JW *et al* (2016) Two Distinct Types of E3 Ligases Work in Unison to Regulate Substrate Ubiquitylation. *Cell* 166: 1198-1214 e1124

Sharma R, Raduly Z, Miskei M, Fuxreiter M (2015) Fuzzy complexes: Specific binding without complete folding. *FEBS Lett* 589: 2533-2542

Shearer RF, Typas D, Coscia F, Schovsbo S, Kruse T, Mund A, Mailand N (2022) K27-linked ubiquitylation promotes p97 substrate processing and is essential for cell proliferation. *EMBO J* 41: e110145

Sherpa D, Chrustowicz J, Qiao S, Langlois CR, Hehl LA, Gottemukkala KV, Hansen FM, Karayel O, von Gronau S, Prabu JR *et al* (2021) GID E3 ligase supramolecular chelate assembly configures multipronged ubiquitin targeting of an oligomeric metabolic enzyme. *Mol Cell* 81: 2445-2459 e2413

Sherpa D, Chrustowicz J, Schulman BA (2022) How the ends signal the end: Regulation by E3 ubiquitin ligases recognizing protein termini. *Mol Cell* 82: 1424-1438

Shi M, Zhao J, Zhang S, Huang W, Li M, Bai X, Zhang W, Zhang K, Chen X, Xiang S (2023) Structural basis for the Rad6 activation by the Bre1 N-terminal domain. *Elife* 12

Shimshon A, Dahan K, Israel-Gueta M, Olmayev-Yaakobov D, Timms RT, Bekturova A, Makaros Y, Elledge SJ, Koren I (2024) Dipeptidyl peptidases and E3 ligases of N-degron pathways cooperate to regulate protein stability. *J Cell Biol* 223

Siepmann TJ, Bohnsack RN, Tokgoz Z, Baboshina OV, Haas AL (2003) Protein interactions within the N-end rule ubiquitin ligation pathway. *J Biol Chem* 278: 9448-9457

Singh A, Vashistha N, Heck J, Tang X, Wipf P, Brodsky JL, Hampton RY (2020) Direct involvement of Hsp70 ATP hydrolysis in Ubr1-dependent quality control. *Mol Biol Cell* 31: 2669-2686

Sitron CS, Brandman O (2019) CAT tails drive degradation of stalled polypeptides on and off the ribosome. *Nat Struct Mol Biol* 26: 450-459

Sontag EM, Samant RS, Frydman J (2017) Mechanisms and Functions of Spatial Protein Quality Control. *Annu Rev Biochem* 86: 97-122

Stewart MD, Ritterhoff T, Klevit RE, Brzovic PS (2016) E2 enzymes: more than just middle men. *Cell Res* 26: 423-440

Streich FC, Jr., Lima CD (2014) Structural and functional insights to ubiquitin-like protein conjugation. *Annu Rev Biophys* 43: 357-379

Sukalo M, Fiedler A, Guzman C, Spranger S, Addor MC, McHeik JN, Oltra Benavent M, Cobben JM, Gillis LA, Shealy AG *et al* (2014) Mutations in the human UBR1 gene and the associated phenotypic spectrum. *Hum Mutat* 35: 521-531

Suresh HG, Pascoe N, Andrews B (2020) The structure and function of deubiquitinases: lessons from budding yeast. *Open Biol* 10: 200279

Suzuki Y, Imai Y, Nakayama H, Takahashi K, Takio K, Takahashi R (2001) A serine protease, HtrA2, is released from the mitochondria and interacts with XIAP, inducing cell death. *Mol Cell* 8: 613-621

Swanson R, Locher M, Hochstrasser M (2001) A conserved ubiquitin ligase of the nuclear envelope/endoplasmic reticulum that functions in both ER-associated and Matalpha2 repressor degradation. *Genes Dev* 15: 2660-2674

Szoradi T, Schaeff K, Garcia-Rivera EM, Itzhak DN, Schmidt RM, Bircham PW, Leiss K, Diaz-Miyar J, Chen VK, Muzzey D *et al* (2018) SHRED Is a Regulatory Cascade that Reprograms Ubr1 Substrate Specificity for Enhanced Protein Quality Control during Stress. *Mol Cell* 70: 1025-1037 e1025

Tan X, Calderon-Villalobos LI, Sharon M, Zheng C, Robinson CV, Estelle M, Zheng N (2007) Mechanism of auxin perception by the TIR1 ubiquitin ligase. *Nature* 446: 640-645

Tang X, Orlicky S, Lin Z, Willems A, Neculai D, Ceccarelli D, Mercurio F, Shilton BH, Sicheri F, Tyers M (2007) Suprafacial orientation of the SCFCdc4 dimer accommodates multiple geometries for substrate ubiquitination. *Cell* 129: 1165-1176

Tasaki T, Mulder LC, Iwamatsu A, Lee MJ, Davydov IV, Varshavsky A, Muesing M, Kwon YT (2005) A family of mammalian E3 ubiquitin ligases that contain the UBR box motif and recognize N-degrons. *Mol Cell Biol* 25: 7120-7136

Tasaki T, Sriram SM, Park KS, Kwon YT (2012) The N-end rule pathway. *Annu Rev Biochem* 81: 261-289

Teale WD, Paponov IA, Palme K (2006) Auxin in action: signalling, transport and the control of plant growth and development. *Nat Rev Mol Cell Biol* 7: 847-859

Thrower JS, Hoffman L, Rechsteiner M, Pickart CM (2000) Recognition of the polyubiquitin proteolytic signal. *EMBO J* 19: 94-102

Timms RT, Koren I (2020) Tying up loose ends: the N-degron and C-degron pathways of protein degradation. *Biochem Soc Trans* 48: 1557-1567

Timms RT, Zhang Z, Rhee DY, Harper JW, Koren I, Elledge SJ (2019) A glycine-specific N-degron pathway mediates the quality control of protein N-myristoylation. *Science* 365

Tompa P, Fuxreiter M (2008) Fuzzy complexes: polymorphism and structural disorder in protein-protein interactions. *Trends Biochem Sci* 33: 2-8

Tsai JM, Aguirre JD, Li YD, Brown J, Focht V, Kater L, Kempf G, Sandoval B, Schmitt S, Rutter JC *et al* (2023) UBR5 forms ligand-dependent complexes on chromatin to regulate nuclear hormone receptor stability. *Mol Cell* 83: 2753-2767 e2710

Tsai JM, Nowak RP, Ebert BL, Fischer ES (2024) Targeted protein degradation: from mechanisms to clinic. *Nat Rev Mol Cell Biol*

Turco E, Gallego LD, Schneider M, Kohler A (2015) Monoubiquitination of histone H2B is intrinsic to the Bre1 RING domain-Rad6 interaction and augmented by a second Rad6-binding site on Bre1. *J Biol Chem* 290: 5298-5310

Turner GC, Du F, Varshavsky A (2000) Peptides accelerate their uptake by activating a ubiquitin-dependent proteolytic pathway. *Nature* 405: 579-583

Twomey EC, Ji Z, Wales TE, Bodnar NO, Ficarro SB, Marto JA, Engen JR, Rapoport TA (2019) Substrate processing by the Cdc48 ATPase complex is initiated by ubiquitin unfolding. *Science* 365

Ubersax JA, Ferrell JE, Jr. (2007) Mechanisms of specificity in protein phosphorylation. *Nat Rev Mol Cell Biol* 8: 530-541

Uckelmann M, Sixma TK (2017) Histone ubiquitination in the DNA damage response. *DNA Repair (Amst)* 56: 92-101

Ungelenk S, Moayed F, Ho CT, Grousl T, Scharf A, Mashaghi A, Tans S, Mayer MP, Mogk A, Bukau B (2016) Small heat shock proteins sequester misfolding proteins in near-native conformation for cellular protection and efficient refolding. *Nat Commun* 7: 13673

Van Roey K, Uyar B, Weatheritt RJ, Dinkel H, Seiler M, Budd A, Gibson TJ, Davey NE (2014) Short linear motifs: ubiquitous and functionally diverse protein interaction modules directing cell regulation. *Chem Rev* 114: 6733-6778

Varadi M, Anyango S, Deshpande M, Nair S, Natassia C, Yordanova G, Yuan D, Stroe O, Wood G, Laydon A *et al* (2022) AlphaFold Protein Structure Database: massively expanding the structural coverage of protein-sequence space with high-accuracy models. *Nucleic Acids Res* 50: D439-D444

Varland S, Silva RD, Kjosas I, Faustino A, Bogaert A, Billmann M, Boukhatmi H, Kellen B, Costanzo M, Drazic A *et al* (2023) N-terminal acetylation shields proteins from degradation and promotes age-dependent motility and longevity. *Nat Commun* 14: 6774

Varshavsky A (1991) Naming a targeting signal. *Cell* 64: 13-15

Varshavsky A (1996) The N-end rule: functions, mysteries, uses. *Proc Natl Acad Sci U S A* 93: 12142-12149

Varshavsky A (2011) The N-end rule pathway and regulation by proteolysis. *Protein Sci* 20: 1298-1345

Varshavsky A (2019a) N-degron and C-degron pathways of protein degradation. *Proc Natl Acad Sci U S A* 116: 358-366

Varshavsky A (2019b) On the cause of sleep: Protein fragments, the concept of sentinels, and links to epilepsy. *Proc Natl Acad Sci U S A* 116: 10773-10782

Walsh I, Martin AJ, Di Domenico T, Tosatto SC (2012) ESpritz: accurate and fast prediction of protein disorder. *Bioinformatics* 28: 503-509

Wang B, Dai T, Sun W, Wei Y, Ren J, Zhang L, Zhang M, Zhou F (2021) Protein N-myristoylation: functions and mechanisms in control of innate immunity. *Cell Mol Immunol* 18: 878-888

Wang F, He Q, Zhan W, Yu Z, Finkin-Groner E, Ma X, Lin G, Li H (2023) Structure of the human UBR5 E3 ubiquitin ligase. *Structure* 31: 541-552 e544

Wang L, Liu C, Yang B, Zhang H, Jiao J, Zhang R, Liu S, Xiao S, Chen Y, Liu B *et al* (2022) SARS-CoV-2 ORF10 impairs cilia by enhancing CUL2ZYG11B activity. *J Cell Biol* 221

Weinelt N, Wachtershauser KN, Celik G, Jeiler B, Gollin I, Zein L, Smith S, Andrieux G, Das T, Roedig J *et al* (2024) LUBAC-mediated M1 Ub regulates necroptosis by segregating the cellular distribution of active MLKL. *Cell Death Dis* 15: 77

Wilkinson KD, Urban MK, Haas AL (1980) Ubiquitin is the ATP-dependent proteolysis factor I of rabbit reticulocytes. *J Biol Chem* 255: 7529-7532

Williamson A, Banerjee S, Zhu X, Philipp I, Iavarone AT, Rape M (2011) Regulation of ubiquitin chain initiation to control the timing of substrate degradation. *Mol Cell* 42: 744-757

Wojcik C, DeMartino GN (2003) Intracellular localization of proteasomes. *Int J Biochem Cell Biol* 35: 579-589

Wright JD, Mace PD, Day CL (2016) Secondary ubiquitin-RING docking enhances Arkadia and Ark2C E3 ligase activity. *Nat Struct Mol Biol* 23: 45-52

Wright MH, Heal WP, Mann DJ, Tate EW (2010) Protein myristoylation in health and disease. *J Chem Biol* 3: 19-35

Wu K, Itskanov S, Lynch DL, Chen Y, Turner A, Gumbart JC, Park E (2024) Substrate recognition mechanism of the endoplasmic reticulum-associated ubiquitin ligase Doa10. *Nat Commun* 15: 2182

Xia Z, Turner GC, Hwang CS, Byrd C, Varshavsky A (2008a) Amino acids induce peptide uptake via accelerated degradation of CUP9, the transcriptional repressor of the PTR2 peptide transporter. *J Biol Chem* 283: 28958-28968

Xia Z, Webster A, Du F, Piatkov K, Ghislain M, Varshavsky A (2008b) Substrate-binding sites of UBR1, the ubiquitin ligase of the N-end rule pathway. *J Biol Chem* 283: 24011-24028

Xie Y, Varshavsky A (1999) The E2-E3 interaction in the N-end rule pathway: the RING-H2 finger of E3 is required for the synthesis of multiubiquitin chain. *EMBO J* 18: 6832-6844

Xie Y, Varshavsky A (2000) Physical association of ubiquitin ligases and the 26S proteasome. *Proc Natl Acad Sci U S A* 97: 2497-2502

Xue H, Yao T, Cao M, Zhu G, Li Y, Yuan G, Chen Y, Lei M, Huang J (2019) Structural basis of nucleosome recognition and modification by MLL methyltransferases. *Nature* 573: 445-449

Yang ZR, Thomson R, McNeil P, Esnouf RM (2005) RONN: the bio-basis function neural network technique applied to the detection of natively disordered regions in proteins. *Bioinformatics* 21: 3369-3376

Yau RG, Doerner K, Castellanos ER, Haakonsen DL, Werner A, Wang N, Yang XW, Martinez-Martin N, Matsumoto ML, Dixit VM *et al* (2017) Assembly and Function of Heterotypic Ubiquitin Chains in Cell-Cycle and Protein Quality Control. *Cell* 171: 918-933 e920

Young TS, Ahmad I, Yin JA, Schultz PG (2010) An enhanced system for unnatural amino acid mutagenesis in E. coli. *J Mol Biol* 395: 361-374

Yuan J, Luo K, Zhang L, Cheville JC, Lou Z (2010) USP10 regulates p53 localization and stability by deubiquitinating p53. *Cell* 140: 384-396

Zenker M, Mayerle J, Lerch MM, Tagariello A, Zerres K, Durie PR, Beier M, Hulskamp G, Guzman C, Rehder H *et al* (2005) Deficiency of UBR1, a ubiquitin ligase of the N-end rule pathway, causes pancreatic dysfunction, malformations and mental retardation (Johanson-Blizzard syndrome). *Nat Genet* 37: 1345-1350

Zhang J, Ma C, Yu Y, Liu C, Fang L, Rao H (2023) Single amino acid-based PROTACs trigger degradation of the oncogenic kinase BCR-ABL in chronic myeloid leukemia (CML). *J Biol Chem* 299: 104994

Zhang Y, Lin S, Peng J, Liang X, Yang Q, Bai X, Li Y, Li J, Dong W, Wang Y *et al* (2022) Amelioration of hepatic steatosis by dietary essential amino acid-induced ubiquitination. *Mol Cell*

Zhu K, Song L, Wang L, Hua L, Luo Z, Wang T, Qin B, Yuan S, Gao X, Mi W *et al* (2024) SARS-CoV-2 ORF10 hijacking ubiquitination machinery reveals potential unique drug targeting sites. *Acta Pharm Sin B*

Zhu K, Suskiewicz MJ, Hlousek-Kasun A, Meudal H, Mikoc A, Aucagne V, Ahel D, Ahel I (2022) DELTEX E3 ligases ubiquitylate ADP-ribosyl modification on protein substrates. *Sci Adv* 8: eadd4253

Zhu K, Song L, Wang L, Hua L, Luo Z, Wang T, Qin B, Yuan S, Gao X, Mi W, Cui S (2024) SARS-CoV-2 ORF10 hijacking ubiquitination machinery reveals potential unique drug targeting sites. *Acta Pharm Sin B* doi: 10.1016/j.apsb.2024.05.018

7. Acknowledgements

First, I would like to thank Sebastian who gave me the opportunity to work on this exciting project that was since the very beginning full of serendipitous discoveries and (biochemical) plot twists. Thank you not only for your support but particularly also for the experimental freedom I highly appreciated.

I would like to thank my TAC members Matthias Mayer and Axel Mogk, who throughout the years provided me with continuous scientific support.

Next, I would like to acknowledge the efforts of Dirk Flemming and Jan Rheinberger to acquire (and process) a cryo-EM dataset of the Roq1-Ubr1 complex. A special thanks goes also to Bram Vermeulen and Stefan Pfeffer for their tremendous input regarding AlphaFold predictions and evaluations. Thank you also to Jörg Malsam for the generous photo-crosslinking advice and experimental assistance.

An enormous appreciation for her contributions to this project goes to Sibylle aka “Schnibi”, without whom the project would have not been where it is right now. Thank you for your being a wonderful project partner, surviving endlessly long SHRED meetings, cold room challenges, paper writing exercises and creating great conference memories with me.

Rafael, many thanks for your enormous contributions to the SHRED project. I always enjoyed your presence in the lab, your attention for details and the stimulating discussions we had.

Tamas, thank you very much for contributions to the SHRED project! You can’t believe how many times I have studied your detailed old lab protocols, have read and cited your work in my thesis.

Well, well, well, my dear (past and present) Schookees: I am absolutely blown away by your never-ending positivity, willingness to help and the constant supplies of C&Cs since the first day I joined the lab. Thank you so much, Oli, Giulia, Dimitris, Jasmin, Rolf, Lis, Natalie, Petra, Inge, Anna, Sneha, Klara and Carlos for everything. I know that during COVID-19 and in between all the moves some of us experienced, we could always count on each other, which is what makes this lab so special.

BZH 3rd floor and old ZMBH buddies: Thank you very much for creating such a great working environment and providing so many reagents at initial stages of the project.

Thank you, Anke, for reliably managing all of our bureaucratic hurdles.

I would also like to thank the ZMBH Spülküche, Melanie and Linda for their tremendous but often underappreciated tasks that are so essential for all of us. Dear Mensa-Team, what would I have done without you?! Thank you so much for providing me throughout all these years with the energy I needed in the lab.
I am particularly grateful by the Boehringer Ingelheim Fonds and Studienstiftung des deutschen Volkes for their support during my academic studies and PhD.
I would like to thank Manu Hegde, Florian Wilfling, Stefan Jentsch, Frau Junker, Frau Rühl and Herr Lommetz for stimulating my scientific curiosity that ultimately enabled me to pursue this journey.
Thank you also, Monday Bouldering People, for all the fun we had at Boulderhaus that made me forget for a few hours the stressful and occasionally frustrating life of a PhD student. Particularly, I would like to thank my climbing partner in crime, Francesco, for all the climbing, bouldering, German language and kebab experiences we enjoyed together.
Robert and Sandra, thank you for being great roommates. Particularly during the harsh COVID-19 lockdowns I enjoyed your company and will always remember the winter BBQs in our garden.
Aye and Lau, I am very grateful for our friendship that goes well beyond the same taste in restaurants and movies.
An enormous appreciation goes also to all my other friends for their continuous support throughout the years, witnessing all ups and downs a PhD can bring: Robert, Vincenz, Dominik, Kenneth, Maxi, Victoria, Silvia, Chris, Darius, Samuel, Lea, Leonie, Alex, Nora, Vivian, Maurice, Anne and Florestan.
Dearest Franzi, how could I have managed this endeavor without your constant support, positiveness, love, and attention. I am so grateful that you are a part of my life, which would not be the same without you.
Mama, Papa, Julia, Claudia, Sepp, Alex, Ralf, Jürgen, Petra, Oma Hilde, Opa Jupp, Oma Fine, Opa Martin: Ich danke Euch von ganzem Herzen, dass Ihr immer an mich geglaubt habt und mich so tatkräftig unterstützt. Letztlich ist das, was am wichtigsten im Leben ist, die eigene Familie. Und dafür bin ich Euch unendlich dankbar.

8. Supplements

8.1 Supplementary Figure 1

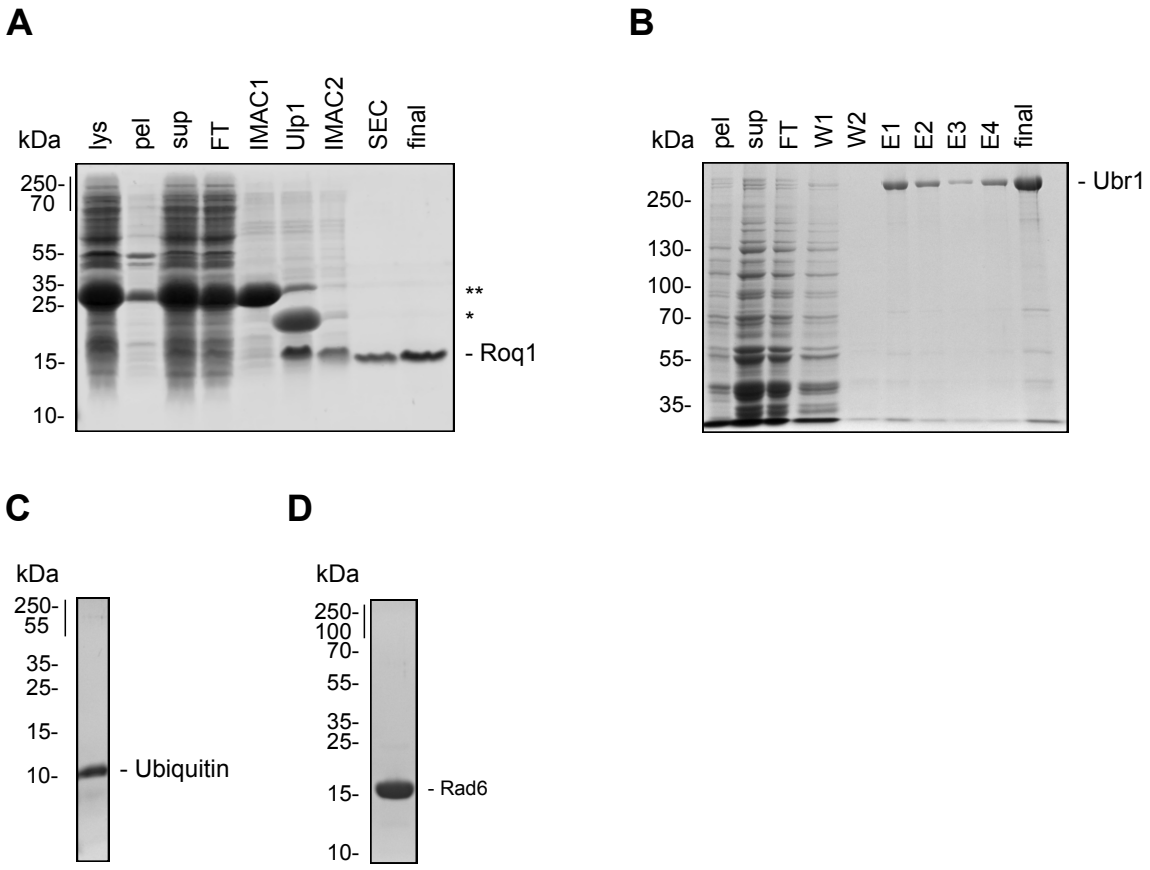

Figure S1. Overview of Roq1, Ubr1, ubiquitin and Rad6 purification

(A) Coomassie-stained SDS-PAGE gel of Roq1 (22-60)-HA purification steps. For a detailed expression and purification protocol, see section 5.2.4.1.2. In brief, I expressed Roq1 in *E. coli* cells as His_6-SUMO-Roq1(22-60)-HA to protect the unstable N-terminal arginine of Roq1. Harvested cells were lysed (lys) and insoluble proteins (pel) were separated. To isolate His_6-SUMO-Roq1(22-60)-HA, I incubated the soluble protein pool (sup) with nickel beads, separated them from soluble unbound proteins (FT), washed and eluted fractions (IMAC1). To remove the N-terminal His_6-SUMO tag and thereby expose the N-terminal arginine residue of Roq1, I added Ulp1 (Ulp1). To remove uncleaved His_6-SUMO-Roq1(22-60)-HA (**) and free His_6-SUMO (*), I performed a second IMAC step (IMAC2). A size exclusion chromatography step (SEC) further increased purity. 1 µl of "lys", "pel", "sup" and "FT" were mixed with 9 µl sample buffer and loaded. 10 µl of "IMAC1", "Ulp1", "IMAC2" and "SEC" and 2.8 µg of final Roq1 (22-60)-HA were loaded. Expression and purification of Roq1 (22-60)-HA was conceptualized and performed by me.

(B) Coomassie-stained SDS-PAGE gel of FLAG-Ubr1 purification steps. For a detailed expression and purification protocol, see section 5.2.4.1.1. In brief, I harvested yeast cells that expressed FLAG-Ubr1, lysed the cells and separated insoluble proteins (pel). To isolate FLAG-Ubr1, I incubated the soluble protein pool (sup) with FLAG beads, separated them from soluble unbound proteins (FT), washed twice (W1 and W2) and eluted fractions (E1-E4). 1 µl of "pel", "sup" and "FT" were mixed with 9 µl sample buffer. 10 µl of "W1", "W2", "E1-4" and 3.4 µg of final FLAG-Ubr1 were loaded. Expression and purification of FLAG-Ubr1 was originally conceptualized and performed by me. Sibylle Kanngießer re-purified FLAG-Ubr1 using slightly adapted protocols.

(C) Coomassie-stained SDS-PAGE gel of purified ubiquitin. 10 µl were loaded after size exclusion but before sample concentration. For a detailed expression and purification protocol, see section 5.2.4.1.8. Ubiquitin purification was conceptualized by Jörg Schweiggert, and collaboratively performed by Gerry (Melchior lab) and me.
(D) As in panel (C), but with Rad6. Rad6 purification was conceptualized by Chi-Ting Ho and performed by me.

8.2 Supplementary Figure 2

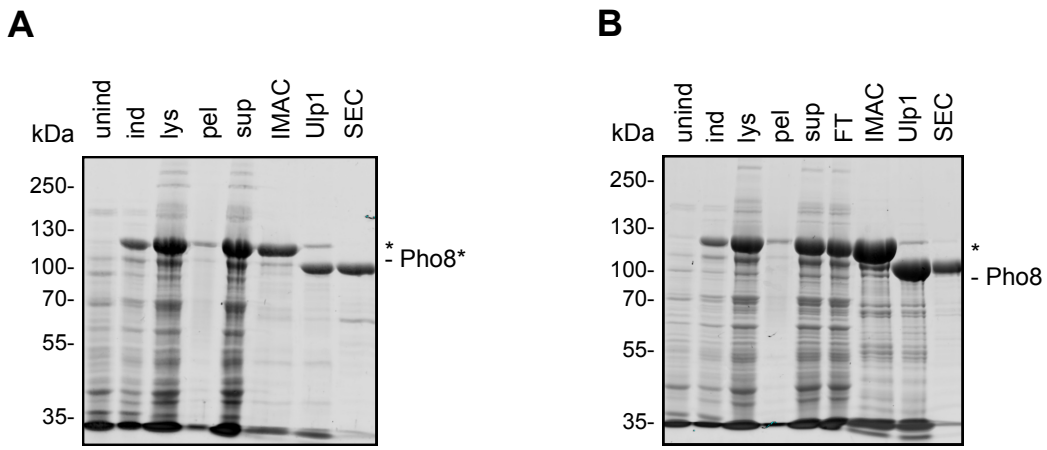

Figure S2. Overview of Pho8* and Pho8 purification
(A) Coomassie-stained SDS-PAGE gel of Pho8*-MBP purification steps. For a detailed expression and purification protocol, see section 5.2.4.1.4. In brief, I expressed Pho8* in *E. coli* as His_6-SUMO-Pho8*-MBP. To monitor His_6-SUMO-Pho8*-MBP expression levels, I loaded 0.05 ODs of uninduced (unind) and IPTG-induced samples (ind). After harvesting, I lysed the cells (lys) and removed insoluble proteins (pel). To purify His_6-SUMO-Pho8*-MBP, I incubated the soluble protein pool (sup) with nickel beads, separated them from soluble unbound proteins, washed and eluted protein-containing fractions (IMAC). To remove the N-terminal His_6-SUMO tag, I added Ulp1 (Ulp1). To remove free His_6-SUMO and Ulp1, I further purified Pho8*-MBP via amylose resin affinity chromatography followed by size exclusion chromatography (SEC). 1 µl of "lys", "pel" and "sup" were mixed with 9 µl sample buffer and loaded. 10 µl of "IMAC", "Ulp1", "SEC" and 4.4 µg of final Pho8*-MBP were loaded. The asterisk (*) indicates uncleaved His_6-SUMO-Pho8*-MBP. Expression and purification of Pho8*-MBP was conceptualized and performed by me.
(B) As in panel (A), but with Pho8-MBP. "FT" denotes an IMAC flow-through sample. 4.6 µg of final Pho8-MBP were loaded

8.3 Supplementary Figure 3

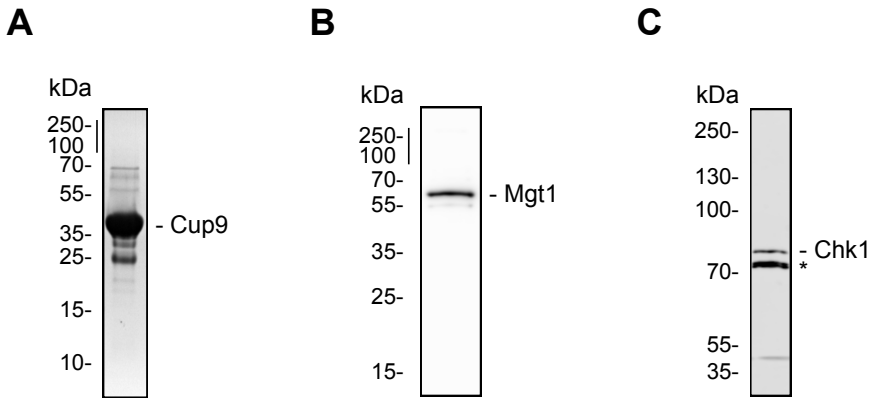

Figure S3. Overview of Cup9, Mgt1 and Chk1 purification
(A) Coomassie-stained SDS-PAGE gel of purified Cup9-Strep. 2.8 µg of purified Cup9 were loaded. For a detailed expression and purification protocol, see section 5.2.4.1.6. Expression and purification of Cup9-Strep was conceptualized and performed by me.
(B) Immunoblot of MBP tag from purified Mgt1-MBP. 0.95 µg of purified Mgt1-MBP were loaded. For a detailed expression and purification protocol, see section 5.2.4.1.5. Expression and purification of Mgt1-MBP was conceptualized and performed by me.
(C) Immunoblot of ALFA tag from purified Chk1-ALFA-FLAG. 1.9 µg of purified Chk1-ALFA-FLAG were loaded. The asterisk (*) denotes a degradation product that arose during expression or purification. For a detailed expression and purification protocol, see section 5.2.4.1.7. Expression and purification of Chk1-ALFA-FLAG was conceptualized and performed by me.

8.4 Supplementary Figure 4

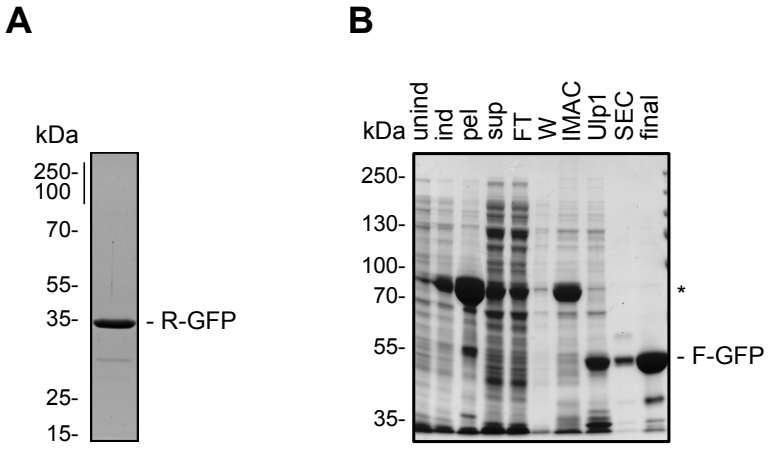

Figure S4. Overview of R-GFP and F-GFP purification

(A) Coomassie-stained SDS-PAGE gel of purified R-GFP. 10 µl were loaded after size exclusion but before sample concentration. For a detailed expression and purification protocol, see section 5.2.4.1.10. Expression and purification of R-GFP was conceptualized by Chi-Ting Ho and performed by me.
(B) Coomassie-stained SDS-PAGE gel of F-GFP purification steps. For a detailed expression and purification protocol, see section 5.2.4.1.10. In brief, I expressed F-GFP in *E. coli* as His_6-SUMO-F-GFP. To monitor His_6-SUMO-F-GFP expression levels, I loaded 0.05 ODs of uninduced (unind) and IPTG-induced samples (ind). After harvesting, I lysed the cells and removed insoluble proteins (pel). To purify His_6-SUMO-F-GFP, I incubated the soluble protein pool (sup) with nickel beads, separated them from soluble unbound proteins (FT), washed (W) and eluted protein-containing fractions (IMAC). To remove the N-terminal His_6-SUMO tag, I added Ulp1 (Ulp1). To remove uncleaved His_6-SUMO-F-GFP, I further purified F-GFP via size exclusion chromatography (SEC). 1 µl of “pel”, “sup” and “FT” were mixed with 9 µl sample buffer and loaded. 10 µl of “W”, “IMAC”, “Ulp1”, “SEC” and 2.6 µg of final F-GFP were loaded. The asterisk (*) indicates uncleaved His_6-SUMO-F-GFP. Expression and purification of F-GFP was conceptualized and performed by me.